

P-NIPAM microgels as stimuli responsive matrix for embedding functional inorganic and organic particles

vorgelegt von
Diplom-Chemikerin
Kornelia Gawlitza
Berlin

Von der Fakultät II - Mathematik und Naturwissenschaften
der Technischen Universität Berlin
zur Erlangung des akademischen Grades

Doktor der Naturwissenschaften
- Dr. rer. nat. -

genehmigte Dissertation

Vorsitzender: Prof. Dr. Reinhard Schomäcker

Gutachter: Prof. Dr. Regine von Klitzing

Gutachter: Prof. Dr. Thomas Hellweg

Tag der wissenschaftlichen Aussprache: 07.12.2012

Berlin 2012

D83

Acknowledgement

This thesis is dedicated to my parents, Waltraud and Peter-Michael Gawlitza.

The presented PhD thesis was elaborated under the supervision of Prof. Regine von Klitzing at the Stranski-Laboratorium for Physical and Theoretical Chemistry at the Technical University Berlin. Parts of the experiments were performed at the Charité Berlin and at the University of Melbourne, Australia.

First of all, I would like to thank Prof. Regine von Klitzing for giving me the opportunity to make my PhD in this laboratory. Many fruitful discussions and her friendly support helped me a lot during the last years. And when I was stuck, she found the right words to keep me going on and to bring out the best of me.

Special thanks go to Dr. Radostina Georgieva for her support, her helpful discussions and her time spending with me at the CLSM.

Dr. Changzhu Wu is kindly acknowledged for helping me in the field of enzyme immobilization. It was always a pleasure to work and discuss with you. At this point, I also want to thank Prof. Marion Ansorge-Schumacher for giving me the opportunity to work in her laboratory. Prof. Möhwald, Prof. Dayang Wang and Dr. Shuo Bai are acknowledged for "introducing" me into this topic.

Furthermore, I want to thank Prof. Paul Mulvaney and his whole group for a memorable time in Australia. Beside the chance to get to know an incredible continent, the work in the laboratory as well as the fruitful discussions gave me a great introduction into the field of inorganic nanoparticles.

I want to thank Sarah Turner and Frank Polzer for performing the exper-

iments at the Electron microscope of the Joint Laboratory for Structural Research (JLSR) of Helmholtz-Zentrum Berlin für Materialien und Energie (HZB), Humboldt-Universität zu Berlin (HU) and Technische Universität Berlin (TU).

To Gabi Hedicke, Jana Lutzki, Michaela Dzionara, Rene Strassnick, Rolf Kunert, Erik Sallwey, Christiane Abu-Hani and Maria Blobel I owe much for their kind and immediate support and also for the helpful coffee breaks.

I want to thank my former and current colleagues in the Stranski-Laboratorium. Nora Konnertz is mentioned for her support with the experiments but much more for the friendship which has been grown. Thanks go to Stefan Wellert for having his ear and for keeping me calm sometimes. Matthias Karg is acknowledged for his constant support during the last years and for spending awesome times on many conferences and in many places. A special thanks also goes to Natascha Schelero for her steady help in scientific but also in private things. Last but not least I want to mention Adrian Carl who was the most important help at work to get through the last years.

And of course, I want to thank my family and friends who have been on my side whenever I needed them. Special thanks go to Kristin Lindner, Friederike Blödorn, Frances Christmann, Gitte und Andreas Jäger, Marko Müller, Tristan Fürst, the girls from Berlinchen and Strupsel to name just a few.

And last but not least my deep appreciation to my mum and dad for their endless support on my path following my dreams.

This work was supported by the DFG via the Cluster of Excellence "Unifying Concepts in Catalysis" and the EU via a STSM within the cost action D43.

Contents

1 Introduction	1
2 Theory	5
2.1 Smart gels	5
2.2 Plasmon resonance of gold nanoparticles	9
2.3 Enzyme immobilization	11
2.4 Methods	13
2.4.1 Dynamic light scattering	13
2.4.1.1 Characterization of the size and diffusion.	13
2.4.1.2 Characterization of the zeta potential.	17
2.4.2 Imaging techniques	19
2.4.2.1 Confocal laser scanning microscopy.	19
2.4.2.2 Transmission electron microscopy.	21
2.4.2.3 Atomic force microscopy.	22
3 Experimental Section	25
3.1 Materials	25
3.2 Synthesis	26
3.2.1 P-NIPAM microgels	26
3.2.2 Large p-NIPAM microgels	27
3.2.3 Copolymers of NIPAM and AA	27
3.2.4 Copolymers of NIPAM and AG	28
3.2.5 Integrated amount of comonomer	28
3.2.6 Au-NPs	29
3.3 Preparation procedures	30
3.3.1 Determination of the amount of water in microgel particles	30
3.3.2 Loading of microgels with Au-NPs	30
3.3.3 Immobilization of enzymes by solvent exchange	31
3.3.3.1 Determination of the purity of enzymes by SDS-	
Page.	31
3.3.3.2 Labeling of the enzymes with FITC.	32

3.3.3.3	Immobilization of CalB.	32
3.3.3.4	Immobilization of HRP.	33
3.3.3.5	Determination of the immobilized amount of enzyme.	33
3.3.4	Covalent immobilization of HRP	33
3.4	Activity Measurements	34
3.4.1	Activity measurements of immobilized CalB in organic solvents	34
3.4.2	Activity measurements of immobilized HRP in organic solvents	35
3.4.3	Activity measurements of immobilized HRP in water	35
3.5	Instruments and sample preparation	36
3.5.1	DLS	36
3.5.2	SLS	36
3.5.3	Zeta potential measurements	37
3.5.4	Gas chromatography	37
3.5.5	CLSM	37
3.5.6	AFM	38
3.5.7	TEM	38
3.5.8	UV-Vis spectroscopy	38
3.5.9	SDS-Page	39
3.5.10	Karl-Fischer titration	39
4	P-NIPAM microgels loaded with Au-NPs	41
4.1	Introduction	41
4.2	Results and Discussion	42
4.2.1	Characterization of different cross-linked p-NIPAM microgel particles	42
4.2.2	Characterization of Au-NPs	46
4.2.3	Low loading regime	46
4.2.4	High loading regime	50
4.3	Conclusion	54
5	Immobilization of enzymes within p-NIPAM microgels	57
5.1	Introduction	57
5.2	Determination of enzyme purity	58

5.3 Immobilization of enzymes by physical adsorption using solvent exchange	59
5.3.1 Characterization of large p-NIPAM microgels	61
5.3.2 Immobilization of CalB	64
5.3.2.1 Determination of the immobilized amount of CalB.	65
5.3.2.2 Activity measurements on the immobilized system.	69
5.3.2.3 Localization of CalB within p-NIPAM microgels using CLSM.	73
5.3.3 Immobilization of HRP	80
5.3.3.1 Determination of the immobilized amount of HRP.	80
5.3.3.2 Activity measurements on the immobilized system.	81
5.3.3.3 Localization of HRP within p-NIPAM microgels using CLSM.	82
5.4 Immobilization of <i>horseradish</i> peroxidase by covalent immobilization using para-benzoquinone	83
5.4.1 Characterization of p-NIPAM- <i>co</i> -AA microgels	84
5.4.2 Immobilization of HRP using BQ	88
5.4.2.1 Activity measurements on the immobilized system.	88
5.4.3 Outlook	90
5.5 Conclusion	91
6 Polyampholyte p-NIPAM-<i>co</i>-AG microgels	93
6.1 Introduction	93
6.2 Results and Discussion	94
6.2.1 Characterization of p-NIPAM- co -AG microgels	94
6.2.2 Switchable aggregation behavior of p-NIPAM- co -AG microgels	100
6.3 Conclusion	104
7 Conclusions and Future Perspectives	107
7.1 Conclusions	107
7.2 Future Perspectives	111

A Further experimental details	113
A.1 Experimental Section	113
A.2 P-NIPAM microgels loaded with Au-NPs	114
A.3 Immobilization of enzymes within p-NIPAM	115
A.4 Conclusions and Future Perspectives	116
B Abbreviations	117

1 Introduction

Polymer materials play an essential role in daily life due to their broad range of specific properties.¹ One type of polymers which is highly interesting for research and industries are gels. Gels consist of a cross-linked, three-dimensional polymer network. Their reversible swelling behavior as well as their unique viscoelastic properties²⁻⁵ make them interesting for many technical and medical applications, e.g. in contact lenses⁶ and as superabsorbers.⁷

A special group of gels can be summarized as microgels which have a size in the submicron range (10 nm to 1000 nm). The smaller size compared to macrogels leads to a faster response to external stimuli as well as to a higher surface-to-volume ratio which forced them into the focus of many investigations during the last decades.⁷⁻⁹

In this PhD thesis polymer particles made of poly-N-isopropylacrylamide (p-NIPAM) were used. They show a reversible volume phase transition (VPT) at around 32°C by changing the temperature.¹⁰⁻¹² Additionally, the properties, e.g. the VPTT, of the microgels can be influenced by changing the amount of cross-linker or integrating comonomers within the polymer network.¹³⁻¹⁷ p-NIPAM microgels offer high potential as stimuli responsive matrices in biocatalysis or sensor designs. Three possible approaches to produce suitable systems for these applications are illustrated in figure 1.1. All of the three approaches were investigated within this PhD thesis.

In order to receive suitable supports for sensors, one strategy is to load the microgel particles with gold nanoparticles (Au-NPs) (figure 1.1a). The production of p-NIPAM microgels with Au-NPs is an interesting topic due to the combination of the thermoresponsive behavior of the polymer and the optical¹⁸⁻²⁰ properties of the NPs. Although there are a huge number of publications on the loading of spherical Au-NPs within p-NIPAM microgels,²¹⁻²³

neither the influence of the cross-linker content on the optical properties nor the internal structure of the Au-NP loaded microgels were investigated in detail.

Chapter 4 of this PhD thesis deals with the loading of spherical, citrate-stabilized Au-NPs with a diameter of 18.5 nm within p-NIPAM microgel particles. The influence of the cross-linker density and the amount of added Au-NPs on the surface plasmon resonance was studied using temperature dependant UV-Vis spectroscopy. Transmission electron microscopy (TEM) was used to study the penetration depth of the Au-NPs for different cross-linker and loading densities. The pure p-NIPAM as well as the loaded microgels were measured by dynamic light scattering (DLS) to investigate the swelling behavior of the polymer systems.

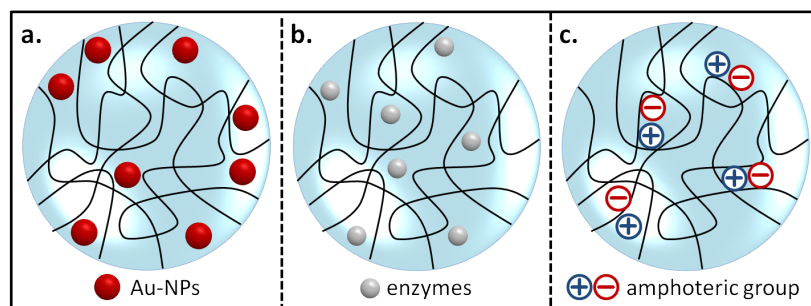


Figure 1.1: Sketch of possible applications of p-NIPAM microgels: loading with Au-NPs (a), immobilization of enzymes (b) and integration of amphoteric comonomers (c).

The main part of the present work deals with the immobilization of enzymes within p-NIPAM microgel particles which is of high research interest (figure 1.1b).^{8,24-28} The focus of the present work lays on the production of biocatalysts for the usage in organic or aqueous environment by either embedding enzymes in the polymer network by physical interactions or covalent binding of enzymes into the polymer particles. In chapter 5 two existing immobilization methods were adapted in order to successfully immobilize enzymes within p-NIPAM microgel particles.

In a first case, the enzymes lipase B from *Candida Antarctica* (CalB) and horseradish peroxidase (HRP) were embedded within large p-NIPAM particles to produce a biocatalyst that works in organic media. The immobilization was done via a gradual solvent exchange from water to isopropanol and finally to n-hexane for the activity test. The usage of confocal laser scanning microscopy (CLSM) to determine the location of the labeled enzymes after

solvent exchange is discussed extensively. The immobilized amount of CalB as well as the activity reaction were investigated at different temperatures for p-NIPAM with 0.25 mol-% cross-linker. Additionally, the reusability and stability of the immobilized CalB were determined. In order to get information about the impact of the cross-linker density on the activity of the system, the immobilization and the following analysis was also done with 5 mol-% of the cross-linker.

In a second case, the covalent immobilization of HRP within p-NIPAM-co-allylamine using para-benzoquinone (BQ) as coupling agent is discussed. In contrast to the immobilization using solvent exchange, the covalent immobilization leads to biocatalysts that can be used in aqueous media. The characterization of the synthesized particles by DLS, zeta potential measurements and atomic force microscopy (AFM) is also presented. The activity and the stability of the produced immobilized system are also discussed. For the immobilization of enzymes, it can be useful to integrate amphoteric comonomers into the polymer network leading to polyampholyte (PA) microgels (figure 1.1c). In literature, there are several studies on the production and characterization of such PA microgel particles.²⁹⁻³³ In contrast to the present work, all investigated polymers were synthesized with two different comonomers to integrate the functional groups so far.

Chapter 6 deals with the synthesis of a novel PA microgel system made of p-NIPAM and allylglycine (AG) as comonomer. In the present case, only one comonomer is integrated within the polymer network leading to a balanced microgel. The characterization by DLS, zeta potential and AFM measurements in dependence of the temperature, the concentration and the pH value is discussed.

2 Theory

2.1 Smart gels

In general a gel consists of two phases. The solid phase is always a three dimensional network with pores. These pores can be filled with either a liquid (lyogel) or a gas (xerogel).³⁴ In case of a highly porous network dispersed in air the system is called aerogel. Lyogels are interesting objects due to the fact that they show liquid-like and solid-like properties.³⁵ Usually, the main component of a lyogel is its liquid which is responsible for the liquid-like properties. The decisive parameter for the solid-like properties is the cross-linking of the polymer network. This cross-linking leads to a shear modulus which becomes apparent when the gel is deformed. Therefore, a gel can retain its shape and shows properties of a solid. One distinguishes between gel networks that are stabilized either by physical or chemical cross-linking. In case of a chemical cross-linking real covalent bonds are present while a physical cross-linking is formed by hydrogen bonds, Coulomb interactions, van-der-Waals forces or entanglements. The viscoelastic properties of a gel are strongly influenced by the number of cross-links in the polymer network.²⁻⁴ An increasing number of cross-links, also known as connectivity,³⁶ leads to an increase in the solid-like properties and a decrease in the swelling capacity.³⁶⁻³⁸ When a solvent is added to a solid gel it swells until the swelling equilibrium is reached which can be up to 97% regarding the total volume of the gel. The driving force for the swelling capacity are the interactions between the network components and the solvent.

Another promising property of a number of gels is their ability to react on external stimuli which is usually defined as "smart" behavior.^{7,10,37} In this case not only the solvent but also outer parameters like temperature,³⁹⁻⁴⁴ pH,^{13,16,45,46} ionic strength,^{15,47} photons^{48,49} or electric field^{50,51} can control the volume of the gel.⁵² In case of a volume phase transition (VPT), which

was experimentally discovered by Tanaka in 1978,⁵³ an enormous change in the volume can be induced by one of these external stimuli. Figure 2.1 schematically illustrates such a responsive gel.

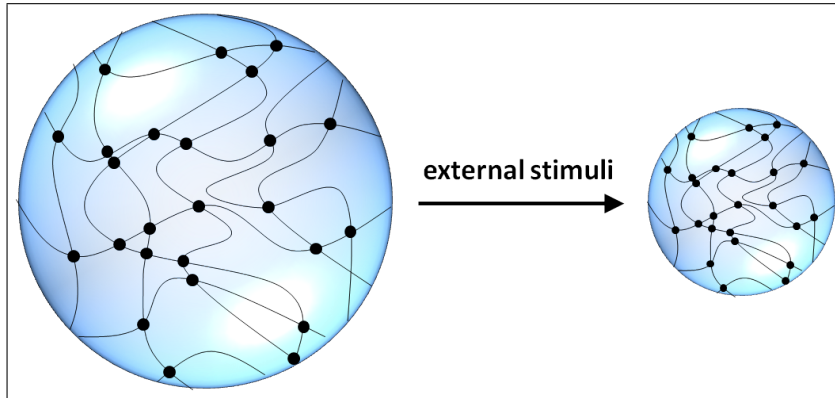


Figure 2.1: Schematic drawing of the VPT of a gel.

According to their size gels can be classified in macrogels and microgels. Microgels were defined by Baker in 1949.⁵⁴ They are colloidal dispersions of gel particles with four criteria:⁵⁵ 1.) Their size has to be in the submicron range which is supposed to be between 10 nm and 1000 nm. 2.) The microgel particles are dispersable and 3.) swellable in a solvent. 4.) They consist of a stable polymer network which is either chemically or physically stabilized.

Especially the usage of microgels which are dispersed in water, so called hydrogels, is of high research interest for technical, medical and biological applications. The VPT induced by external stimuli is much faster for microgels than for macrogels. Additionally, they show a higher surface to volume ratio. Both properties make them promising systems for a wide field of applications: drug delivery, emulsion stabilizations, microlenses, coatings, sensors and so on.^{56–65}

The microgel particles used within this work are made of the monomer N-Isopropylacrylamide (NIPAM). The synthesis of p-NIPAM microgel particles is done by surfactant free precipitation polymerization which was firstly reported in 1986.⁶⁶ The advantage of this method is the production of monodisperse, spherical polymer particles in the submicron range. Due to the lower critical solution temperature (LCST) of individual p-NIPAM chains the formed microgel particles show a VPT with increasing temperature.

In general, a gel can have a LCST or an upper critical solution temperature (UCST). Figure 2.2 presents phase diagrams of a gel with a lower miscibility

gap (a) and an upper miscibility gap (b). It is shown that for both cases a

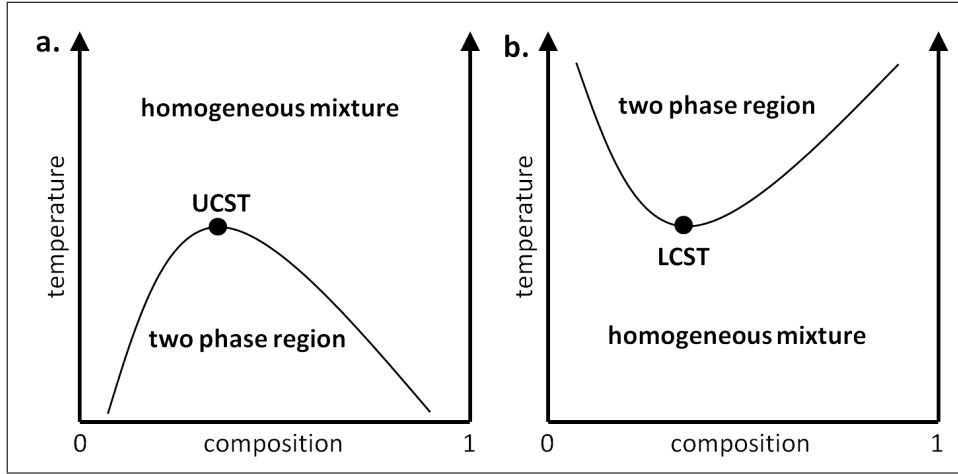


Figure 2.2: Phase diagrams of a gel with a lower miscibility gap or UCST (a) and an upper miscibility gap or LCST (b) where the critical temperatures are illustrated as filled points.

transition from a homogeneous to a two phase region can be observed by a change in temperature depending on the gel composition. The filled points represent the critical temperatures while the LCST corresponds to an upper miscibility gap and the UCST corresponds to a lower miscibility gap.

Microgels made of p-NIPAM show a VPT at a temperature of approximately 32°C (VPTT). According to figure 2.2, water is a good solvent for the p-NIPAM particles below this temperature due to hydrogen bonds between the polymer network and the water molecules. Hence, the microgel exists in a swollen state. Increasing the temperature above the VPTT leads to a shrinking and water is expelled. Therefore, water turns into a bad solvent by surpassing the VPTT. The swelling behaviour of the microgel particles is controlled by the amount of cross-linker and can be characterized by the deswelling ratio α , as shown in equation 2.1.

$$\alpha = \frac{V_H}{V_{H,0}} = \frac{R_H^3}{R_{H,0}^3} \quad (2.1)$$

where V_H and $V_{H,0}$ are the volumes of the microgel particles in the collapsed and swollen state, respectively. Due to the spherical character of the microgel particles the hydrodynamic radii (R_H) can be used instead of the volume. Within this work the R_H values detected at 25°C and 40°C were used to calculate the deswelling ratios.

The VPT can be described by the classical FLORY-REHNER theory.⁶⁷ The basic idea of this theory is the assumption that the free energy of the gel F_{gel} is a sum of three components:

$$F_{gel} = F_{mix} + F_{el} + F_{ion} \quad (2.2)$$

where F_{mix} is the free mixing energy of the gel and the surrounding solvent, F_{el} the free energy of the network elasticity and F_{ion} the free energy of charged gels. The volume change leads to a change in free energy which can be described by the internal osmotic pressure of a gel particle. According to equation 2.2 the osmotic pressure is also a sum of these three contributions:

$$\Pi_{gel} = - \left(\frac{\partial F}{\partial V} \right)_T = \Pi_{mix} + \Pi_{el} + \Pi_{ion}. \quad (2.3)$$

Π_{mix} , Π_{el} and Π_{ion} can be defined by the following equations:

$$\Pi_{mix} = - \frac{N_A k_B T}{v} (\phi + \ln(1 - \phi) + \chi \phi^2) \quad (2.4)$$

$$\Pi_{el} = - \frac{N_c k_B T}{V_0} \left(\left(\frac{\phi}{2\phi_0} \right) - \left(\frac{\phi}{\phi_0} \right)^{\frac{1}{3}} \right) \quad (2.5)$$

$$\Pi_{ion} = - \frac{f N_c k_B T}{V_0} \frac{\phi}{\phi_0} \quad (2.6)$$

where V is the volume, N_A the Avogadro constant, k_B the Boltzmann constant, T the absolute temperature, v the molar volume of the solvent, ϕ the volume fraction of the polymer, ϕ_0 the volume fraction of the polymer at reference conditions, N_c the number of chains contained in the gel network, V_0 the volume of the relaxed Gaussian gel network, f the number of counterions per chain and χ the polymer-solvent interaction parameter (FLORY-HUGGINS parameter).⁵⁵

When molecules of the solvent get into contact with the polymer particles the free energy per solvent molecule is changed. This change can be described by χ :

$$\chi = \frac{\Delta F}{k_B T} = \frac{\Delta H - T \Delta S}{k_B T} \quad (2.7)$$

where ΔH and ΔS are the changes in enthalpy and entropy per monomeric unit of the polymer network during the VPT. Gel particles with a LCST lead to negative values of ΔH and ΔS while for a UCST behavior it is the oppo-

site.

In summary, p-NIPAM microgel particles combine a number of promising properties such as the small dimensions in size and therefore a large surface area, a low polydispersity and a spontaneous and reversible response to external stimuli. The VPT behavior of pure p-NIPAM microgels can be influenced by integrating comonomers such as acrylic acid¹⁶ and allylacetic acid¹⁵ into the polymer network. This gives the opportunity to tune the VPTT and the deswelling ratio α as well the sensitivity to pH and ionic strength.

2.2 Plasmon resonance of gold nanoparticles

Due to their interesting optical properties, gold nanoparticles (Au-NPs) have been used since the antiquity. In the 17th century it was developed that a combination of an aqua regia solution of gold and tin leads to a deep red colorant. This so called "purple of Cassius" became one of the most used red pigments in the production of glass and ceramics.⁶⁸

One special property of Au-NPs is the surface plasmon resonance which leads to a specific absorption band in the visible range. This behavior is based on the collective resonant oscillation of the free electrons in the conduction band of the gold. Therefore, an oscillating dipole is created. Figure 2.3 illustrates this charge oscillation induced by excitation with light.

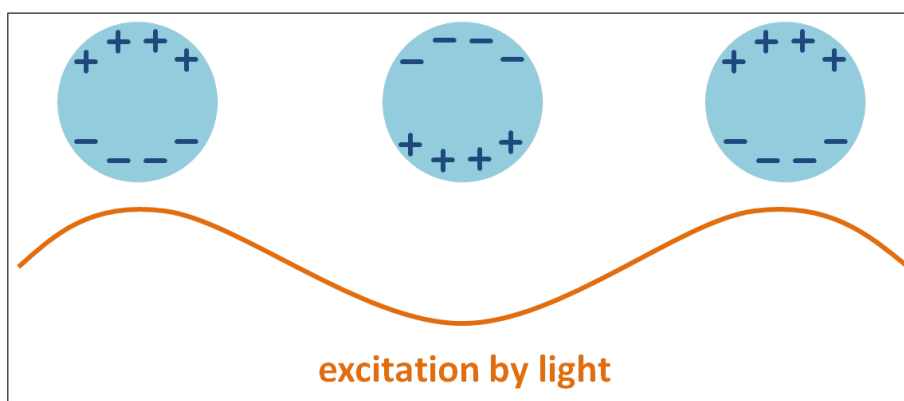


Figure 2.3: Sketch of the surface plasmon oscillations of Au-NPs induced by light.

The properties of these plasmon resonances are influenced by the refractive index of the surrounding medium^{69,70} as well as by the size^{18,71} and

shape⁷²⁻⁷⁴ of the Au-NPs.

For spherical Au-NPs with a diameter smaller than the wavelength of the incident light, the dipole oscillations and therefore the absorption behavior can be described by the classical MIE theory.⁷⁵ In this theory the extinction cross-section of a single spherical particle with the dielectric function $\epsilon = \epsilon' + i\epsilon''$ is given by equation 2.8:

$$C_{ext} = \frac{2\pi}{k^2} \sum (2n+1) \text{Re}(a_n + b_n) \quad (2.8)$$

where $k = 2\pi\sqrt{\epsilon_m}/\lambda$ with ϵ_m as dielectric constant of the surrounding medium, λ as wavelength, n as refractive index of the surrounding medium and a_n and b_n as the scattering coefficients, which are functions of the radius R and λ in terms of Ricatti-Bessel functions.⁶⁹

In case of very small NPs ($kR \ll 1$) the extinction cross-section is given by:

$$C_{ext} = \frac{24\pi^2 R^3 \epsilon_m^{3/2}}{\lambda} \frac{\epsilon''}{(\epsilon' + 2\epsilon_m)^2 + \epsilon''^2}. \quad (2.9)$$

Equation 2.9 shows that the maximum of C_{ext} and hence an absorption peak is obtained when the denominator becomes minimal. This condition is achieved (if ϵ'' is small) when:

$$\epsilon' = -2\epsilon_m. \quad (2.10)$$

This clearly demonstrates that the surface plasmon resonance is highly influenced by the dielectric constant ϵ_m and hence by the refractive index n of the surrounding medium. Therefore, equal Au-NPs possess different absorption maxima in dependence of the refractive index of the solvent used. This was demonstrated by Underwood et. al using UV-Vis spectroscopy.⁷⁶ The interesting optical properties make Au-NPs highly attractive for formation of functional hybrid microgels. In the present work, differently cross-linked p-NIPAM microgel particles were loaded with spherical shaped Au-NPs to produce a system which can change the optical properties by a change in temperature.

2.3 Enzyme immobilization

Enzymes are biocatalysts which catalyze reactions in all living cells. Therefore, enzymes are able to catalyze a wide range of chemical reactions even if these reactions are extremely complex to perform by chemical synthesis.⁷⁷ The presence in the metabolism of all living cells requires that enzymes show special properties like working under mild reaction conditions (physiological pH and temperature), high activity, high stereo-, regio- and chemoselectivity as well as high biodegradability.⁷⁸ These properties make them useful for many applications: pharmaceuticals, chemicals, food, organic synthesis and detergents. Nevertheless, the low long-term stability, the high costs of isolation as well as the difficulty to reuse the enzymes often prevents their use in large-scale applications under industrial conditions (extreme pH, high temperature and high shear force in reactors). These drawbacks could be solved by immobilization of the enzyme catalysts. Therefore, the immobilization of enzymes is of high interest for research since several decades. In 1971 at the first Enzyme Engineering Conference at Henniker (New Hampshire, USA) the term "immobilized enzyme" was defined as "enzymes physically confined or localized in a certain defined region of space with retention of their catalytic activities, and which can be used repeatedly and continuously".^{79,80} The production of the new biocatalysts is not only useful for applications in industrial processes but also for the synthesis of a number of biotechnological products with applications in diagnostics and biosensors.^{80,81} For the production of an immobilized enzyme system it is important to choose the enzyme, the matrix and the immobilization method carefully.

Firstly, a suitable support has to be considered. Depending on the chemical composition, they can be classified into inorganic and organic supports. Beside the swelling behavior, the mechanical strength as well as the compression behavior, the pore diameter and the particle size are important physical characteristics of the matrix. Due to the fact that the size of the matrix and the pores defines the total surface area these parameters have a high impact on the binding capacity for enzymes. Porous materials have a high surface area and hence a high capacity for enzyme immobilization as well as the possibility to protect enzymes against chemical and mechanical stress. Therefore, these materials are often preferred as enzyme supports. The immobilization methods can be classified in different types such as

1.) support binding, entrapment and cross-linking,⁷⁸ 2.) chemical binding and physical retention⁸² and 3.) attachment and entrapment.⁸³ In 1983 the methods for immobilization were firstly defined as adsorption, covalent binding, cross-linking, entrapment and encapsulation which can be sorted to the classification of entrapment and attachment.⁸⁴ These different methods are illustrated in figure 2.4.

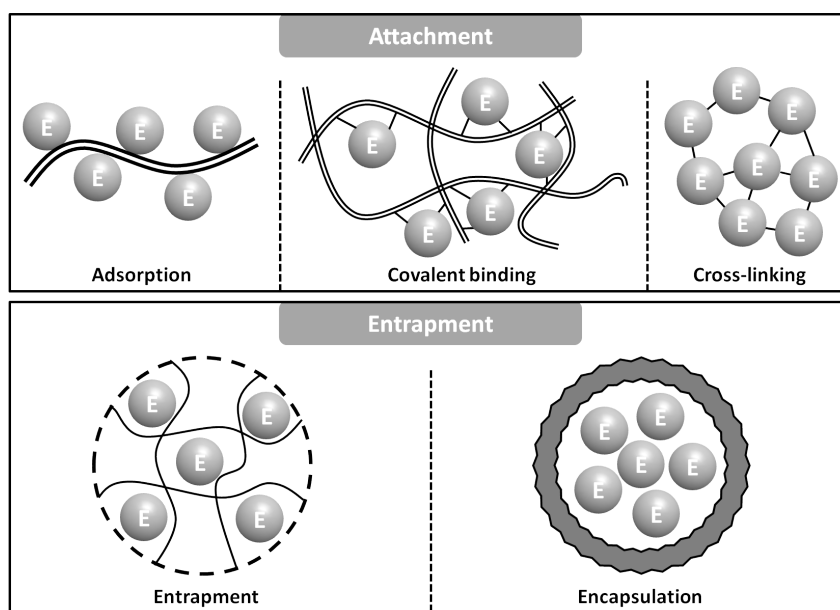


Figure 2.4: Classification of enzyme immobilization.

Immobilization by adsorption is reached by reversible non-covalent interactions between the enzyme and the support.⁸⁵ These interactions include van-der-Waals forces, ionic bonding, hydrogen bonding and hydrophobic bonding. Although the interactions are rather weak, they are large enough in number to provide good binding. The prominent advantages of this method are little damage to the biocatalyst, no required modification to the enzyme or matrix and the possibility to exchange the used enzyme against fresh one. Beside, there are also some disadvantages known for this immobilization method. The biocatalyst can leak or desorb from the support material and the support can lead to a steric hindrance. The desorption can be also an advantage if it is used for the regeneration of the biocatalyst by exchanging used enzyme against fresh ones.

Immobilization by covalent binding can be obtained by the formation of covalent bonds between the enzyme and the support.⁸⁵ Normally, these bonds are received between functional groups situated at the matrix and

functional groups of amino acids existing in the structure of every enzyme. Basically, the covalent binding is done in two steps. Firstly, either the support (e.g. dextran or agarose gel⁸⁶) or the enzyme is activated by a specific chemical reagent (e.g. BQ) followed by a coupling reaction with the unactivated part of the biocatalyst. The covalent binding of enzymes using BQ has not been done with microgels as support so far.

The third immobilization method in the field of attachment is the cross-linking of enzymes by chemical or physical attachment where a three-dimensional complex structure is achieved.⁸⁵ The characteristic property of this method is the absence of a support. Chemical cross-linking includes the formation of covalent bonds between the enzymes using a reagent like glutaraldehyde. A drawback of this cross-linking regarding application to living cells is the toxicity of the reagents. The cross-linking by physical attachment is realized by flocculation of the enzymes. As flocculation agents polyamines and polystyrene sulfonates are used.

In case of entrapment, the enzyme is immobilized into a cross-linked polymer matrix. Hence, the enzymes are free in solution but restricted in movement by the surrounding matrix.⁸⁵ An important aspect is that the pore sizes of the support need to be large enough for immobilization but small enough to prevent leakage of the enzymes. Additionally, the substrate and products have to be able to move freely.

For the last immobilization method enzymes are encapsulated within a semi-permeable membrane.⁸⁵ As described for entrapment, the enzyme is free in solution but restricted in space through the matrix.

Within this study, enzymes are immobilized by entrapment within p-NIPAM microgel particles to reach an active biocatalyst in organic media. Furthermore, covalent binding using BQ as coupling reagent was used to produce a biocatalyst that is active in aqueous environment.

2.4 Methods

2.4.1 Dynamic light scattering

2.4.1.1 Characterization of the size and diffusion. To characterize the size and the thermoresponsive behavior of the synthesized microgel particles dynamic light scattering (DLS) was applied.⁸⁷ Figure 2.5a shows a typical setup of a scattering experiment.

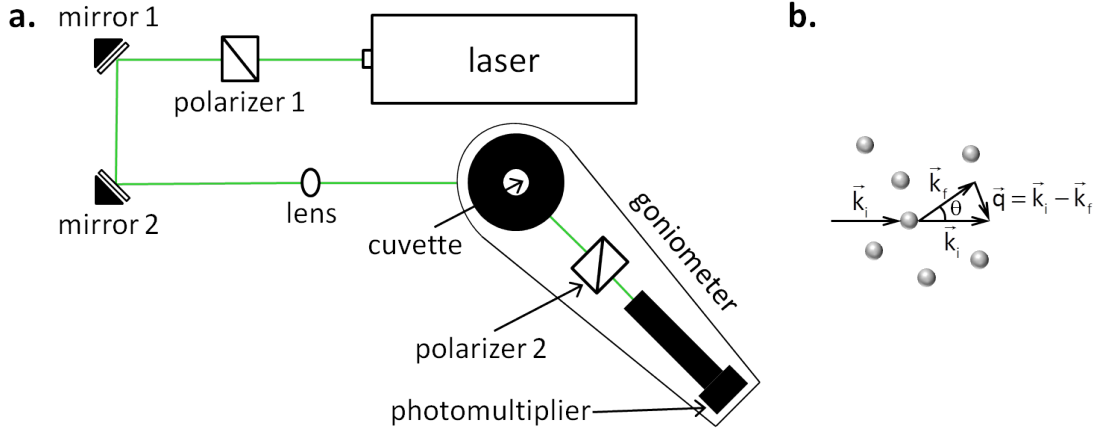


Figure 2.5: (a) Schematic drawing of a setup of a DLS experiment. (b) Illustration of the scattering vector \vec{q} . \vec{k}_i is the wave vector of the incident light and \vec{k}_f is the wave vector of the scattered light.

In order to receive radiation with a narrow frequency distribution and an almost constant output power, usually continuous wave lasers are used as light source. The polarized laser beam is reflected by two mirrors and focused on the sample by a convex lens. The sample leads to a scattering of the light which passes a second polarizer and is detected by a photomultiplier. The scattered light can be collected under different scattering angles due to the fact that the photodiode is placed on a goniometer arm. The sample is placed in a toluene bath which matches the refractive index of the used quartz bath and cuvettes as well as serves as a temperature control. Additionally, a PT 100 thermoelement is used to control the sample temperature.

The movement of particles which is related to Brownian motion leads to fluctuation of the scattered light intensity. In DLS measurements these fluctuations are measured leading to the intensity time autocorrelation function $g^2(\tau)$:

$$g^2(\tau) = \frac{\langle I(\vec{q}, t) I(\vec{q}, t + \tau) \rangle}{\langle I(\vec{q}, \tau) \rangle^2} \quad (2.11)$$

where $I(\vec{q}, t)$ is the intensity of the scattered light, τ is the correlation time and \vec{q} is the scattering vector. Figure 2.5b shows the construction of this scattering vector for a single scattering event. The magnitude of \vec{q} is given by equation 2.12.

$$|\vec{q}| = q = \frac{4\pi n}{\lambda} \sin\left(\frac{\theta}{2}\right) \quad (2.12)$$

where n is the refractive index, λ the wavelength of the incident beam and θ

the scattering angle.

For further investigations on the diffusion of particles this second order autocorrelation function is converted into the first order field time autocorrelation function $g^1(\tau)$ by using the SIEGERT relation:

$$g^2(\tau) = 1 + \beta |g^1(\tau)|^2 \quad (2.13)$$

where β is a parameter which depends on the experimental geometry.

In case of monodisperse particles $g^1(\tau)$ can be described by a simple exponential function with the relaxation rate Γ :

$$g^1(\tau) = e^{-\Gamma\tau} \quad (2.14)$$

For monodisperse particles and a factor β of 1 equations 2.13 and 2.14 show that both autocorrelation functions have a simple relation which is illustrated in figure 2.6.

For particles with a certain polydispersity a distribution in size is existent leading to different diffusion coefficients and relaxation rates. In this case $g^1(\tau)$ can not be described by a single exponential function. Instead a sum has to be considered:

$$g^1(\tau) = a_0 + a_1 e^{-\Gamma'\tau} + a_2 e^{-\Gamma''\tau} + a_3 e^{-\Gamma'''\tau} + \dots \quad (2.15)$$

where $a_0, a_1, a_2 \dots$ are amplitudes and $\Gamma', \Gamma'', \Gamma''' \dots$ are relaxation rates. Usually, the methods of cumulants is used to analyze the first order autocorrelation function which was firstly proposed by Koppel.⁸⁸ Therefore, the logarithm of $g^1(\tau)$ is expanded in terms of the cumulants of the distribution:⁸⁹

$$\ln[g^1(\tau)] = -\Gamma_1\tau + \frac{1}{2!}\Gamma_2\tau^2 - \frac{1}{3!}\Gamma_3\tau^3 + \dots \quad (2.16)$$

To take advantage of this form the baseline is assumed to be exactly one and a fit can be made by the following fitting function:

$$\ln[g^2(\tau) - 1] = \ln\beta - 2\Gamma_1\tau + \frac{2}{2!}\Gamma_2\tau^2 - \frac{2}{3!}\Gamma_3\tau^3 + \dots \quad (2.17)$$

The first cumulant describes the average decay rate of the distribution. Hence, Γ_1 can be used to calculate the diffusion coefficient D:

$$\Gamma_1 = Dq^2. \quad (2.18)$$

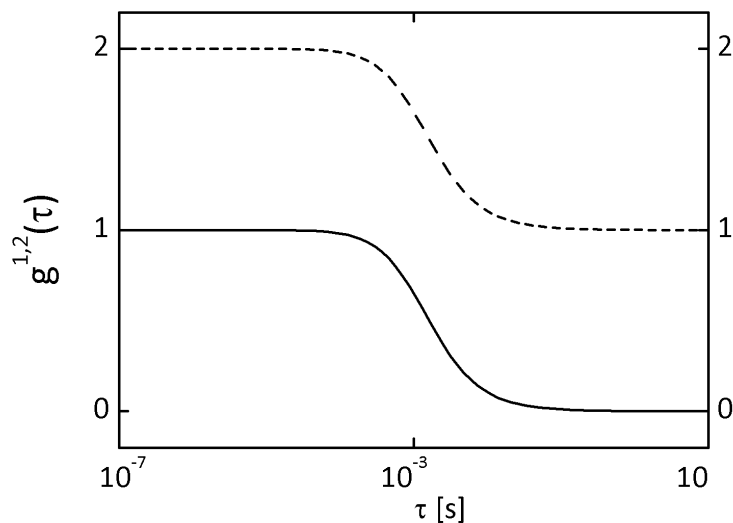


Figure 2.6: Scheme of the first (straight line) and second (dashed line) order autocorrelation function for monodisperse particles.

Finally, the STOKES-EINSTEIN equation can be used to calculate the R_H values of monodisperse particles:

$$D = \frac{k_B T}{6\pi\eta R_H} \quad (2.19)$$

where k is the Boltzmann constant, T the temperature of the sample and η the viscosity of the solution.

The polydispersity index (PDI) is another characteristic parameter for the monodispersity of a sample which can be obtained by the cumulant expansion:

$$PDI = \frac{\Gamma_2}{\Gamma_1^2}. \quad (2.20)$$

Especially for the characterization of thermoresponsive microgel particles DLS is an important technique. It gives the opportunity to investigate the behavior of the R_H in dependence from the temperature and hence the deswelling ratio α can be determined.

2.4.1.2 Characterization of the zeta potential. Combining DLS with electrophoresis can be used to receive informations on the charge of a colloidal dispersions which is directly related to their stability and therefore an important property. In a dispersion of colloidal particles an electrical double layer is formed. To describe the charge situation usually the STERN model is used which was developed in 1924 by combining the earlier models of Helmholtz and Gouy-Chapman.⁹⁰ Figure 2.7 schematically shows the distribution of ions at the interface for the case of a negatively charged particle surface.

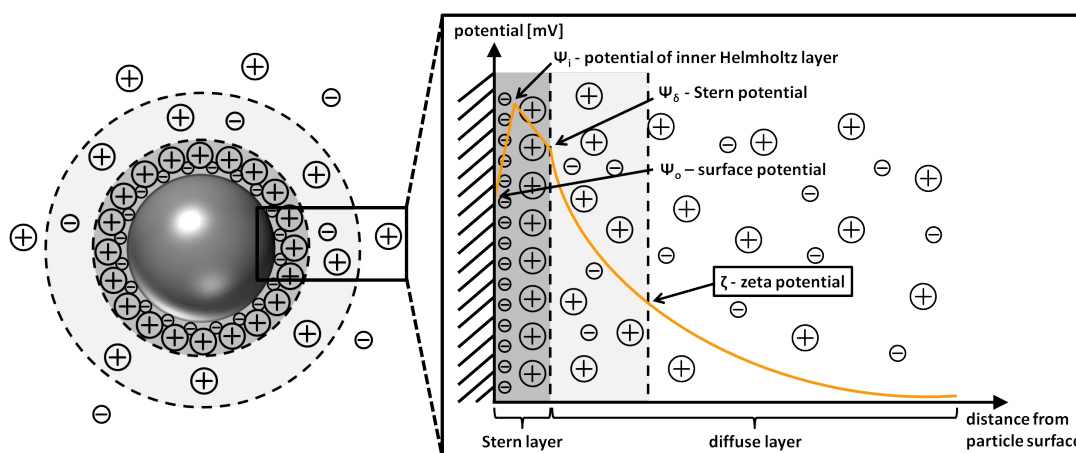


Figure 2.7: Structure of the electrochemical double layer on a negative particle surface.

In an electrolyte solution one monolayer of dehydrated anions is directly adsorbed at the particle surface (inner Helmholtz layer). This leads to an increase in the surface potential (Ψ_0) to the potential of the inner Helmholtz layer (Ψ_i). The next layer (outer Helmholtz layer) consists of fixed hydrated cations leading to a reduction of the potential to the so called Stern potential (Ψ_δ). The combination of the inner and the outer Helmholtz layer is the Stern layer with the thickness δ . In the following part of the electrical double layer the distribution of the charge carriers is diffuse. The potential shows an exponential decay till the electric neutrality is reached. If the particles move, e.g. by applying an electric field, parts of the diffuse layer can be sheared off. This region separates the ions associated with the particle from those in the bulk phase. The potential at this shear plane is defined as the zeta potential (ζ). The value of the determined zeta potential can be a strong indication for the stability of a colloidal system. If the particles show a high zeta potential the tendency to repel each other is high and therefore in most

cases a high stability of the system is obtained. Especially, two kinds of dispersions are interesting for this technique: a solid dispersed in a liquid, and a liquid dispersed in a liquid.

The principle of the zeta potential measurement is based on electrophoresis which means that the movement of charged particles in an electric field is investigated. The observed velocity of the particles (v) is proportional to the electrophoretic mobility (μ_E) with the applied electric field (E) as proportionality factor:

$$v = \mu_E E. \quad (2.21)$$

From the measured mobility the zeta potential can be calculated using the Henry equation:

$$\mu_E = \frac{2\epsilon_0\epsilon_r\zeta}{3\eta} f(\kappa a) \quad (2.22)$$

where ζ is the zeta potential, ϵ_0 the electric field constant, ϵ_r a relative dielectric constant, η the viscosity of the medium and $f(\kappa a)$ a correction function (Henry's function) which considers the thickness of the double layer and the particle diameter. Regarding Henry's function one distinguishes between two laws: the Helmholtz-Smoluchowski law and the Hueckel-Onsager law. The first law can be used for large particles in polar media ($\kappa a \gg 1$, where κ is the Debye-length and a is the particle radius).⁹¹

$$\mu_E = \frac{\epsilon_0\epsilon_r\zeta}{\eta}. \quad (2.23)$$

The second law is valid for small particles ($\kappa a \ll 1$) and highly diluted electrolyte solutions:

$$\mu_E = \frac{2\epsilon_0\epsilon_r\zeta}{3\eta}. \quad (2.24)$$

The setup of the experiment is similar to the DLS setup shown in figure 2.5. Instead of Brownian motion the movement of the charged particles in an applied electric field is investigated. The particles scatter the incident laser light and due to the movement the Doppler effect leads to a shift of the scattered compared to the incident light. The magnitude of this shift is proportional to the velocity of the particles. Hence, μ_E can be determined (equation 2.21). This measurement principle is defined as laser doppler anemometry.^{92,93}

Especially in the characterization of the synthesized copolymers this method is needed to proof the integration of the comonomer within the poly-

mer network.

2.4.2 Imaging techniques

2.4.2.1 Confocal laser scanning microscopy. Confocal laser scanning microscopy (CLSM) is a technique for obtaining high-resolution optical images and is frequently applied in biology and chemistry.⁹⁴ The principle of the confocal microscopy was patented by Marvin Minsky in 1957 which shows that this technique is a relatively new characterization method.⁹⁵ In the following years Davidovits and Egger were able to engineer a confocal laser microscope and published the images of cells in 1971^{96,97} Due to the usage of lasers for CLSM this technique became a standard method not before the end of the 1980s.

A scheme of an experimental setup of a CLSM is shown in figure 2.8. As

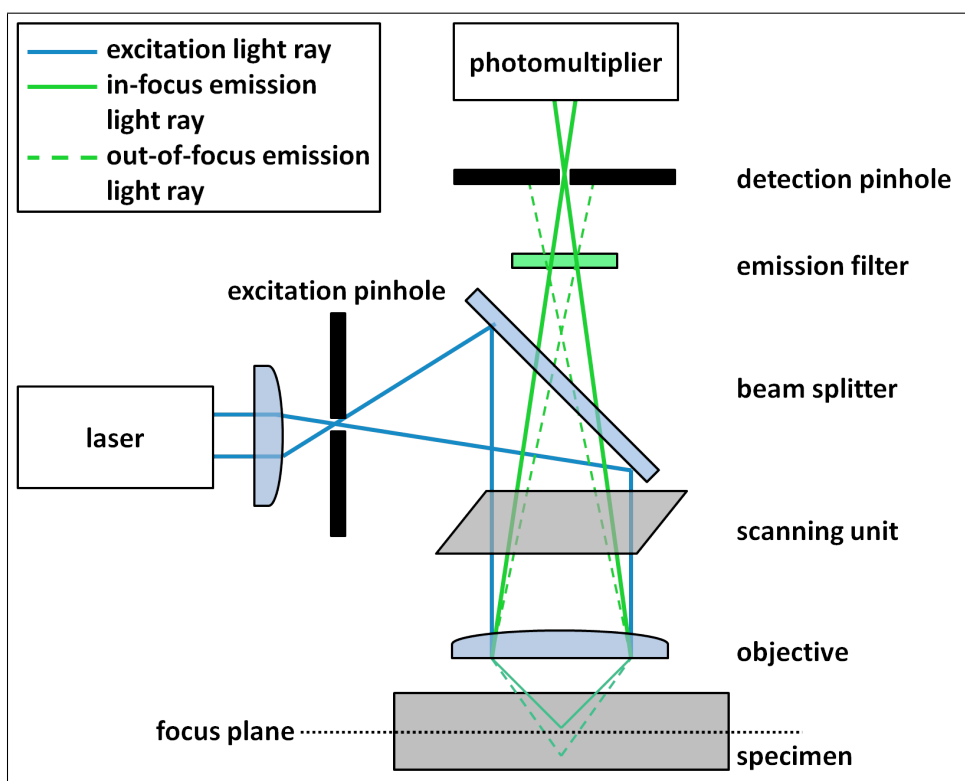


Figure 2.8: Principal function and beam pathway of a CLSM.

light source a laser is used which produces coherent light of a defined wavelength. By passing the excitation pinhole a sufficiently thin laser beam is produced which is afterwards reflected into the objective by a dichroic mirror. The objective focuses the light on the focal plane within the specimen.

If a fluorescent probe is excited by the incident laser beam, the light emitted from the sample passes the dichroic mirror and the emission pinhole before it is detected by the photomultiplier. The scanning unit which is responsible to shift the laser spot in x- and y-direction is usually controlled by two galvanometers.

In comparison to a conventional wide field fluorescence microscope a CLSM shows great advantages. Firstly, in conventional fluorescence microscopy a wide region of the sample is exposed to the excitation light while in CLSM the laser beam is focused to a very small spot at the focal plane (figure 2.9). Secondly, the emission pinhole used in a CLSM is in confocal position to the excitation pinhole and therefore the out-of-focus light is suppressed. Compared to a conventional wide field fluorescence microscope sharper images can be obtained.

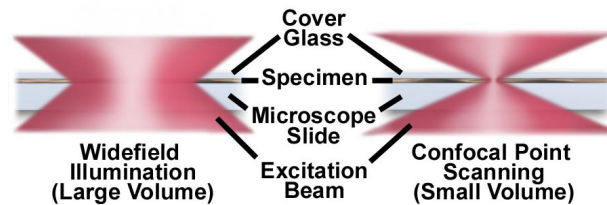


Figure 2.9: Comparison between widefield and confocal microscopy illumination volumes. Figure taken from.⁹⁸

An important characteristic of CLSM is its resolution which refers to the smallest distance (r) between two objects at which the objects still appear distinct. The lateral resolution of a CLSM can be described by:

$$r_{lateral} = \frac{0.4\lambda}{NA} \quad (2.25)$$

where λ is the emitted light wavelength and NA is the numerical aperture of the objective. Especially for CLSM it is also important to consider the axial resolution which is given by equation 2.26:

$$r_{axial} = \frac{1.4\lambda n}{NA^2}. \quad (2.26)$$

Beside the advantages of this technique, there are also some drawbacks which have to be mentioned. The usage of lasers as excitation source limits the number of wavelength which can be selected. Furthermore, the sample is bombarded with intense, focused laser light which can lead to a damage

of the sample or, if the sample is labeled with a fluorescent dye, to a bleaching of the used dye.

Nevertheless, CLSM is an important technique for numerous biological applications, especially due to the possibility of 3D-imaging. Therefore, several xy planes can be measured with small steps in z-direction in between. This provides all necessary information to reconstruct a 3D-model of the interior of a sample.

2.4.2.2 Transmission electron microscopy. Another optical method with higher resolutions than obtained in classical light microscopy is represented by electron microscopy. The imaging process is done by using electrons whose wavelength can be described by the DE BROGLIE relation:⁹⁹

$$\lambda = \frac{h}{mv} \quad (2.27)$$

where λ is the wavelength, h Planck's constant, m the mass and v the velocity of the electrons.

Equation 2.27 shows that a higher velocity leads to lower values for λ . It is also known that smaller λ gives a high resolution which is the case for electrons.

In principle, there are two different types of electron microscopes, transmission electron microscopes (TEM) and scanning electron microscopes (SEM). Within this PhD thesis TEM was used to characterize hybrid samples. Figure 2.10 illustrates a typical setup of a TEM.

The basic setup is very similar to that of a light microscope. The electrons are generated by a glowing wolfram wire and focussed by passing the Wehnelt cylinder. The electron beam is accelerated to the anode by using acceleration voltages between 20 and 100 kV. Afterwards, a condensor lense focusses the electron beam on the sample which is prepared on a copper grid. The following part of the TEM is responsible for the imaging of the sample. Therefore, electromagnetic as well as projector lenses are used.

Especially, for the prepared hybrid systems made of Au-NPs within p-NIPAM microgel particles, TEM is a suitable method for visualization. Due to the higher electron density of Au-NPs compared to the surrounding polymer, large contrast is expected and the Au-NPs within the polymer network can be imaged.

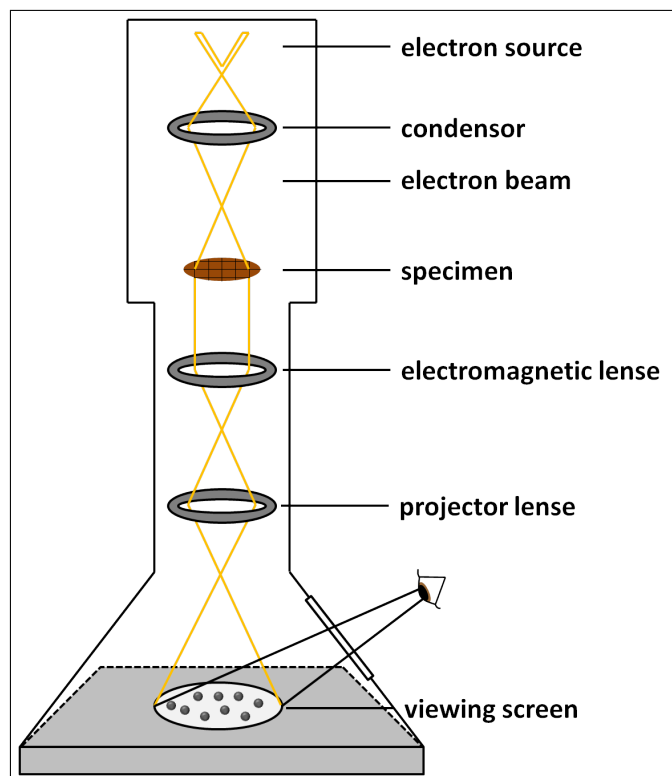


Figure 2.10: Principal function and beam pathway of a TEM.

2.4.2.3 Atomic force microscopy. Atomic force microscopy (AFM) is a very high-resolution type of scanning probe microscopy which was developed by Binnig, Quate and Gerber in 1986.¹⁰⁰ Three years later the first commercially available AFM was introduced leading to the possibility to scan a wide range of surfaces on atomic scale including ceramic materials, biological samples and polymers.¹⁰¹

Figure 2.11 illustrates a typical setup of an AFM. The basic principle is the scanning of the surface of a sample with a sharp tip. This tip has a radius of curvature in the order of 10's of nanometers and is fixed at a cantilever which is typically made of silicon or silicon nitride. A laser beam is focused on the back of the cantilever and the reflected light is detected by a photodiode. The usage of piezoelectric scanners give the possibility to move the cantilever and hence the tip in xyz-direction. The distance between tip and sample is controlled by a feedback loop. Finally, the results are evaluated by a computer leading to a topographical image of the sample.

The great advantage of AFM over many other microscopes available is the possibility to make measurements in x, y and z-direction and hence to receive a three dimensional image of a sample surface. The samples can be

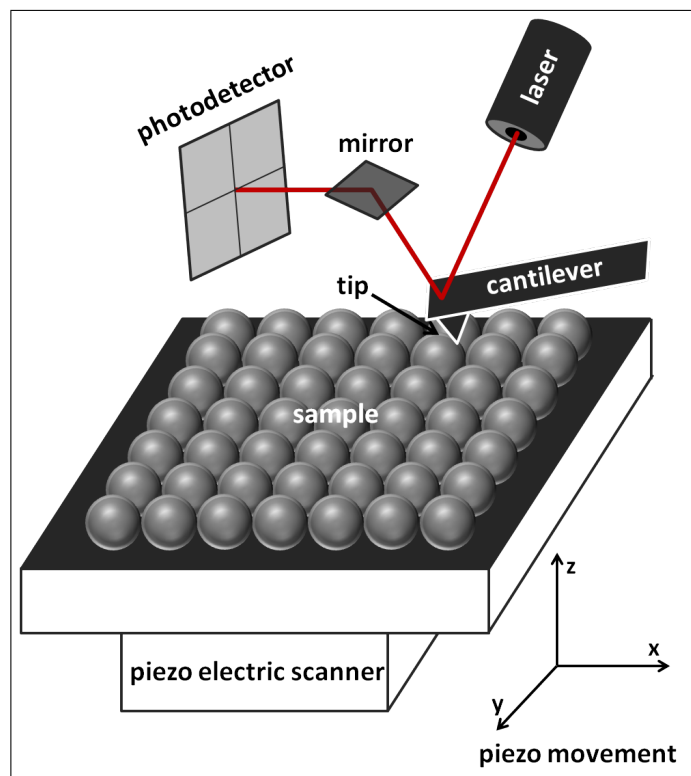


Figure 2.11: Sketch of an AFM setup.

studied in air or in liquid environment and the resolution in the x-y direction ranges from 0.1 nm to 1.0 nm while the resolution in the z-direction is 0.01 nm. Additionally, the height profiles of the measured samples can be used to determine the height of the sample.

An AFM can operate in three different modes, named contact mode, non-contact mode and tapping mode. In the first mode an extremely low and constant force is executed on the cantilever which leads to a continuous contact between the tip and the surface while the sample is scanned. The repulsive force between the sample and the tip or the tip deflection is monitored. Afterwards, this signal is converted into an image of the surface. The disadvantage of this mode is that soft surfaces can be damaged by the constant contact with the tip. Therefore, the other modes were developed. In non-contact mode the frequency of the oscillation is higher than the frequency of the tip leading to no contact between the tip and the sample during the whole scanning process. Although this is a really gentle method concerning the damage of the sample, the interactions are rather weak leading to a low resolution.

The tapping mode is a good compromise between damage of the sample and

resolution. There, the frequency of the oscillation is slightly lower than the resonance frequency of the tip. The surface-to-tip distance is set and hence the surface is only touched ("tapped") at the bottom of these oscillations. This means the cantilever oscillates at the surface during the scanning process and hence the pushing on the substrate is reduced. Additionally, the tapping mode can be used in wet and dry state of the investigated sample. Due to the fact that p-NIPAM microgel particles are quite soft all measurements were done in the tapping mode.

As described before, the force between the sample and the cantilever is determined by AFM. Using HOOKE's law, this force can be calculated if the distance between sample and tip is constant:

$$F = -kx \tag{2.28}$$

where F is the force, k the spring constant of the cantilever and x the cantilever deflection.

In summary, AFM is a powerful technique for the imaging of polymeric and biological samples.

3 Experimental Section

3.1 Materials

The monomer N-Isopropylacrylamide (NIPAM; 97%, Aldrich) was purified by recrystallization in n-hexane. The cross-linker N,N'-methylenebis(acrylamide) (MBA; $\geq 99.5\%$, Fluka), potassium peroxydisulfate (KPS; $\geq 99\%$, Fluka), allylamine (AA; $\geq 99\%$, Aldrich) and DL-2-allylglycine (AG; Aldrich) were used as received for microgel synthesis.

HYDRANAL-Methanol dry (Riedel-de Haen) and HYDRANAL-Composite 5 (Fluka) were used for Karl-Fischer-titration.

Tetrachloroauric(III)-acid (HAuCl_4 ; $\geq 99\%$, Fluka) and sodium citrate dihydrate ($> 99\%$, Fluka) were used without further purification for gold nanoparticle synthesis.

Lipase B from *Candida antarctica* L (CalB) was generously donated by Novozymes A/S (Bagsvaerd, Denmark) and dialyzed for the labeling procedure. Horseradish peroxidase (HRP; Sigma), bovine serum albumin (BSA; 2 mg protein/ml, Sigma), Bradford Reagent (Sigma-Aldrich), Fluorescein-5-isothiocyanate (FITC; $\geq 95\%$, Merck), octanoic acid ($\geq 99\%$, Sigma-Aldrich), 1-octanol ($\geq 99\%$, Sigma-Aldrich), pyrogallol ($\geq 99\%$, Sigma), hydrogen peroxide (H_2O_2 ; 30% in water, ChemSolution), n-hexane ($\geq 99.5\%$, Fluka), isopropanol ($\geq 99.5\%$, Chem Solution), para-benzoquinone (BQ; $\geq 99.5\%$, Fluka), ethanol ($\geq 99.5\%$, Merck), methanol ($\geq 99.9\%$, Sigma-Aldrich), sodium carbonate (Na_2CO_3 ; $> 99.9\%$, Merck), sodium hydrogen carbonate (NaHCO_3 ; $\geq 99.5\%$, Merck), sodium phosphate dibasic dihydrate ($\text{Na}_2\text{HPO}_4 \cdot 2\text{H}_2\text{O}$; $\geq 99.5\%$, Sigma-Aldrich), potassium dihydrogen phosphate (KH_2PO_4 ; $\geq 99.5\%$, Merck), dipotassium hydrogenphosphate (K_2HPO_4 ; Merck), sodium chloride (NaCl ; $\geq 99\%$, Chem Solution) and potassium chloride (KCl ; $\geq 99.5\%$, Merck) were not purified and used for enzyme immobilization as well as the characterization of the immobilized systems.

For the adjustment of the pH value sodium hydroxide (NaOH; Titrisol, Merck) and hydrogen chloride (HCl; Titrisol, Merck) were used as received. Tris(hydroxymethyl)aminomethane (TRIS; $\geq 99.9\%$, Roth), glycerine (ACS, Reag. Ph Eur, Merck), sodium dodecyl sulfate (SDS; $\geq 99\%$, Roth), mercaptoethanol (98%, PlusOne), glycine ($>99\%$, Roth), acrylamide mixture (30% in water, Roth), ammonium persulfate (APS; $\geq 98\%$, Affymetrix/USB) and N,N,N',N'-tetramethylethylenediamine (TEMED; 99%, Roth) were used for SDS-Page without further purification.

A three-stage Millipore Milli-Q Plus 185 purification system was used for water purification leading to a final resistance of 18 M Ω .

3.2 Synthesis

3.2.1 P-NIPAM microgels

The p-NIPAM microgel particles with cross-linker concentrations of 0.25 mol-%, 5 mol-% and 10 mol-% were synthesized by surfactant free precipitation polymerization according to the protocol reported by Pelton and Chibante.⁶⁶ The cross-linker concentrations refer to the molar concentration of the monomer NIPAM. In order to receive particles with a cross-linker content of 5 mol-%, 1.132 g (0.01 mol) of NIPAM and 0.078 g (5×10^{-4} mol) of the cross-linker MBA were dissolved in 100 mL of water in a three-neck flask equipped with a reflux condenser. The temperature of the solution was increased to 70°C and degassed for 30 min. Afterwards, 1 mL of an aqueous solution of KPS (3.7×10^{-3} M) was added rapidly to the mixture while stirring continuously to initiate the radical polymerization. The clear solution became turbid within the first 10 min indicating the beginning polymerization. After 4 h of reaction time the temperature was decreased to room temperature and the mixture was stirred overnight under N₂-atmosphere. The crude microgel particles were purified by filtering over glass wool, dialysis for 2 weeks with daily water exchange and finally freeze drying at -85°C and 1×10^{-3} bar for 48 h. The received solid microgel particles were dissolved in methanol to determine the residual amount of water after freeze-drying by Karl-Fischer titration.

For the preparation of p-NIPAM microgel particles with a different content of MBA the same experimental setup and amounts of reagents were used. Just the amount of added MBA was adjusted to 0.0038 g (2.5×10^{-5} mol) for

0.25 mol-% MBA and to 0.154 g (1×10^{-3} mol) for 10 mol-% MBA.

3.2.2 Large p-NIPAM microgels

Micron-sized p-NIPAM microgel particles with a cross-linker content of 0.25 mol-% were synthesized by surfactant free precipitation polymerization via a temperature ramp according to Meng et al.¹⁰² The cross-linker concentrations refer to the molar concentration of the monomer NIPAM. Therefore, 1.8 g (0.015 mol) of the monomer NIPAM and 0.006 g (3.75×10^{-5} mol) of the cross-linker MBA were dissolved in 125 mL water using the same experimental equipment described in 3.2.1. The solution was degassed for 1 h at 45°C. Afterwards, a solution of 1 mL KPS (0.08 M) was added to the mixture while stirring continuously at 450 rpm. The temperature was slowly increased to 65°C at a rate of 1°C per 2 minutes. During the temperature ramp the solution became turbid. Finally, the polymerization was completed by stirring overnight at 65°C under N₂ atmosphere. The received microgel particles were purified by filtering over glass wool, dialysis for 2 weeks and finally freeze drying at -85°C under 1×10^{-3} bar for 48 h. After dissolving the dried microgels in methanol the residual amount of water was determined by Karl-Fischer titration.

In order to synthesize large p-NIPAM microgels with a MBA content of 5 mol-%, the added amount of cross-linker was increased to 0.116 g (7.5×10^{-4} mol). All other parameters and amounts of reagents were the same as described for a MBA content of 0.25 mol-%.

3.2.3 Copolymers of NIPAM and AA

The synthesis of p-NIPAM-*co*-AA microgel particles with a cross-linker and comonomer amount of 5 mol-% was done using the same experimental setup described in 3.2.1. The cross-linker as well as the comonomer concentrations refer to the molar concentration of the monomer NIPAM. Briefly, 1.132 g (0.01 mol) NIPAM, 0.078 g (5×10^{-4} mol) MBA and 0.038 mL (5×10^{-4} mol) were dissolved in 100 mL of water. The clear solution was degassed for 30 min using nitrogen while the mixture was heated to 70°C. 1 mL (3.7×10^{-3} M) of the radical initiator dissolved in water was added leading to a clouding of the solution after a few minutes. After 4 h the solution was cooled down to room temperature and stirred overnight under N₂-atmosphere. The received white dispersion was purified by filtering over glass wool, dialysis for

2 weeks with daily water exchange and finally freeze drying at -85°C and 1×10^{-3} bar for 48 h. The received solid microgel particles were dissolved in methanol to determine the residual amount of water after freeze-drying by Karl-Fischer titration.

3.2.4 Copolymers of NIPAM and AG

In order to synthesize p-NIPAM-*co*-AG microgels with a cross-linker content of 0.25 mol-%, 2.263 g (0.02 mol) NIPAM, 0.0078 g (5×10^{-5} mol) and the desired amount of the comonomer AG were dissolved in 200 mL of water using the same experimental equipment described in 3.2.1. The MBA as well as the AG concentrations refer to the molar concentration of the monomer NIPAM. While degassing the mixture with nitrogen for 30 min the temperature was increased to 70°C . To initiate the polymerization 1 mL of an aqueous solution of KPS (3.7×10^{-3} M) was added rapidly. The solution became turbid after a few minutes indicating a successful beginning of the radical polymerization. After 4 h the white dispersion was allowed to cool down to room temperature followed by stirring overnight under N_2 -atmosphere. To purify the synthesized polymer particles they were filtered over glass wool, dialyzed for 2 weeks with daily water exchange and finally freeze dried at -85°C and 1×10^{-3} bar for 48 h.

The initial amounts of AG as comonomer were 3 mol-% (0.069 g, 6×10^{-4} mol) and 25 mol-% (0.576 g, 5×10^{-3} mol).

3.2.5 Integrated amount of comonomer

The determination of the integrated amount of comonomer was tried via titration as described for p-NIPAM-*co*-acrylic acid.³⁶ Briefly, 100 mg of p-NIPAM_{AA-5} were dissolved in 20 mL water. The pH value of the solution was pH 5 indicating the formation of ammonium ions from amine during the freeze drying of the polymer particles. Therefore, the sample was titrated with 0.01 M NaOH to determine the buffer plateau and hence the amount of AA in the polymer network. The received titration curve is shown in figure A1. Additionally, figure A1a shows the fitting procedure done with CurTiPot¹⁰³ assuming carbonic acid (H_2CO_3) in the titrant but not in the sample. Figure A1b presents the fitting data assuming H_2CO_3 in both components. The calculated amounts of all components are summarized in table 3.1.

Table 3.1: M_W and zeta potential at 25°C for p -NIPAM_{0.25}, p -NIPAM₅ and p -NIPAM₁₀ determined by Light Scattering.

	c_{AA} [mol/L]	$c_{H_2CO_3}$ [mol/L] titrant	$c_{H_2CO_3}$ [mol/L] titrand
Fit1	2.8×10^{-4}	4.7×10^{-3}	0
Fit 2	1.8×10^{-4}	4.7×10^{-3}	9.9×10^{-5}

Figure A1a shows that the fit correlates with the buffer range at pH 6 and pH 10. Adding small amounts of H_2CO_3 to the sample leads to a change in the determined amount of AA of $\approx 35\%$. Hence, the evaluation of the data led to the problem of H_2CO_3 in the sample and the titrant. A small amount of that acid is formed by dissolved carbon dioxide present in air which is not avoidable under ambient conditions. Due to the fact that the pK_a values of H_2CO_3 and AA are very close (pK_a (AA) = 9.5, pK_a (H_2CO_3) = 10.3) it is difficult to quantify small amounts of AA.

As conclusion, only a low amount of the initial comonomer is integrated into the polymer network. Due to the amine groups in the comonomer AG, the same problems occur in case of p -NIPAM co -allylglycine. In contrast to acrylic acid, which is integrated in a higher amount, the concentration of AA and AG within p -NIPAM microgel particles cannot be determined by titration.

3.2.6 Au-NPs

Spherical Au-NPs with a diameter of 18.5 nm were synthesised using the well known method of Enüstün and Turkevich.⁷² For the preparation citrate is used as reduction reagent and as stabilizer. All glassware involved in the synthesis was carefully cleaned with aqua regia. Briefly, 5 mL of a hot citrate solution (0.6 wt%) were added to 100 mL of a boiling gold salt solution (5×10^{-4} M $HAuCl_4$) under vigorous stirring. Within the first three minutes, the light yellow solution changed its colour to almost black, which is related to the reduction of Au^{3+} to Au^0 . Afterwards, the speed of the stirrer was lowered from 500 rpm to 200 rpm. The growth of the Au-NPs was continued for 17 min leading to a deep red dispersion. Finally, the solution was cooled down to room temperature under continuous stirring.

3.3 Preparation procedures

3.3.1 Determination of the amount of water in microgel particles

Karl-Fischer-titration was used to determine the water content in p-NIPAM microgel particles before and after solvent exchange.

In case of freeze-dried polymers a solution of 20 mg of the microgel per mL methanol was prepared under ambient conditions and titrated with a mixture of Sulphur dioxide, Imidazole and Iodine (Hydranal). In the presence of water the components react in a molar ratio of 1:1:1 as shown in figure 3.1. The endpoint of the titration is determined by a platinum electrode. If

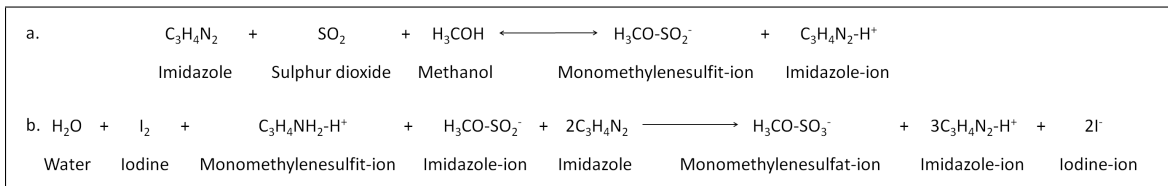


Figure 3.1: Reactions of Karl-Fischer-titration.

no more water is present in the solution, an excess of iodine is produced and hence a current flow is measured. The consumed amount of titrand is used to calculate the amount of water in the sample. The water content in the pure methanol was also determined to receive the exact value of water content for the freeze-dried microgels.

The determination of the residual water content after solvent exchange was done by dissolving 20 mg microgel in 1 mL buffer (0.1 M potassium phosphate buffer, pH 7) followed by two centrifugation steps (10 min at 9000 g) and redispersion in 1 mL isopropanol. The received solutions as well as pure isopropanol were titrated and the residual amount of water was calculated. All measurements were done in triplicate.

3.3.2 Loading of microgels with Au-NPs

Au-NPs were loaded within p-NIPAM microgel particles with a cross-linker content of 0.25 mol-%, 5 mol-% and 10 mol-% (see 3.2.1). The incorporation of the Au-NPs was achieved by adding 0.943 mL of the synthesised Au-NPs to 0.057 mL of p-NIPAM microgel solutions resulting in a concentration of 1.9×10^{15} Au-NPs per liter. The concentration of the microgel particles was varied to yield Au-NP loadings of 241 and 1133 Au-NPs per microgel particle, respectively. The mixture obtained was homogenized for 10 min using a

vortex mixer and centrifuged at 8000 rpm for 4 min. The received residue was redispersed in 1 mL water. This washing procedure was repeated two times.

3.3.3 Immobilization of enzymes by solvent exchange

3.3.3.1 Determination of the purity of enzymes by SDS-Page. In order to determine the purity of the commercially available enzymes, sodium dodecyl sulfate polyacrylamide gel electrophoresis (SDS-Page) was done. Firstly, the separation and stacking gel were prepared by polymerization. The composition of these gels is shown in table 3.2.

Table 3.2: Composition of stacking and running gel for 12% SDS gels. The acrylamide mixture contains acrylamid and bisacrylamide (37.5:1).

components	5% stacking gel [mL]	12% running gel [mL]
H ₂ O	9.9	6.9
30% acrylamide mixture	1.7	12.0
1.5 M TRIS (pH 8.8)	-	7.5
1.5 M TRIS (pH 6.8)	1.25	-
10% SDS	0.1	0.3
10% APS	0.1	0.3
TEMED	0.01	0.012

Afterwards, HRP, CalB as received and CalB after dialysis were dissolved in buffer (0.1 M potassium phosphate buffer, pH 7) with a concentration of 0.5 mg/mL. The samples were mixed with the Laemmli buffer¹⁰⁴ (pH 6,8, 126 mM TRIS-HCl, 20% glycerine, 4% SDS, 0,02% bromophenol blue, 2.5% mercaptoethanol) in a 1:1 ratio and denaturated at a temperature of 95°C for 5 min. 10 μ L of each sample was deposited at the top of the stacking gel. As molecular mass standard 10 μ L of the PageRuler Prestained Protein Ladder (10 kDa to 170 kDa, Fermentas) were also separated by the gel. After surrounding the gel with a running buffer (3.03 g TRIS, 14.41 g glycine, 10 mL of a 10% SDS-solution) 50 V were applied to the system till the samples reached the separation gel followed by applying a voltage of 100 V for 1h. After separation the gel was stained with Coomassie dye (PageBlue Protein Staining Solution, ThermoScientific) on the one hand and with silver nitrate on the other hand. After washing the received gels with water the molecular weight of the enzymes was determined.

3.3.3.2 Labeling of the enzymes with FITC. While HRP was used as bought, CalB was dialyzed and freeze-dried in advance to receive a solid. The labeling procedure was done with FITC according to the literature.¹⁰⁵ Therefore, 25 mg of either HRP or CalB were dissolved in 2 mL buffer (0.07 M sodium carbonate buffer, pH 9.5). While stirring, 200 μL of a FITC solution in carbonate buffer (1 mg/mL) were added dropwise leading to a slightly turbid and yellow mixture. Afterwards, the solution was stirred for 2 h in the dark. To separate the labeled enzymes from the unreacted FITC the received sample was purified using PD-10 desalting columns packed with Sephadex G-25 with the carbonate buffer as eluant. The greenish yellow fraction was collected and freeze-dried leading to a fluffy sample.

3.3.3.3 Immobilization of CalB. For the immobilization process, 5 mg of large p-NIPAM particles with either 0.25 mol-% or 5 mol-% MBA and 0.1 mL CalB ($c = 4.32$ mg/mL) were dissolved in 1.4 mL buffer (0.1 M potassium phosphate buffer, pH 7) at room temperature, stirred overnight and centrifuged for 15 min at 9000g. The received residues were redispersed in the water miscible solvent, isopropanol, and washed three times by centrifugation and redispersion. After the last centrifugation step, one part of the samples was dissolved in buffer to determine the immobilized amount using Bradford assay. The other part of the samples was used for another solvent exchange by the exchange of isopropanol against the water immiscible solvent, n-hexane to investigate the catalytic activity.

In case of immobilization within large p-NIPAM microgel particles with a cross-linker content of 0.25 mol-% the immobilization experiment was done at 25°C and 50°C during the whole immobilization procedure. Furthermore, CalB and p-NIPAM microgel particles were mixed at 25°C, stirred for 30 minutes followed by heating the mixture to 50°C for the immobilization over night. As reference un-immobilized CalB was treated the same way for all temperature procedures.

To determine the location of the immobilized CalB within the polymer particles, two samples for each microgel system consisting of 5 mg p-NIPAM microgel particles, 1.1 mg FITC-CalB and 1 mL buffer (0.1 M potassium phosphate buffer, pH 7) were prepared. After stirring overnight, the samples were centrifuged for 10 min at 9000g. The residue of one sample was redispersed in buffer while isopropanol was added to the other sample followed by one further washing step.

Additionally, the residual amount of water within the p-NIPAM microgel particles after solvent exchange from water to isopropanol was determined by Karl-Fischer titration.

3.3.3.4 Immobilization of HRP. For the immobilization process, 5 mg of large p-NIPAM particles with a cross-linker content of 0.25 mol-% and 0.7 mg of HRP were mixed with 1.5 mL buffer (0.1 M potassium phosphate buffer, pH 7) at room temperature. The amount of HRP was determined using Bradford reagent leading to an initial concentration of 0.061 mg per mg p-NIPAM. The solution was stirred overnight and centrifuged for 15 min at 9000g. The residues were redispersed in isopropanol and washed three times by centrifugation and redispersion. To determine the immobilized amount one part of the samples was redispersed in water while the other part of the samples was redispersed in isopropanol again for investigations on the catalytic activity.

The preparation for the determination of the localization of HRP within the p-NIPAM microgel particles was done as described in 3.3.3.3 by using FITC-HRP instead of labeled CalB.

Furthermore, the residual amount of water within the p-NIPAM microgel particles after solvent exchange from water to isopropanol was determined by Karl-Fischer titration.

3.3.3.5 Determination of the immobilized amount of enzyme. The amounts of CalB and HRP which were immobilized within the large p-NIPAM microgel particles were achieved using the Bradford reagent according to the manufacturer's instruction. After the solvent exchange to isopropanol described in 3.3.3.3 and 3.3.3.4 the samples were centrifuged for 15 min at 9000g and redispersed in 50 mL buffer (0.1 M potassium phosphate buffer, pH 7). This solution was used for the Bradford reagent and via UV-Vis spectroscopy the total concentration of enzyme in the sample was calculated. Detailed informations are given in 5.3.2.1.

3.3.4 Covalent immobilization of HRP

For the covalent immobilization of HRP within p-NIPAM-**co**-AA microgel particles (see 3.2.3) the coupling reagent BQ was bound to HRP. Therefore, 0.025 mL of a BQ solution in ethanol (15 mg/mL) were added to 0.25 mL

of a HRP solution in buffer (20 mg/mL, 0.1 M potassium phosphate buffer, pH 5.98). After stirring for 30 min at 37°C the solution was diluted with 1 mL of the same buffer. The received mixture was purified by using PD-10 desalting columns packed with Sephadex G-25 with the phosphate buffer as eluant. The first fraction was collected and purified again with the same column. Afterwards, 0.5 mL of a sodium carbonate solution in water (0.1 g/mL) was added to the obtained sample.

In the second step the BQ-HRP complex was covalently attached to the microgel particles with AA as comonomer by adding 15 mg of the polymer particles to the solution received in the first step. The mixture was stirred overnight at room temperature. The obtained p-NIPAM_{AA-5}-BQ-HRP complex was purified by centrifugation for 10 min at 9000g and redispersion in buffer (0.1 M potassium buffer saline, pH 7.14). This was repeated three times followed by a third centrifugation step with redispersion in phosphate buffer. The received solution was stored at 4°C.

3.4 Activity Measurements

3.4.1 Activity measurements of immobilized CalB in organic solvents

The catalytic performance of CalB was determined via the esterification of 1-octanol and octanoic acid in n-hexane. Typically, 50 μL droplets of the aqueous solution of un-immobilized CalB ($c = 4.32 \text{ mg/mL}$) or 5 mg of p-NIPAM particles loaded with CalB were given to a 1.0 mL of substrate solution in n-hexane containing 100 mM 1-octanol and 100 mM octanoic acid. These dispersions were shaken at 25°C, 32°C or 50°C for 15 min. The supernatant of the immobilized CalB or the upper part of the solution with un-immobilized CalB was investigated with a gas chromatograph to determine the activity of CalB. Every 5 min 150 μL of solution were withdrawn and analyzed for ester concentration via gas chromatography. The concentration of the product, octyl octanoate, was calculated from the peak area at a typical retention time of 10 min. All reactions were performed in triplicate. One unit per μg ($\text{U}/\mu\text{g}$) of specific activity of free or immobilized CalB was defined as 1 μmol of product produced per min per μg of free or immobilized CalB.

To investigate the stability of the system, some samples of immobilized CalB were stored in n-hexane and after different time intervals the samples were

used as catalyst for the esterification reaction. The reusability of the system was investigated by testing the activity of one sample followed by testing the same sample again after centrifugation and washing. This procedure was repeated four times.

3.4.2 Activity measurements of immobilized HRP in organic solvents

The reaction to investigate the catalytic activity of HRP is based on the oxidation of pyrogallol to purpurogallin in the presence of hydrogen peroxide. The formation of the product can be determined via UV-Vis spectroscopy at a wavelength of 420 nm. 0.4 mL of the immobilized sample redispersed in 1.5 mL isopropanol was mixed with 0.4 mL of a pyrogallol solution in isopropanol (1 mg/mL) and 0.132 mL of hydrogen peroxide [48 μL H_2O_2 (35%) in 20 mL water]. For the determination of the activity of free enzyme 1 mL of a solution of HRP in isopropanol (1 mg/mL) was mixed with 0.1 mL of the pyrogallol and hydrogen peroxide solution, respectively. As reference the same compositions of the reagents were used unless the samples were replaced by isopropanol. Afterwards, the solution was measured via UV-Vis spectroscopy for 1 min at 420 nm. Due to a linear behavior of the increase in absorption with time, the volume activity can be calculated using equation 3.1.

$$U_V = \frac{\Delta E V_{total}}{V_S \epsilon d} \quad (3.1)$$

where U_V is the volume activity, ΔE the change of the absorption per minute, V_{total} the total volume, V_S the volume of the sample, ϵ the extinction coefficient of purpurogallin and d the thickness of the used cuvette. For the calculation the extinction coefficient of purpurogallin was determined to be $1.976 \text{ mL} \mu\text{mol}^{-1} \text{cm}^{-1}$. Therefore, one unit is defined as the formation of 1 μmol product per minute per mL.

3.4.3 Activity measurements of immobilized HRP in water

The received sample from the covalent immobilization was used as is for the activity reaction. The used reaction and procedure is similar to that described in 3.4.2. The composition for the immobilized system is as follows: 1.68 mL water, 0.216 mL buffer (0.1 M potassium phosphate buffer, pH 5.98), 0.12 mL sample, 0.256 mL of a pyrogallol solution in water (0.05 g/mL) and 0.128 mL hydrogen peroxide [0.253 mL H_2O_2 (35%) in 20 mL

water]. In order to have a comparison, the same activity reaction was done with free HRP. Therefore, 1.68 mL water, 0.266 mL buffer (0.1 M potassium phosphate buffer, pH 5.98), 0.07 mL of a HRP solution (4.95 $\mu\text{g}/\text{mL}$), 0.256 mL of a pyrogallol solution in water (0.05 g/mL) and 0.128 mL hydrogen peroxide [0.253 mL H_2O_2 (35%) in 20 mL water] were mixed. In both cases the blind samples have the same composition, only the sample is replaced by buffer. The formation of the product was investigated via UV-Vis spectroscopy at 420 nm. To calculate the volume activity the extinction coefficient of purpurogallin in water was found to be 2.642 $\text{mL}\mu\text{mol}^{-1}\text{cm}^{-1}$. Therefore, one unit is defined as the formation of 1 μmol product per minute per mL.

3.5 Instruments and sample preparation

3.5.1 DLS

DLS measurements were done using an ALV goniometer setup with either a frequency doubled Nd:YAG laser (Compass 150, Coherent, USA) with a wavelength of $\lambda = 532$ nm and an output power of 150 mW or a He-Ne laser with a wavelength of $\lambda = 632.8$ nm as the light source. The correlation functions were recorded at a constant scattering angle of 60° . The data were analyzed by a regularized fit routine supplied by the ALV instrument, which is similar to CONTIN^{106,107} when cumulant analysis failed to fit the data due to polydispersity. The swelling behavior was investigated over a temperature range from 15°C to 50°C using a thermostated toluene bath. All measurements were done in cylindrical quartz cells of 10 mm in diameter (Hellma, Germany). To inhibit multiple scattering in the samples, very low concentrations were prepared for DLS (0.0015 wt%). To study the aggregation behavior of p-NIPAM-**co**-AG microgels the concentration was increased to 0.015 wt%.

3.5.2 SLS

Static light scattering (SLS) data were recorded at scattering angles from 17° to 37° with 2° steps in between using an ALV/CGS-3 compact goniometer system equipped with an ALV/LSE-7004 correlator to determine the M_W of the polymer particles. The temperature was controlled with a Huber Compatible Control thermostat. As light source a He-Ne laser ($\lambda = 632.8$

nm) was used and the laser light was polarized vertically with respect to the instrument table. The concentration of the polymer particles was varied from 1×10^6 g/g to 7×10^6 g/g.

3.5.3 Zeta potential measurements

Zeta potential measurements were carried out with a Malvern Zetasizer NanoZS ($\lambda = 633$ nm, 4 mW) using highly diluted microgel solutions in water (0.0015 wt%) and the synthesised solution of gold nanoparticles. The temperature during the measurements was varied from 15°C to 50°C .

3.5.4 Gas chromatography

The formation of octyloctanoate was determined using a Shimadzu 2010 gas chromatograph equipped with a BPX5 column from SGE (length = 25 m, internal diameter = 0.22 mm). The film thickness is $0.25 \mu\text{m}$ and the detector is a flame ionization detector at 300°C . Furthermore a split injector is used at 275°C with an injection volume of $1 \mu\text{L}$. The temperature program is separated in three parts. Firstly, the starting temperature of 80°C is kept constant for 0.5 min. Afterwards, the temperature increases with a rate of 20°C per minute from 80°C to 170°C . The last ramp leads to a further increase to the final temperature of 200°C using a rate of 5°C per minute.

3.5.5 CLSM

As described in section 3.3.3.3 the samples were redispersed either in buffer or in isopropanol. To measure the samples, roughly $20 \mu\text{L}$ of the immobilized sample was placed between two cover slides. The location of the enzymes within the microgel particles was investigated using an inverted microscope Axiovert 200 M equipped with a 100x oil immersion objective (numerical aperture 1.3) and a Zeiss LSM 510Meta confocal scanning unit (Zeiss MicroImaging GmbH, Jena, Germany). The CLSM images were prepared using the 488 nm line of the argon laser for excitation and a 505 nm long-pass emission filter. Z-stacks were performed with a step of 50 nm upwards starting at the surface of the cover slips. Different Z-stacks of the samples were analyzed using the LSM 510 software and displayed as an overlay of transmission and fluorescence channels in orthogonal section views.

3.5.6 AFM

Most of the images were measured with an Asylum Cypher using Igor Pro 6.20 for the analysis of the received images.

Some particles were measured with a Veeco nanoscope III controller on a multimode microscope working in tapping mode. The images were analyzed using the WSxM 5.0 software.¹⁰⁸

The samples for AFM measurements were prepared by spin-coating. Therefore, solutions of the microgel particles in water (0.1 wt%) were dropped on a silicon wafer ($\approx 1 \text{ cm}^2$) and spin-coated for 200s at 2000 rpm. As substrates silicon wafers from Olympus (OMCL-AC160TS) with spring constants between 12-103 N/m were used. More information on spin-coating procedures can be found in the literature.¹⁰⁹

3.5.7 TEM

Each TEM specimen was prepared using $5 \mu\text{L}$ of solution (see 4.2.1 for concentration used) on a 200-mesh TEM copper grid with carbon support film. Excess liquid was blotted from the grid using filter paper after 2 min. The specimen was inserted into the sample holder after sufficient drying and transferred to JEOL JEM-2100 operating at an acceleration voltage of 200 kV. Images were recorded digitally with a bottom-mounted 4k TVIPS CMOS camera system (TemCam-F416) and processed with a digital imaging processing system (EM-Menu 4.0). Final image analysis was completed using ImageJ 1.42q. The adsorbed amount of Au-NPs was determined by counting the nanoparticles in ten different microgel particles.

3.5.8 UV-Vis spectroscopy

UV-Vis spectra were collected using a Perkin Elmer Lambda 35 UV-Vis spectrophotometer at a temperature of 25°C .

In order to obtain temperature dependent UV-Vis spectra in a range from 20°C to 50°C a Varian Cary 50 spectrophotometer equipped with a temperature controlled sample holder was used.

All spectra were recorded in standard 10 mm quartz cells (Hellma, Germany).

3.5.9 SDS-Page

For the separation of the enzymes by the molecular weight a Mini Trans-Blot Electrophoretic Transfer Cell (Bio-Rad) was used.

3.5.10 Karl-Fischer titration

Karl-Fischer titration was done with a 836 Titrande from Metrohm to determine the residual amount of water in the microgel particles.

4 P-NIPAM microgels loaded with Au-NPs^{1,2}

4.1 Introduction

As described in Chapter 1 hybrid materials can be prepared by combining responsive microgels with inorganic nanoparticles to create multifunctional particles.¹¹⁰⁻¹¹³ Ideally such hybrid materials combine the sensitivity of the microgel to temperature and pH with the optical, catalytic or magnetic properties of the inorganic material. Many hybrid materials are based on polymer coating of preformed nanoparticles^{18,114,115} or the in-situ synthesis of inorganic nanoparticles in a polymer matrix.^{21,116,117} In both cases, the nanoparticles are larger than the mesh size and immobilized in the gel matrix. In the study of Lange et. al it was presented that the plasmon coupling due to Au-NPs is induced by shrinking of the thermoresponsive p-NIPAM matrix. Related simulations show that the plasmon coupling becomes pronounced, if the distance between the nanoparticle surfaces is below 5 nm.²¹ Only a few studies deal with the loading of microgels with preformed nanoparticles^{9,22,23} or nanorods.¹⁹ However, neither the internal structure of the Au-NP loaded microgels nor any plasmon coupling effects during the volume phase transition of the Au-NPs were investigated in these studies.

Karg et. al attached polyelectrolyte-coated gold nanorods at the surface of

¹Similar content is included in *Interaction of gold nanoparticles with thermoresponsive microgels: Influence of the cross-linker density on optical properties* Gawlitza, K.; Turner, S. T.; Karg, M.; Mulvaney, P.; von Klitzing, R. **2012**, in preparation.

²TEM images were measured by Sarah T. Turner from TU Berlin at the Electron microscope of the Joint Laboratory for Structural Research (JLSR) of Helmholtz-Zentrum Berlin für Materialien und Energie (HZB), Humboldt-Universität zu Berlin (HU) and Technische Universität Berlin (TU).

oppositely charged microgels and investigated the optical properties of the gold nanorods as a function of microgel swelling.^{20,118} The microgel collapse led to a significant decrease in the surface area, thereby reducing the distance between the attached gold nanorods. Plasmon coupling was observed below a certain nanorod spacing and the longitudinal plasmon resonance was found to be significantly red-shifted. Variation of the gel structure offers new perspectives for tuning the optical properties. This topic has not been studied so far.

In the following the physical entrapment of spherical, citrate stabilised Au-NPs in chemically cross-linked p-NIPAM microgels is described. Changes to the Au-NP loading density and the microgel cross-linking density lead to altered distances between the Au-NPs in the microgels. The resulting variation in the surface plasmon resonances is investigated using UV-Vis absorption spectroscopy. TEM is used to study the penetration depth of the Au-NP and DLS is used to investigate the temperature dependant size changes of the hybrid particles. Due to the sensitivity of the Au-NP plasmon resonance to changes in the dielectric environment, the plasmon resonance is also used as a monitor of the particle size distribution and structural changes during microgel collapse.

4.2 Results and Discussion

4.2.1 Characterization of different cross-linked p-NIPAM microgel particles

Three p-NIPAM microgel systems with nominal cross-linker concentrations of 0.25, 5 and 10 mol-% were prepared by surfactant-free precipitation polymerization. For the sake of clarity, the samples are denoted as p-NIPAM_x where x describes the mol-% of MBA.

The size and the shape of the synthesized polymer particles were investigated by performing AFM measurements against air. The images of one microgel particle for each sample and the corresponding cross-sections are summarized in figure 4.1. It is shown that the diameter in dried state is ≈ 600 nm for p-NIPAM_{0.25} (figure 4.1a) and p-NIPAM₅ (figure 4.1b) and ≈ 550 nm for p-NIPAM₁₀ (figure 4.1c). The height of the microgel particles adsorbed on the silicon wafer increases with increasing cross-linker content. Due to the decrease in the polymer network density the drying process

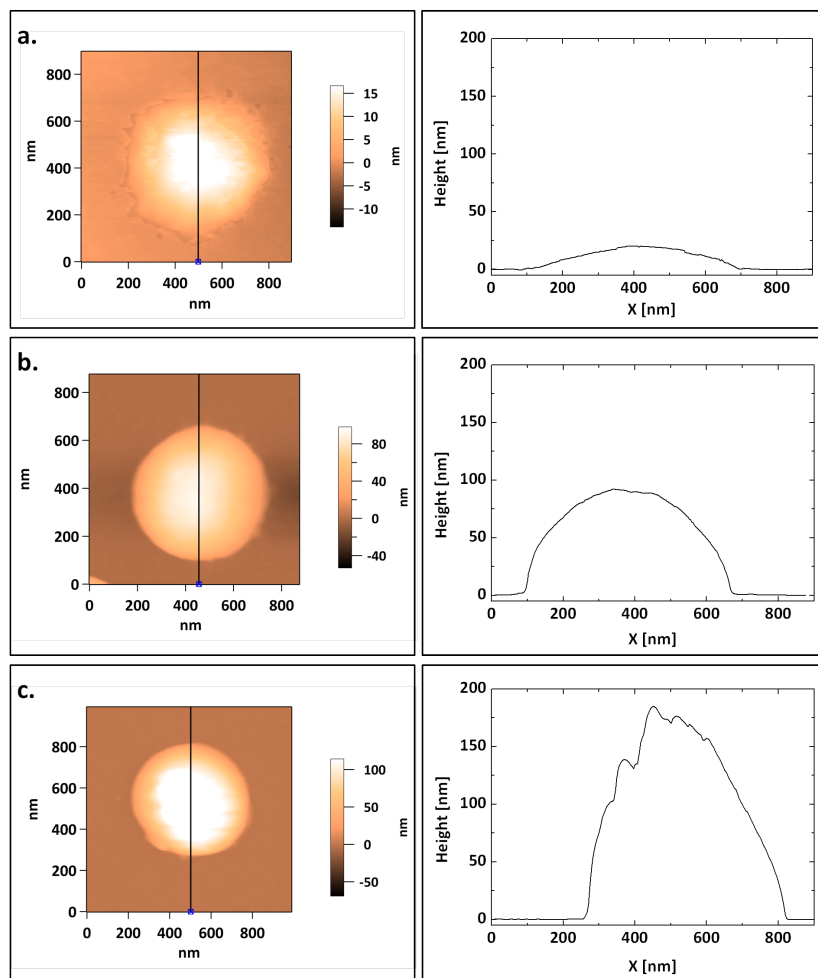


Figure 4.1: AFM images of $p\text{-NIPAM}_{0.25}$ (a), $p\text{-NIPAM}_5$ (b) and $p\text{-NIPAM}_{10}$ measured against air and the corresponding cross-sections.

leads to a higher amount of expelled water and a less pronounced flattening with increasing cross-linker content. Additionally, the images confirm the spherical shape of the synthesized microgel particles.

The molecular weight (M_W) of the $p\text{-NIPAM}$ microgels was determined using SLS and Zimm-plot analysis. Karl-Fischer titration was used to determine a residual water content of around 10 wt% which was considered for the concentrations of the samples. A refractive index increment $dn/dc = 0.167 \text{ cm}^3/\text{g}^{119}$ was used for calculation and the received Zimm-plots can be found in the Appendix (figure A2). Table 4.1 summarizes the M_W values for the three microgels. For $p\text{-NIPAM}_{0.25}$ the M_W ($1.7 \times 10^9 \text{ g/mol}$) is found, whereas the values for $p\text{-NIPAM}_5$ and $p\text{-NIPAM}_{10}$ are in a similar range.

Zeta potential measurements were performed at 25°C as an estimate of

Table 4.1: M_W and zeta potential at 25°C for $p\text{-NIPAM}_{0.25}$, $p\text{-NIPAM}_5$ and $p\text{-NIPAM}_{10}$ determined by Light Scattering.

MBA content [mol-%]	M_W [g/mol]	ζ [mV]
0.25	$1.7 \times 10^9 \pm 7 \times 10^7$	-6.5 ± 0.5
5	$8.4 \times 10^9 \pm 3 \times 10^8$	-5.7 ± 0.5
10	$6.9 \times 10^9 \pm 1 \times 10^8$	-7.9 ± 0.9

the $p\text{-NIPAM}$ surface charge. Small, negative values from -6 to -8 mV were measured for all three microgels (see table 4.1). This negative charge is due to the anionic radical initiator used for the polymerization. Note that zeta potential values are rather difficult to interpret for large, gel-like particles such as $p\text{-NIPAM}$ microgels and therefore ζ serves only as an indication of the slightly negative microgel surface charge.

The temperature dependant R_H values of the microgel particles were measured by DLS. The received swelling curves are presented in figure 4.2a for $p\text{-NIPAM}_{0.25}$, 4.2c for $p\text{-NIPAM}_5$ and 4.2e for $p\text{-NIPAM}_{10}$.

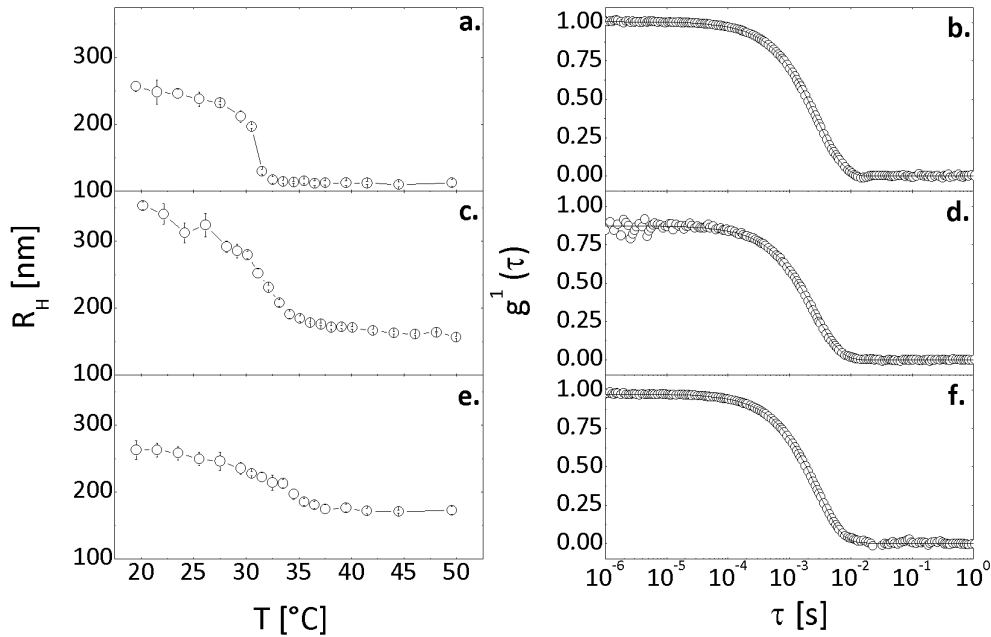


Figure 4.2: Swelling curves for $p\text{-NIPAM}_{0.25}$ (a), $p\text{-NIPAM}_5$ (c) $p\text{-NIPAM}_{10}$ (e) and correlation functions with cumulant fit at 25°C for $p\text{-NIPAM}_{0.25}$ (b), $p\text{-NIPAM}_5$ (d) $p\text{-NIPAM}_{10}$ (f) dispersed in water.

The fitting of the received correlation functions leads to the corresponding values of R_H . One correlation function for each microgel including the cumulant fit is given in figure 4.2 and polydispersity indices (PDI) of 0.042

for p-NIPAM_{0.25} (figure 4.2b), 0.059 for p-NIPAM₅ (figure 4.2d) and 0.033 for p-NIPAM₁₀ (figure 4.2f) were determined revealing the low polydispersity of the synthesized polymer particles. All characteristic values which were obtained from DLS measurements are summarized in table 4.2.

In order to compare the sizes of the synthesized microgel particles, the hydrodynamic radii have to be compared in the collapsed state ($T = 40^\circ\text{C}$) of the polymer particles where the polymerization is done. Interestingly, the hydrodynamic dimensions for the microgel system with the lowest crosslinker density (p-NIPAM_{0.25}) are significantly smaller than those of the p-NIPAM₅ and p-NIPAM₁₀ particles. As assumption this is attributed to a less efficient polymerization for a very low amount of cross-linker. The

Table 4.2: R_H , α and VPTT of p-NIPAM microgel particles with MBA-contents of 0.25, 5 and 10 mol-%.

MBA content [mol-%]	$R_H(25^\circ\text{C})$ [nm]	$R_H(40^\circ\text{C})$ [nm]	α	VPTT [$^\circ\text{C}$]
0.25	238 ± 11	112 ± 2	0.10	31
5	281 ± 16	173 ± 2	0.23	32
10	249 ± 10	176 ± 6	0.35	32

deswelling ratio α increases linearly with increasing MBA content as shown in table 4.2. Due to the higher connectivity in the polymer network at higher MBA concentrations, the microgel particles become less elastic and therefore the swelling capacity decreases. This leads to the largest R_H value for p-NIPAM₅ at 25°C which is in good agreement with the received M_W values determined at 25°C (table 4.1). Furthermore, the VPTT is almost constant which indicates that the interactions between the polymer chains and the solvent were not changed with increasing MBA content. These aspects of p-NIPAM microgel particles are in good agreement with studies of Kratz et al.^{37,38}

Additionally, the swelling curves show the characteristic shrinking with increasing temperature for all three microgels. Besides, the sample with the lowest cross-linker content of 0.25 mol-% shows a nearly discontinuous shrinking while an increase in the cross-linker content leads to a broadening of the transition range. The less denser polymer network of p-NIPAM_{0.25} leads to a faster and more abrupt expulsion of water above the VPTT. These investigations are in good agreement with results from literature.³⁷

4.2.2 Characterization of Au-NPs

The Au-NPs were characterized using TEM and UV-Vis spectroscopy. Figure 4.3a shows a representative TEM image of the nearly spherical particles. Figure 4.3b shows the size distribution of the Au-NPs with an average diameter of 18.5 nm obtained from measuring the size of at least 100 individual particles from different TEM images. A UV-Vis spectrum recorded from an aqueous dispersion of the particles at 25°C is presented in figure 4.3c. The spectrum shows the typical localized surface plasmon resonance leading to an absorption maximum at ≈ 525 nm. Using the optical density of 0.17 of the Au-NP solution at 400 nm the number concentration of Au-NPs was calculated (2×10^{15} particles/L).

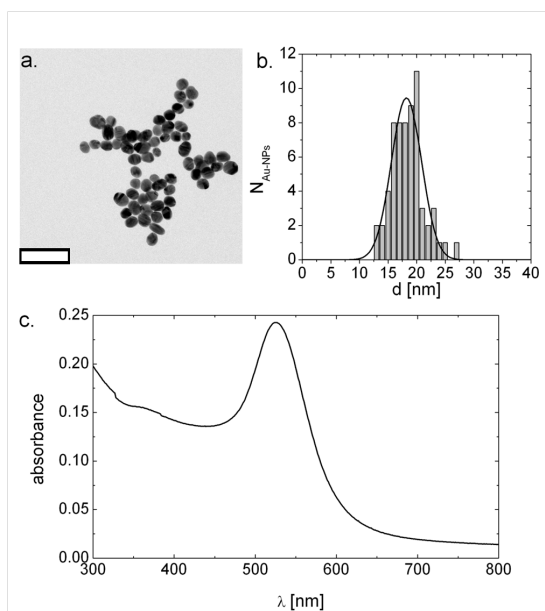


Figure 4.3: TEM-image (scale bar: 80 nm) (a), size distribution (b) and UV-Vis spectrum (c) of synthesised Au-NPs.

The zeta potential of the citrate stabilized Au-NPs was measured from dilute aqueous dispersion at 25°C and yielded a potential of -30 ± 2 mV.

4.2.3 Low loading regime

The synthesised Au-NPs with an average diameter of 18.5 nm were used to load the p-NIPAM microgel particles. The M_W of the microgels (table 4.2) allows calculation of the number density of microgel particles in dispersion. At the same time the number concentration of the Au-NPs dispersion can be

calculated using the extinction cross-section of gold. Therefore, the theoretical number of Au-NPs per p-NIPAM microgel particle could be calculated. For experiments with a low degree of loading the ratio of Au-NPs per microgel particle was kept constant at 241 for the different microgels. The results obtained by TEM and UV-Vis are shown in figure 4.4.

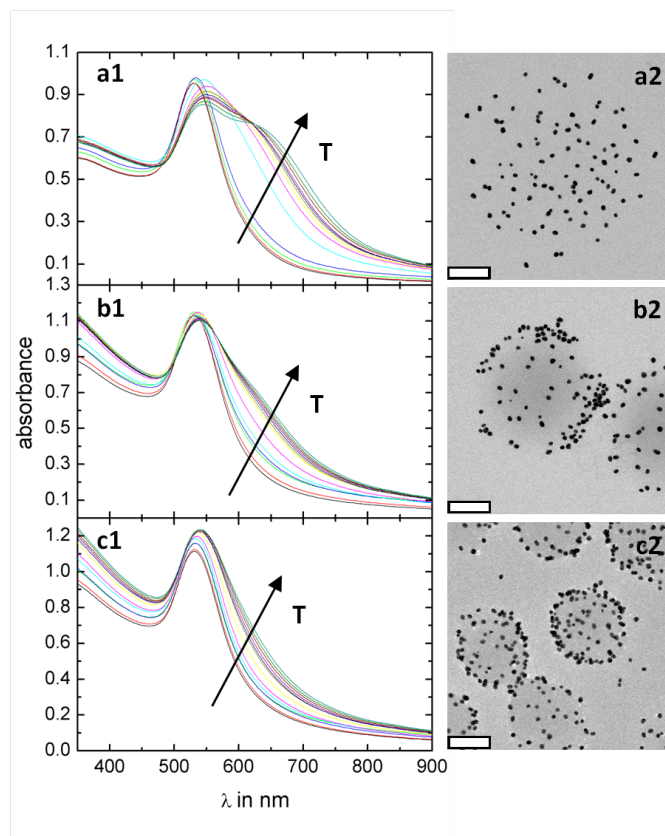


Figure 4.4: UV-Vis spectra and TEM images (scale bar: 300 nm) of $p\text{-NIPAM}_{0.25}$ (a1, a2), $p\text{-NIPAM}_5$ (b1, b2) and $p\text{-NIPAM}_{10}$ (c1, c2) for the low loading regime of Au-NPs.

Although the microgel particle is only barely visible by electron microscopy due to its very low contrast, the circular assembly of Au-NPs allows the microgel particle to be easily recognized in the images, and even for the size to be estimated (figures 4.4a2, 4.4b2 and 4.4c2). The Au-free areas around the Au-NP loaded microgels on the TEM images suggest that the nanoparticles are strongly adsorbed and no diffusion out of the network occurs during the sample preparation. Image analysis reveals an average diameter of the Au-NPs of 18.5 nm, which is in good agreement with the diameter obtained for the bare gold nanoparticles prior to mixing with the microgels. Table 4.3 summarizes the Au-NP loading efficiency for the different microgel particles,

determined by counting the number of nanoparticles per microgel particle in different TEM-images.

Table 4.3: Loading efficiency of p-NIPAM microgels for low loading regime of Au-NPs.

MBA content [mol-%]	$N_{Au,max}$	$N_{Au,adsorbed}$	$N_{Au,adsorbed}$ [%]
0.25	241	99	41
5	241	86	36
10	241	83	34

The loading efficiency is around 35% for p-NIPAM₅ and p-NIPAM₁₀ but higher (41%) for the lowly cross-linked microgel. Therefore, the loaded amount of Au-NPs decreases with increasing cross-linker content. Polymerization with a low amount of cross-linker leads to a more flexible and less narrow polymer network compared to a high content of MBA. Due to the fact that diffusion of Au-NPs in a more flexible structure is favored a higher number of Au-NPs is embedded within p-NIPAM_{0.25}.

Furthermore, the TEM images show that the Au-NPs seem to be located in the outer part of the microgel network in case of p-NIPAM₅ and p-NIPAM₁₀. This suggests that the transport of the gold particles into the core of the microgels is hindered due to blocking of the microgel pores. Access to the centre of the microgels is controlled by the cross-linker density, which is responsible for the mesh size distribution within the microgel particles. In contrast, the TEM images of p-NIPAM_{0.25} show that the Au-NPs are distributed throughout the microgel particles.

To receive more information on this issue, the samples were measured with UV-Vis spectroscopy (figure 4.4a1, 4.4b1 and 4.4c1). It is shown that compared to the spectrum of bare Au-NPs (figure 4.3c), the localized surface plasmon resonance is red shifted by ≈ 10 nm to 535 nm at low temperatures, where the p-NIPAM particles are in the swollen state. It is well-known that an increase in the refractive index leads to a shift of the plasmon resonance towards higher wavelengths. This red shift is attributed to the increase in the local refractive index of the environment in the presence of p-NIPAM chains. The plasmon resonance of the Au-NPs is very sensitive to changes in the dielectric environment. Hence, the observed shift of ≈ 10 nm indicates a strong interaction between the Au-NPs and the polymer network of the microgels.²¹

If spectra recorded at different temperatures are compared, two effects can

be observed: 1.) The plasmon resonance at 535 nm red shifts with increasing temperature, which is related to a refractive index increase during the microgel collapse. 2.) A shoulder appears at ≈ 675 nm when the temperature increases. The appearance of this absorption band at higher wavelengths can be explained by surface plasmon resonance coupling between individual Au-NPs. If the distance between individual Au-NPs is less than the particle diameter, dipolar coupling shifts the resonance to higher wavelength. Due to the VPT behavior of p-NIPAM, the microgel network collapses with increasing temperature, which significantly decreases the distance between the adsorbed Au-NPs. The spectra show that the absorption maximum at 675 nm decreases in intensity with increasing cross-linker content and that the effect is more pronounced for p-NIPAM_{0.25} (figure 4.4a1) due to its much smaller value of α . In other words the relative volume change induced by temperature is much more pronounced for the weakly cross-linked microgel compared to the higher cross-linked microgels. The spectra of p-NIPAM_{0.25} at higher temperatures are hence a superposition of the spectra of individual Au-NPs and aggregates of Au-NPs present in the microgel. Due to the rather low loading density these aggregates are assumed to be almost exclusively pairs of Au-NPs.

The strong plasmon coupling measured by UV-Vis spectroscopy implies nearby Au-NPs. In contrast, the Au-NPs seem to be homogeneously distributed within p-NIPAM_{0.25} particles on TEM images. In Table 4.4 the interparticle spacing is shown for the swollen and collapsed state assuming homogeneously distributed particles. The interparticle spacing is much larger than the particle diameters and strong NP coupling should not be evident, even in the fully collapsed state.

Table 4.4: Average distance of Au-NPs within the microgel network for p-NIPAM_{0.25} for the low loading regime assuming a homogeneous distribution over the entire microgel.

$N_{Au,adsorbed}$	d_{298K} [nm]	d_{323K} [nm]
99	103	49

The results for the low loading regime demonstrate that there is a high affinity of citrate stabilized Au-NPs for p-NIPAM microgels, despite the fact that both the gold and gel particles are negatively charged. This affinity may be attributed to attractive interactions between the nanoparticles and the acrylamide functionalities of the p-NIPAM network as amines are known

to chemisorb strongly to gold metal surfaces. With increasing temperature a strong plasmon coupling can be observed for low cross-linked microgel particles. Such strong effects are expected for higher cross-linked microgel particles by increasing the amount of Au-NPs in the polymer network. This will be treated in the next subsection.

4.2.4 High loading regime

The results obtained by TEM and UV-Vis spectroscopy for hybrid samples in the high loading regime (1133 Au-NPs per p-NIPAM microgel particle) are presented in figure 4.5a1 and a2 for p-NIPAM_{0.25}, in figure 4.5b1 and b2 for p-NIPAM₅ and in figure 4.5c1 and c2 for p-NIPAM₁₀.

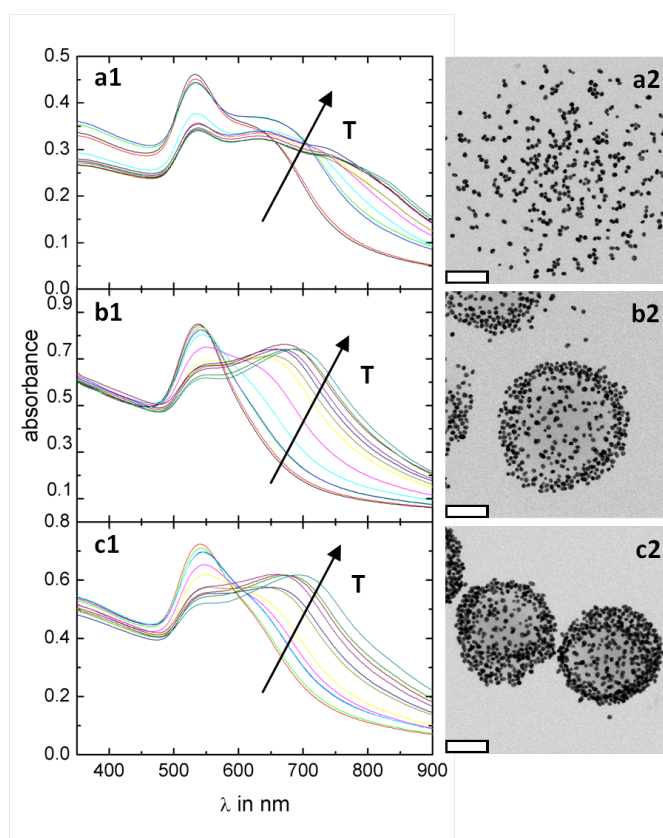


Figure 4.5: UV-Vis spectra and TEM images (scale bar: 300 nm) of p-NIPAM_{0.25} (a1, a2), p-NIPAM₅ (b1, b2) and p-NIPAM₁₀ (c1, c2) for high the loading regime of Au-NPs.

It is shown that increasing the amount of added Au-NPs leads to a higher density of Au-NPs in the polymer network. Therefore, there has to be a high affinity of citrate stabilized Au-NPs for p-NIPAM microgels, despite the

fact that both the gold and gel particles are negatively charged which was already discussed in section 4.2.3. To further prove this assumption, swelling curves of all three systems without Au-NPs and for hybrid samples in the high loading regime were measured using DLS (figure 4.6).

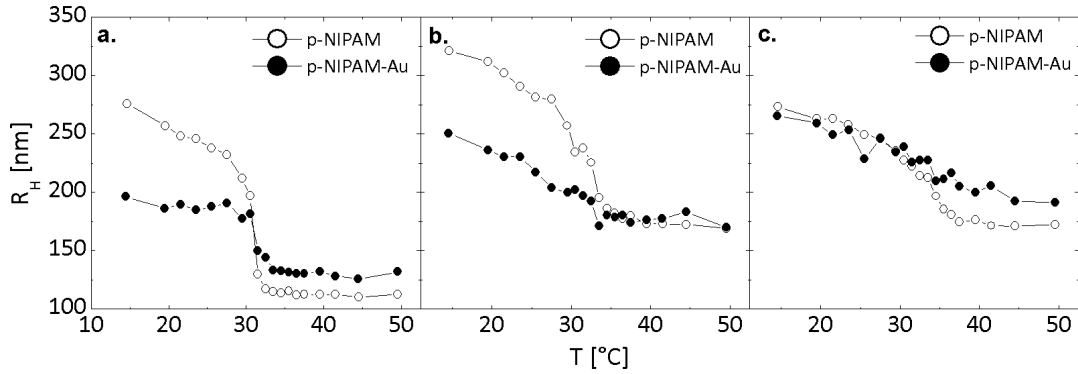


Figure 4.6: Swelling curves of pure $p\text{-NIPAM}_{0.25}$ (a.), $p\text{-NIPAM}_5$ (b.) and $p\text{-NIPAM}_{10}$ (c.) compared to swelling curves after loading with Au-NPs.

It can be seen that the loading of p-NIPAM microgels with Au-NPs has a strong influence on the swelling behavior as well as on the size of the particles. A decrease in hydrodynamic dimensions is most significant for the lowest and the medium cross-linked microgels. These changes are strongly pronounced in the swollen state, e.g. at temperatures below the VPTT of the respective microgels. The decrease in volume demonstrates that the polymer network is contracted due to the encapsulation of the Au-NPs. For the highest cross-linked sample ($p\text{-NIPAM}_{10}$), no change occurs below the VPTT. The Au-NP immobilization was performed at room temperature and hence far below the VPTTs. The low and medium cross-linked microgels are rather elastic and flexible and consequently network deformation is already observed in the swollen state. The sample with the highest cross-linker density is less flexible and therefore the loading of Au-NPs has a minor effect. Burmistrova et. al showed by AFM indentation measurements that the elastic modulus increases with increasing amount of cross-linker.¹²⁰ The Au-NPs partially hinder the particle collapse at the VPTT which leads to a slightly higher final volume of the microgel in comparison to that of the unloaded polymer particles.

Comparing the dimensions of $p\text{-NIPAM}_{0.25}$ from the presented TEM images (figure 4.4a2, 4.5a2) and as obtained by DLS (figure 4.6) a large deviation is observed. TEM images indicate a diameter of more than $1 \mu\text{m}$ while DLS

measurements give a maximum diameter of about 550 nm. The TEM image represents the microgel particles after drying (drop casting) and under high vacuum in the microscopy chamber. The low cross-linker content of 0.25 mol-% leads to a high flexibility in the polymer network and to a strong flattening of the microgel particles during the drying process.

The TEM-images in figure 4.5 clearly reveal a substantially higher degree of Au-NP loading compared to the microgels with less initial Au-NP added (see 4.2.3), as expected. Nevertheless, the TEM images show the same arrangement of Au-NPs in the polymer particles. The NPs are still located in the outer part of the polymer network for p-NIPAM₅ and p-NIPAM₁₀ but in a denser packing. Even for the high loading regime the Au-NPs seem to be distributed throughout the microgel particles in case of p-NIPAM_{0.25}.

Table 4.5 presents the loading efficiency of approximately 30% for the high loading regime. There is a slight decrease in the efficiency compared to the low loading regime (table 4.3) which is an indication for a saturation at high added amounts of Au-NPs. Due to the dense packing of Au-NPs in the microgel particle, the diffusion of additional Au-NPs can be inhibited. Nevertheless, this observed effect is too weak for a strong statement.

Table 4.5: Loading efficiency of the p-NIPAM microgels for high loading regime of Au-NPs.

MBA content [mol-%]	$N_{Au,max}$	$N_{Au,adsorbed}$	$N_{Au,adsorbed}$ [%]
0.25	1133	359	32
5	1133	319	28
10	1133	337	30

The UV-Vis-spectra in figure 4.5 show that even for low temperatures all three loaded p-NIPAM microgel particles possess a shoulder at higher wavelengths than the absorbance maximum at ≈ 535 nm which can be explained by the changing refractive index after adsorption (see 4.2.3). Especially for p-NIPAM₅ and p-NIPAM₁₀, the spectra additionally represent that increasing temperature leads to an increasing intensity of the shoulder at ≈ 675 nm which was also found for the low loading regime. As described in 4.2.3 the shrinking behavior of the loaded microgel particles with increasing temperature is directly related to this shoulder due to plasmon coupling of the Au-NPs. For further investigation the change in intensity (ΔI) at a wavelength of 675 nm was plotted against α (figure 4.7).

It is shown that ΔI increases with decreasing α which is directly related to

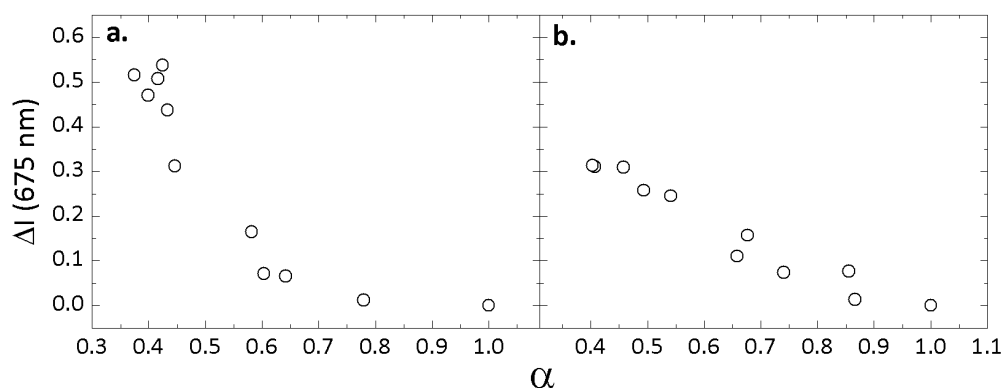


Figure 4.7: Change of intensity at a wavelength of 675 nm during microgel collapse for p-NIPAM₅ (a) and p-NIPAM₁₀ (b).

the decrease in volume. Figure 4.6 makes clear that the nanoparticle loaded microgels with 5 mol-% and 10 mol-% MBA have a less discontinuous VPT compared to the pure microgels. This can be clearly regained in the change of intensity. For p-NIPAM₅ the shoulder at 675 nm increases weakly for a low decrease in volume (figure 4.7a). If an α of around 0.75 is reached a pronounced plasmon coupling and thus an increase in intensity at 675 nm can be observed. At some point the final volume of the microgel particles and therefore α is reached and the intensity remains more or less constant. In case of p-NIPAM₁₀ (figure 4.7b), α changes more continuous, which can be also seen in figure 4.6c, leading to a temporary linear increase of the shoulder at 675 nm. Here, it is also shown that the achievement of the final volume results in a constant intensity.

To conclude, at high values for α the plasmon coupling is more pronounced for highly cross-linked microgel particles. Due to the fact that in case of p-NIPAM₅ the Au-NPs are able to diffuse deeper into the polymer network and that the adsorbed amount is similar for both polymer particles (see table 4.5), the same number of Au-NPs is situated in a larger area for p-NIPAM₅. Hence, the probability that two Au-NPs become close enough to show plasmon coupling by a weak decrease in volume is higher for highly cross-linked microgel particles.

Whereas the shoulder at ≈ 675 nm appears only at high temperatures for the systems in the low loading regime, in the higher loading regime, the shoulder already appears in the fully swollen state of the microgels at room temperature. This effect is most pronounced for highly loaded p-NIPAM_{0.25}. In this case the distance between adsorbed Au-NPs is already small enough

at room temperature (swollen state) so that plasmon coupling is observed (figure 4.5a1). Hence, the results from TEM images and UV-Vis spectroscopy for p-NIPAM_{0.25} for the high loading regime are also contradictory. As described in 4.2.3 the interparticle spacing was calculated for a homogeneous distribution of Au-NPs within p-NIPAM_{0.25}. The results are shown in table 4.6. The average distance between Au-NPs within p-NIPAM_{0.25} is

Table 4.6: Average distance of Au-NPs within the microgel network for p-NIPAM_{0.25} assuming a homogeneous distribution over the entire microgel.

$N_{Au,adsorbed}$	d_{298K} [nm]	d_{323K} [nm]
359	67	32

determined to be 32 nm even in the collapsed state. Due to the fact that this distance is much higher than the diameter of the Au-NPs no plasmon coupling would be observed for a homogeneous distribution.

Furthermore, a third shoulder appears at around 750 nm at high temperatures which indicates the formation of even larger resonantly coupled Au-NPs.

4.3 Conclusion

By simply mixing dilute microgel dispersions with different amounts of citrate-stabilized gold particles, hybrid microgel systems with different gold contents could be achieved. Increasing the added number of Au-NPs a higher concentration of these NPs within the p-NIPAM microgel networks could be obtained. Independent from the amount of Au-NPs the measured TEM images after loading show that the Au-NPs are situated in the outer part of the polymer network for p-NIPAM₅ and p-NIPAM₁₀. In case of p-NIPAM_{0.25} a homogeneous distribution of the Au-NPs in the polymer network was excluded by calculating the interparticle spacing between Au-NPs after loading. Due to the different reaction kinetics of the cross-linker MBA and the monomer NIPAM, it is expected that the microgel particles have a rather pronounced radial gradient of cross-links.¹²¹ The access of Au-NPs to the center of the microgel particles is controlled by the cross-linker density which determines the mesh sizes in the polymer network. This results in a deeper penetration depth of Au-NPs for loosely cross-linked polymer particles which is demonstrated in figure 4.8a and b. During the mixing process the citrate stabilized Au-NPs are able to diffuse rather freely in and out of the polymer network

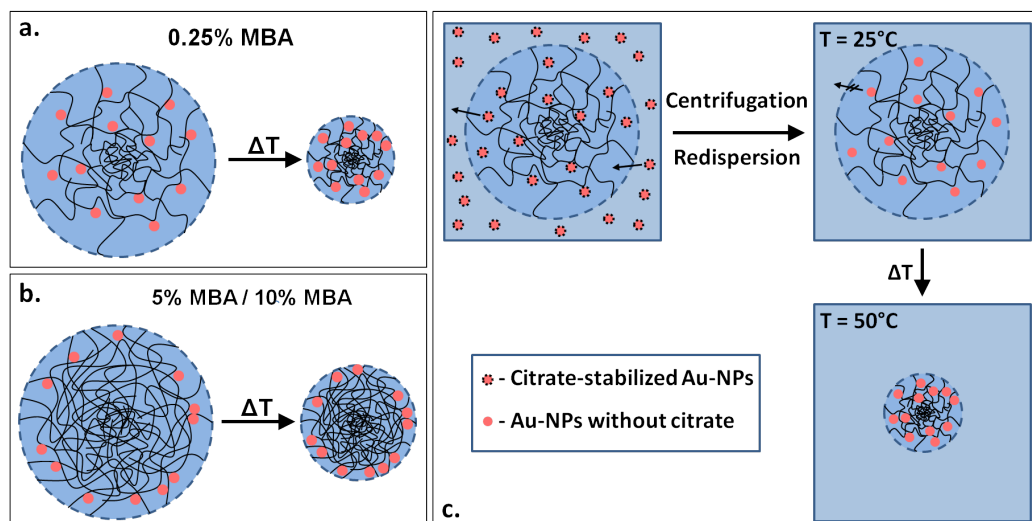


Figure 4.8: Effects of cross-linker concentration on the distribution of Au-NPs in the microgel during collapse (a,b) and schematic process during loading with Au-NPs.

but the maximum penetration depth is limited by the mesh size. Therefore, the loading of Au-NPs within p-NIPAM microgels can be used to get information on the structure. Here, one can roughly estimate that the mesh size in the outer regions is 18.5 nm at minimum since the Au-NPs can be embedded within the polymer network.

In contrast to other studies in literature, the presented work shows a strong adsorption of spherical Au-NPs without using covalent attachment.^{19,21} These strong interactions between the polymer network and the Au-NPs are confirmed by the Au-free areas around the microgel particles on TEM images which proves that no leakage of the Au-NPs occur. Additionally, a strong effect on the swelling behavior is obtained after loading with Au-NPs which was not determined in other studies.¹⁹ The reason for the strong interactions although both components are negatively charged is related to a ligand exchange from citrate to the polymer chains. The centrifugation during the loading procedure supports the removal of the citrate which is located at the surface of the Au-NPs (figure 4.8).

An increase in temperature above the VPTT leads to a partial aggregation of the metastable Au-NPs which is more pronounced for microgels with a low content of MBA. Compared to studies in literature, the presented system can be used to precisely adjust the distance between the Au-NPs by increasing the temperature. Therefore, the received plasmon coupling leads to a controllable tuning of the absorption wavelength. In contrast to many

studies in literature, where the hybrids are investigated regarding the photothermally driven VPT, the plasmon coupling is obtained by an increase in temperature.¹⁹

To create microgels with homogeneously distributed nanoparticle dopants, it may be necessary to reduce their size to facilitate deeper diffusion into the microgel interior. Controlling the polymer-particle interactions by electrolyte screening or pH may also enable the particles to penetrate further into the core of the gels. However, a temperature sensitive absorption behavior is a promising approach for sensor applications.

5 Immobilization of enzymes within p-NIPAM microgels

Parts of the measurements using Bradford reagent were performed by Nora M. Konnertz from TU Berlin under the supervision of Kornelia Gawlitza. A large part of the experimental work of section 5.4 was done by Nora M. Konnertz during her Vertiefungspraktikum at TU Berlin in 2011. The basic concept and planning of this part was done by the author of this PhD thesis.

5.1 Introduction

In the last decades, application of enzymes in technical processes has been grown tremendously leading to a strong competition between biocatalysts and chemical catalysts. Beside the mild conditions during reactions, one of the most important advantages of biocatalysts is their high chemo-, stereo- and regioselectivity.^{122,123} Enzymes are able to produce chiral building blocks with an enantiomeric purity of $\geq 99\%$ which is of great importance for the production of pharmaceuticals. For the application in industrial processes it is necessary that the used enzymes are stable at high temperatures, at different pH values and in the presence of organic solvents. To achieve this stability as well as recyclability and high catalyst density many methods have been developed, among them immobilization.⁸³

Since immobilization also improves the handling of the catalysts during their application in synthesis, it has grown into an important and challenging research field. By definition, the methods are divided into two main categories. The first one is the immobilization by attachment where either macroscopic insoluble aggregates are formed by linking the biocatalysts to each other (cross-linking) or by binding them to the surface of an organic

or inorganic support (adsorption, covalent binding). The second category is entrapment which involves encapsulation in semi-permeable membranes and embedding into a matrix.⁸³ For attachment as well as for entrapment microgel particles made of p-NIPAM represent a suitable support. Due to the reversible shrinking above the VPTT the supply of the substrate can be controlled by changing the temperature.

The following subsection shows the immobilization of two model enzymes within p-NIPAM particles by entrapment on the one hand and attachment on the other hand. By applying these different immobilization procedures two biocatalysts working in different solvents were received.

5.2 Determination of enzyme purity

In order to determine the immobilized amount of enzyme, it is necessary to investigate the purity of the used enzymes. Therefore, SDS-Page was performed using a Polyacrylamide-gel (12% MBA) with Coomassie-dye and silver-staining for analysis. Figure 5.1 shows the received images. The investigations were done for CalB as received (figure 5.1a1,b1) and CalB after dialysis (figure 5.1a3,b3) with an expected M_W of 33273 Da¹²⁴ and for HRP as received (figure 5.1a2,b2) with an expected M_W of 44000 Da.

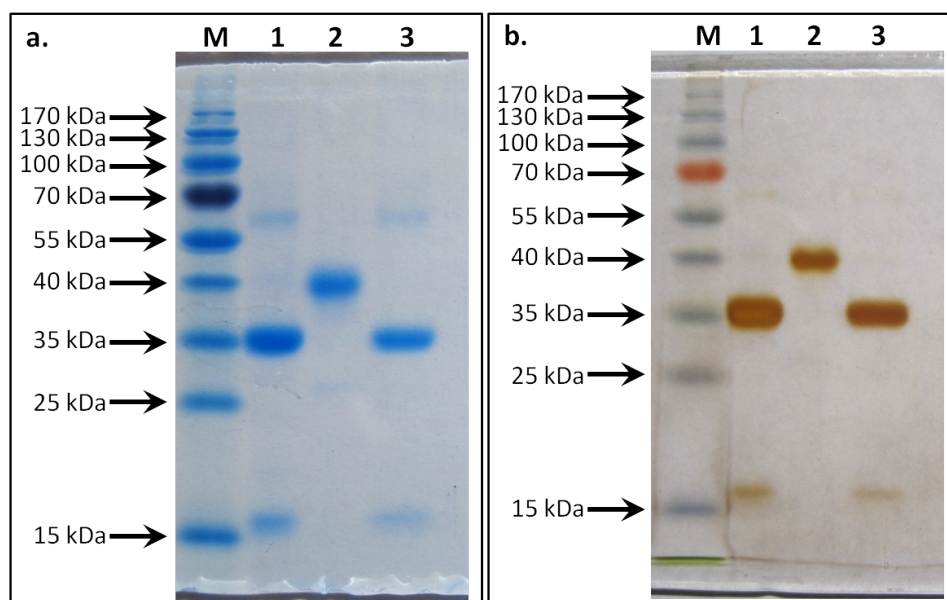


Figure 5.1: Results from SDS-Page after staining with Coomassie-dye (a) and silver nitrate (b) for CalB as received (1), HRP as received (2), CalB after dialysis (3) and the used protein standard (M).

The chromatograms prove that all three samples have a high purity. CalB as received and CalB after dialysis show an intensive band at around 35 kDa after staining with Coomassie-dye as well as with silver nitrate. This M_W is in good agreement with the expected value for CalB. Only a weak staining is visible at around 15 kDa which could be either due to protein fractions from the denaturation process or due to a very small content of proteins with a lower M_W . It is also shown that even after dialysis this band is visible. Due to the fact that, especially in the more sensitive Silver staining, this band is negligible weak in comparison to the band at 35 kDa CalB can be considered to be pure. The investigation on HRP results in an intensive stained band at around 40 kDa which is the only visible band on the chromatograms for this enzyme. The fact that the determined M_W is in good agreement with the expected value proves the high purity of this enzyme. It can be concluded that both enzymes show an acceptable purity for the following immobilizations and investigations on the formed biocatalysts when used as received.

5.3 Immobilization of enzymes by physical adsorption using solvent exchange^{1,2,3}

Especially in chemical synthesis, the usage of organic solvents in enzyme-catalysed reactions is essential to increase the solubility of organic substrates and therefore to improve the formation of the products.¹²⁵⁻¹²⁷ Despite the fact that many substrates and products are rather soluble in organic solvents, many enzymes are soluble in water. The challenge is to design an efficient system, where both compounds are in their suitable environment.

Therefore, enzymes were immobilized by embedding within p-NIPAM microgel particles based on non-specific adsorption using van-der-Waals forces and hydrogen bonds. Due to the reduced contact to the carrier compared to the immobilization by attachment, the residual mobility and flexibility

¹Similar content has been published in Bai, S.; Wu, C.; Gawlitza, K.; von Klitzing, R.; Ansorge-Schumacher, M. B.; Wang, D. *Langmuir* **2010**, *26*, 12980-12987.

²Similar content has been published in Gawlitza, K.; Wu, C.; Georgieva, R.; Wang, D.; Ansorge-Schumacher, M. B.; von Klitzing, R. *Phys. Chem. Chem. Phys.* **2012**, *14*, 9594-9600.

³Similar content has been published in Gawlitza, K.; Wu, C.; Georgieva, R.; Ansorge-Schumacher, M. B.; von Klitzing, R. *Z. Phys. Chem.* **2012**, *226*, 749-759.

of the biocatalysts are much higher.⁸³ There are two other advantages for using embedding in combination with thermoresponsive polymer particles: 1.) Due to non-specific adsorption, the microgel particles can be recycled by exchange the immobilized enzyme against unused enzyme. 2.) The immobilized amount of enzyme can be controlled by temperature.

In the early 1990s the adsorption of proteins onto p-NIPAM microgels was studied intensively.^{128,129} In the following years, the immobilization of enzymes within p-NIPAM particles was investigated in several groups.^{25-28,130} Beside the fact that all of these studies were performed in water, either no enhanced specific activity could be obtained or the localization of the enzyme within the polymer structure was not studied.

In the present work, the immobilization of two enzymes within large p-NIPAM microgel particles by exchanging water against the organic solvents, isopropanol and n-hexane, was studied. The principle is illustrated in figure 5.2.

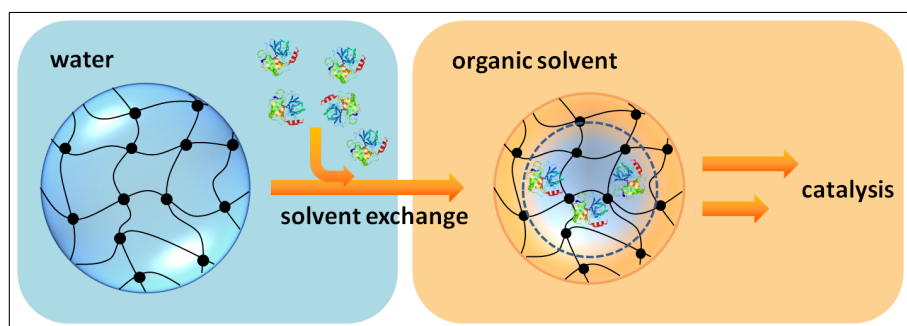


Figure 5.2: Sketch of the immobilization of enzymes within p-NIPAM microgel particles by solvent exchange. The internal structure of the polymer particles was simplified for the sake of clarity.

The immobilized amount of enzyme at different temperatures, the enzyme distribution within the polymer particles, the activity at different reaction temperatures and the reusability of the system applying CLSM and gas chromatography were investigated. In literature, the usage of immobilized systems in organic solvents was either shown for macrogels with no enhanced specific activity¹³¹⁻¹³³ or for reversed micelles where the location of the enzyme was not investigated.¹³⁴ Here, the location of the enzymes was determined and an enhanced activity in organic solvents was reached.

5.3.1 Characterization of large p-NIPAM microgels

Surfactant free emulsion polymerization applying a temperature ramp was used to synthesize large p-NIPAM microgels with a MBA content of 0.25 mol-% (p-NIPAM_{l-0.25}) and 5 mol-% (p-NIPAM_{l-5}).

The size and the shape of the prepared microgel particles were investigated using AFM against air. Figure 5.3 presents an image of one individual particle of p-NIPAM_{l-0.25} and p-NIPAM_{l-5} and the corresponding cross-sections. The measured AFM images show the spherical shape of both synthesized p-NIPAM microgel particles. The diameter in the dried state increases with decreasing cross-linker content leading to a diameter of around 1.4 μm for p-NIPAM_{l-0.25} and around 0.8 μm for p-NIPAM_{l-5}. This decreasing size is in good agreement with the received results by DLS which are discussed below. The height of the polymer particles attached to the silicon surface is similar but taking the different sizes into account the relative height is lower for less amount of cross-linker used for the synthesis. This is related to the more flexible and open structure which leads to a pronounced flattening during the drying process.

In order to investigate the M_W of the synthesized microgel particles SLS measurements were done. A residual water content of around 12 wt% at ambient conditions was determined by Karl-Fischer titration and considered for sample preparation. Due to the larger dimensions of p-NIPAM_{l-0.25} and p-NIPAM_{l-5}, they adsorb a higher amount of water than the smaller microgel particles (see section 4.2.1). A refractive index increment $dn/dc = 0.167 \text{ cm}^3/\text{g}^{119}$ was used for calculation. The received Zimm-Plots for p-NIPAM_{l-0.25} and p-NIPAM_{l-5} are presented in the Appendix (figure A3). The extrapolation of the angle and the concentration to 0 leads to the M_W values which are summarized in table 5.1.

Table 5.1: M_W and zeta potential at 25°C for p-NIPAM_{l-0.25} and p-NIPAM_{l-5} determined by Light Scattering.

MBA content [mol-%]	M_W [g/mol]	ζ [mV]
0.25	$3.0 \times 10^{10} \pm 2 \times 10^9$	-9.9 ± 0.9
5	$5.9 \times 10^{10} \pm 6 \times 10^9$	-21.7 ± 0.9

Additionally, table 5.1 shows the zeta potentials for the microgels to get information on the charge. The zeta potentials are negative due to the initiator KPS used during the synthesis. The zeta potential gets more negative

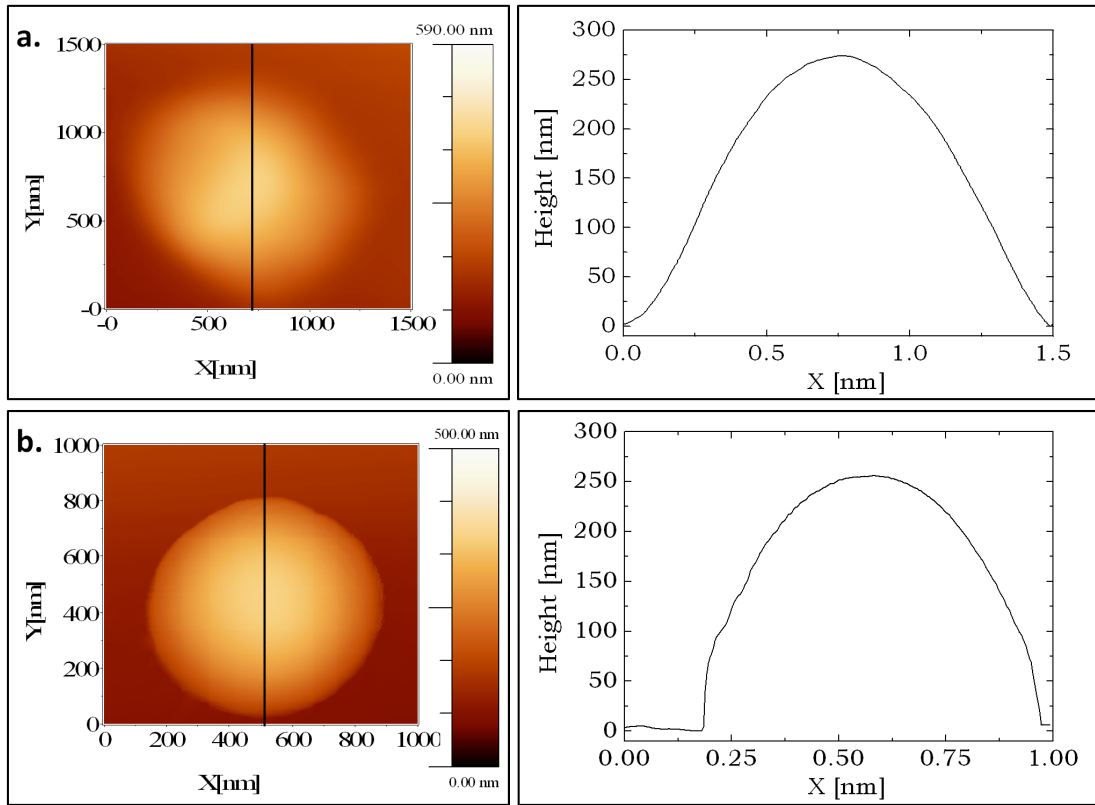


Figure 5.3: AFM images of $p\text{-NIPAM}_{l-0.25}$ (a) and $p\text{-NIPAM}_{l-5}$ (b) measured against air and the corresponding cross-sections.¹⁰⁸

with increasing cross-linker content. This is related to the structure of the microgels which show a denser polymer network in the outer region for increasing amount of MBA. Therefore, the higher cross-linked microgel has more functional groups of the initiator in the outer part of the polymer network in the swollen state leading to this higher zeta potentials measured at 25°C. Note that zeta potentials are rather difficult to interpret for large, gel like particles and hence are only an indication for the charge of the microgels.

The size and the swelling behavior of the synthesized microgel particles were investigated by DLS measurements. Due to the fact that isopropanol is used for the solvent exchange, the measurements were done in water and isopropanol. The R_H values were determined by fitting the correlation functions. The received swelling curves and selected correlation functions including the cumulant fits for the microgel particles in water and isopropanol are presented in figure 5.4.

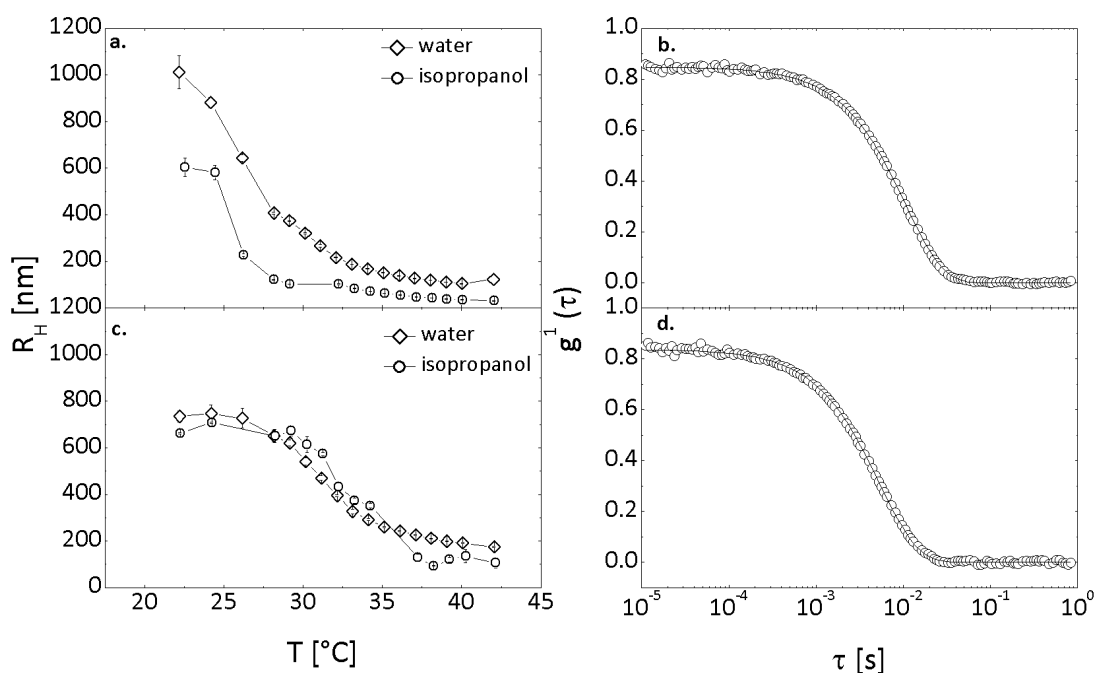


Figure 5.4: Swelling curves of $p\text{-NIPAM}_{l-0.25}$ (a) and $p\text{-NIPAM}_{l-5}$ (c) dissolved in water and isopropanol and correlation functions with cumulant fit for $p\text{-NIPAM}_{l-0.25}$ (b) and $p\text{-NIPAM}_{l-5}$ (d) dissolved in water at 25°C.

Due to the fact that the swelling behavior of the microgel particles is controlled by the connectivity it can be characterized by the deswelling ratio α . All determined hydrodynamic radii in the swollen and collapsed state, the deswelling ratio α and the VPT temperatures of both investigated systems are shown in table 5.2.

Figure 5.4b gives one correlation function of $p\text{-NIPAM}_{l-0.25}$ in water at 25°C leading to a R_H of 881 nm and a PDI of 0.076. This PDI proves the low polydispersity of the synthesized polymer particles. An increase in temperature to 40°C leads to a decrease in R_H to 105 nm. The swelling curve in water shows a VPTT at around 28°C which is about 4°C lower compared to $p\text{-NIPAM}$ microgel particles which are synthesized without temperature ramp.¹³⁵ Meng et. al synthesized $p\text{-NIPAM}$ microgel particles with 0.25 mol-% MBA and acrylic acid as comonomer using the temperature ramp leading to a VPTT of around 31°C.¹⁰² As known from literature, the VPTT of $p\text{-NIPAM}$ with acrylic acid as comonomer is higher than of pure $p\text{-NIPAM}$ particles.¹⁶ The decreased VPTT of the particles synthesized in the presented work are in good agreement with these investigations.

Since later a solvent transfer to isopropanol will be described, the swelling behavior was also studied in isopropanol leading to a R_H of 580 nm at

25°C. The swelling curve of the synthesized microgel particles in isopropanol shows a steep decrease of the R_H to 35 nm at 40°C. The reduced VPTT from 28°C in water to 27°C in isopropanol (see table 5.2) shows that water is a better solvent than isopropanol for this system. A comparison of the microgel particles in water and isopropanol at 25°C leads to a decrease in radius of 300 nm in isopropanol due to the increased hydrophobicity compared to water.

A correlation function for p-NIPAM_{l-5} at 25°C dissolved in water is shown in figure 5.4d. The cumulant analysis of this example leads to a R_H of 727 nm and a PDI of 0.134. This PDI indicates still a low polydispersity of the sample although the p-NIPAM particles with a low cross-linker content of 0.25 mol-% show a much lower polydispersity. The VPTT for p-NIPAM_{l-5} is around 31°C in water which is in good agreement with the results for p-NIPAM in literature.¹³⁵ The increase in temperature to 40°C leads to a decrease in R_H to 175 nm. The cumulant analysis after dissolving the particles in isopropanol give a R_H of 680 nm at 25°C and of R_H of 105 nm at 40°C.

The VPTT for this system is roughly at 33°C. In contrast to p-NIPAM_{l-0.25} a similar VPTT is determined in both environments which reflects that isopropanol is also a good solvent for large microgels with a cross-linker content of 5 mol-%. This different behavior can be explained by a higher content of hydrophobic segments with increasing amount of cross-linker. Therefore, the solubility in the slightly more hydrophobic isopropanol varies. However, p-NIPAM_{l-0.25} as well as p-NIPAM_{l-5} show a suitable size for investigations of the enzyme distribution after immobilization using CLSM.

Table 5.2: R_H , α and VPTT of large p-NIPAM microgel particles with MBA-contents of 0.25 and 5 mol-% in water and isopropanol.

MBA content [mol-%]	R_H at 25°C [nm]	R_H at 40°C [nm]	α	VPTT[°C]
0.25 (H_2O)	881 ± 23	105 ± 2	1.7x10 ⁻³	28
0.25 (iso)	580 ± 31	35 ± 1	2.2x10 ⁻⁴	27
5 (H_2O)	727 ± 42	175 ± 3	1.4x10 ⁻²	31
5 (iso)	680 ± 28	105 ± 21	3.7x10 ⁻³	33

5.3.2 Immobilization of CalB

The first model enzyme is water-soluble CalB which cleaves lipids. These lipids are solely soluble in organic solvents. One effective and well known

strategy is to bring the lipase into a polymer matrix. The advantages of the embedding is given by the fact that the polymer matrix can be dispersed in the organic phase and is permeable for the substrate.

5.3.2.1 Determination of the immobilized amount of CalB. A suitable parameter for the quality of an immobilized system is the specific activity. For the calculation of this value it is necessary to determine the amount of enzyme which is immobilized within the polymer particles. The embedded amount of CalB was investigated using the Bradford assay.

Therefore, three calibration curves have to be measured. At first, different concentrations of pure p-NIPAM in water were measured at 595 nm using UV-Vis spectroscopy. The calibration curve for p-NIPAM_{*l*-0.25} is shown in figure 5.5b leading to the calibration equation

$$abs = 15.84 \cdot c. \quad (5.1)$$

Due to the fact that Bradford reagent is sensitive to nitrogen and p-NIPAM

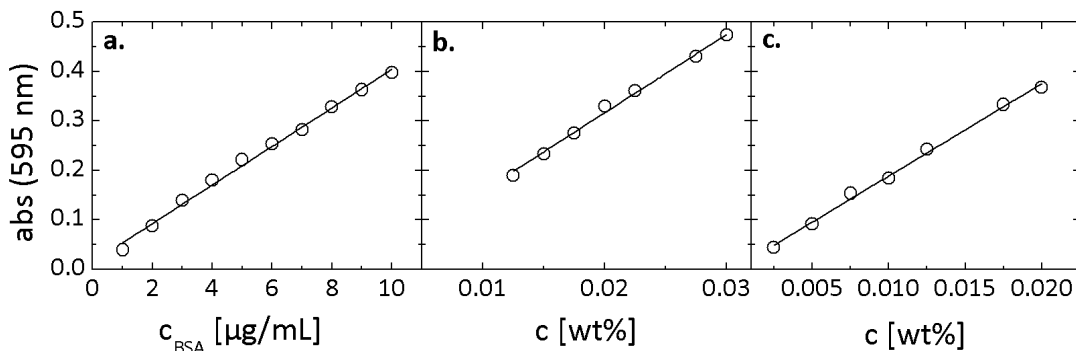


Figure 5.5: Calibration curves of BSA using the Bradford assay (a), p-NIPAM_{*l*-0.25} in water (b) and p-NIPAM_{*l*-0.25} in water using the Bradford assay (c).

microgels contain nitrogen in the polymer network, the influence of pure p-NIPAM on the Bradford assay has to be investigated. Therefore, different concentrations of pure microgel particles in water were measured at 595 nm using the Bradford reagent. The received result for p-NIPAM_{*l*-0.25} is shown in figure 5.5c and leads to the calibration equation

$$abs = 18.70 \cdot c + 0.002. \quad (5.2)$$

The determination of the concentration of an unknown enzyme can be done by using a calibration equation of a known protein with Bradford reagent. Therefore, different concentrations of the protein BSA were mixed with Bradford reagent and measured at 595 nm. The calibration curve is shown in figure 5.5a where the calibration equation is determined to be

$$abs = 0.04 \cdot c + 0.015. \quad (5.3)$$

These three calibration curves were used to calculate the immobilized amount of CalB within p-NIPAM microgel particles. Therefore, the immobilized systems were measured with UV-Vis spectroscopy at 595 nm giving only the absorption of pure p-NIPAM. Using equation 5.1 the microgel concentration in the sample can be calculated. Afterwards, equation 5.2 is used to calculate the correspondent absorption value at 595 nm for pure p-NIPAM with the same concentration in the presence of Bradford reagent. By subtracting this calculated absorption value from the measured absorption of the immobilized sample at 595 nm using the Bradford reagent, the real amount of CalB within the polymer particles can be calculated by equation 5.3. The correspondent calibration curves and equations for p-NIPAM_{l-5} are presented in the appendix (figure A4).

As shown in table 5.1 the M_W of p-NIPAM_{l-0.25} was determined to be 3.0×10^{10} g/mol. Using this M_W and the M_W of CalB (33273 Da¹²⁴) the amount of immobilized CalB per p-NIPAM particles can be calculated.

In order to profit from the thermosensitivity of p-NIPAM particles, the immobilization procedure for the system with 0.25 mol-% MBA was done 1.) at 25°C, 2.) at 50°C before and during the immobilization process and 3.) by heating to 50°C after mixing of CalB and p-NIPAM microgel particles. The schematic process for the immobilization at different temperatures is shown in figure 5.6 and 5.7.

The results for the immobilized amount of CalB for the different immobilization procedures are summarized in table 5.3.

Table 5.3: Adsorbed amount of CalB within p-NIPAM_{l-0.25} particles after immobilization via solvent exchange at different temperatures

T [°C]	m_{CalB} [μ g per mg p-NIPAM]	N_{CalB} per p-NIPAM
25	$6 \pm 1 \times 10^{-2}$	$5.4 \times 10^3 \pm 1 \times 10^1$
50	0	0
50 (after mixing)	14 ± 3.4	$12.6 \times 10^3 \pm 3.1 \times 10^3$

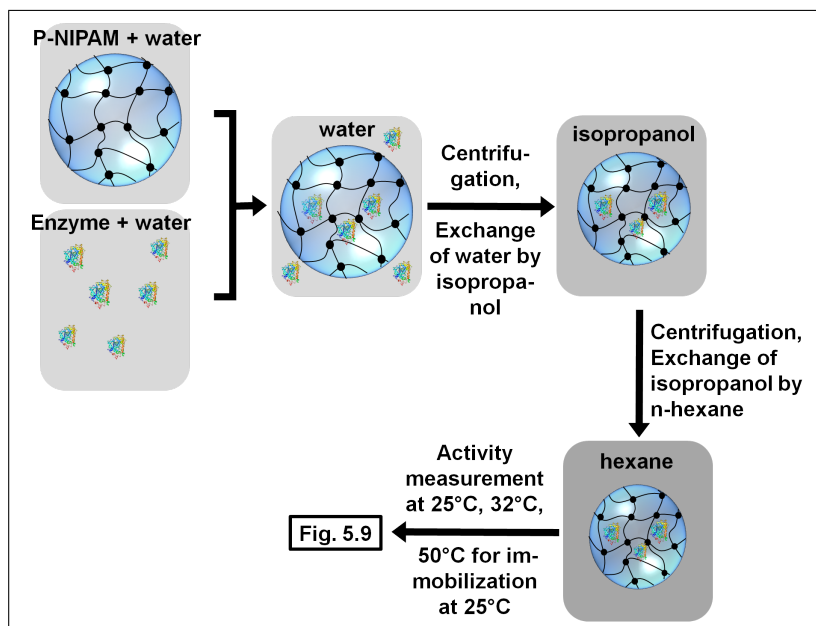


Figure 5.6: Scheme of the process of the immobilization of CalB within p-NIPAM microgel particles at 25°C and 50°C. Due to the fact that after immobilization at 50°C no enzyme is adsorbed, the activity measurement was only performed for the immobilization at 25°C. The internal structure of the polymer particles was simplified for the sake of clarity.

The immobilization at 25°C results in a loading of 5.4×10^3 CalB molecules per p-NIPAM_{*l*-0.25} particle. No enzyme is immobilized when p-NIPAM_{*l*-0.25} and CalB were mixed after increasing the temperature above the VPTT leading to collapsed polymer particles. Due to the denser polymer network the enzyme has no possibility to diffuse into the p-NIPAM_{*l*-0.25} particles. In contrast, the increase of the temperature to 50°C after mixing of enzyme and polymer particles leads to a much higher loading efficiency of 12.6×10^3 CalB molecules per polymer particle. At room temperature the enzyme is diffusing through p-NIPAM_{*l*-0.25} particles. The increase in temperature and the following collapse leads to enzyme entrapment within the p-NIPAM microgel network.

The collapse of the system at 50°C makes the p-NIPAM_{*l*-0.25} microgel particles more hydrophobic. Therefore, water is pressed out of the polymer network while CalB remains inside. By the exchange of water against hot isopropanol the rest amount of water within the microgels is replaced by the more hydrophobic isopropanol. The enzyme is not able to diffuse out of the polymer system due to its size. To investigate the reversibility of this absorption, the system was cooled down to room temperature and washed

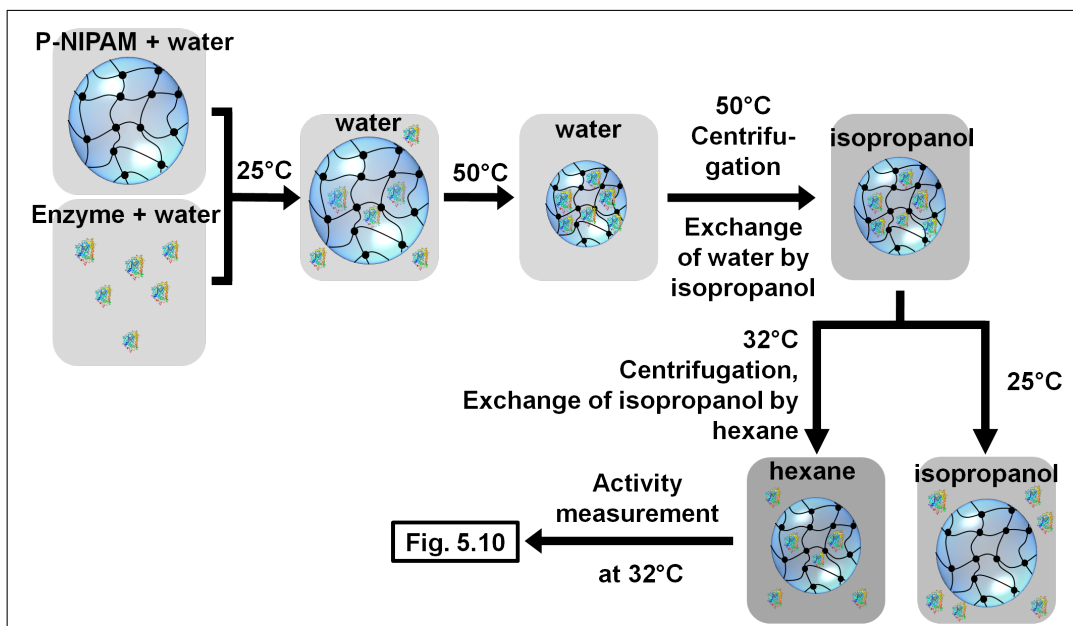


Figure 5.7: Scheme of the process for the immobilization of CalB within p-NIPAM microgel particles by increasing the temperature to 50°C after mixing. The internal structure of the polymer particles was simplified for the sake of clarity.

with isopropanol again. Afterwards, no more enzyme was left within the p-NIPAM_{*l*-0.25} particles, which indicates that CalB diffuses out of the system. By cooling the sample down to room temperature the p-NIPAM_{*l*-0.25} microgel particles swell leading to a larger mesh size and an emersion of CalB. Therefore, no CalB is determined within p-NIPAM_{*l*-0.25}. The dimensions of CalB are supposed to be 3nm x 4nm x 5nm.¹²⁴ Hence, the assumption can be made that the microgel particles have a mesh size below these dimensions in the collapsed state and above these dimensions in the swollen state.

The influence of the cross-linker density on the immobilized amount of CalB was investigated by performing the immobilization procedure for p-NIPAM_{*l*-5} at 25°C. Using the determined M_W of 5.9×10^{10} g/mol (see 5.3.1) and 33273 Da¹²⁴ as the M_W for CalB, an immobilized amount of $5.2 \times 10^3 \pm 7 \times 10^2$ CalB molecules per p-NIPAM microgel particle is determined. The value is in good agreement with the embedded amount found for p-NIPAM with 0.25 mol-% MBA. This leads to the conclusion that the cross-linker content does not influence the loading efficiency. Additionally, the largest mesh size of p-NIPAM_{*l*-5} in the swollen state is above the dimensions of CalB ($> 3\text{nm} \times 4\text{nm} \times 5\text{nm}$ ¹²⁴).

5.3.2.2 Activity measurements on the immobilized system. For catalytic applications, it is required that the enzyme is still active after immobilization within the p-NIPAM matrix. The catalytic activity was determined using an esterification reaction of 1-octanol and octanoic acid in n-hexane with octyloctanoate as a product (figure 5.8). To compare the activity of non-immobilized and immobilized CalB, the same esterification reaction was performed in both systems. One has to take into account that non-immobilized CalB is dissolved in a buffer solution. Therefore, even non-immobilized CalB is surrounded by hydration water even when added to n-hexane.

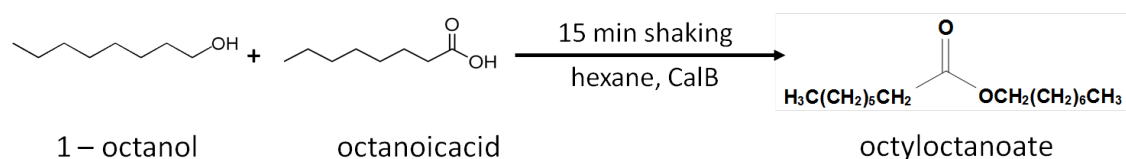


Figure 5.8: Activity reaction for CalB.

At first, the activity of CalB immobilized within p-NIPAM_{*l*-0.25} was investigated. The reaction was performed at 25°C, 32°C and 50°C to investigate if the collapse of the p-NIPAM microgel particles influences the diffusion of the substrate into the polymer particles and the formation of the product by reaction with the enzyme. The specific activity for non-immobilized CalB in n-hexane and immobilized CalB in p-NIPAM_{*l*-0.25} redissolved in n-hexane for the three temperatures is shown in figure 5.9a.

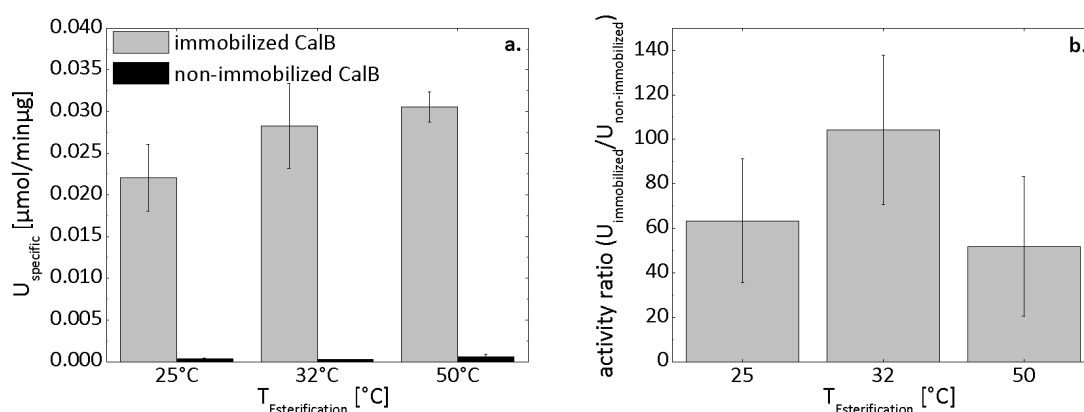


Figure 5.9: Specific activity in n-hexane of non-immobilized and immobilized CalB investigated at 25°C, 32°C and 50°C after immobilization at 25°C within p-NIPAM_{*l*-0.25} (a) and the calculated activity ratio (b).

The immobilization before was performed at 25°C. Accordingly, the specific activity for all three temperatures of immobilized CalB is much higher than for non-immobilized CalB. This enhanced activity can be explained by the more homogeneous distribution of the immobilized enzyme in n-hexane. Due to the fact that CalB is added dissolved in aqueous solution a phase separation occurs after addition to n-hexane which leads to an internal hexane/water interface. The biocatalysis takes place at the enzymes which are located at this internal hexane/water interface. In comparison, the immobilization within p-NIPAM particles creates a much larger total internal interface at which the esterification reaction normally takes place.

Another explanation can be given by the higher density of CalB within the polymer particles compared to the non-immobilized CalB in the reaction solution. The diffusion of the substrate molecules into the p-NIPAM microgel particles leads to an increased collision frequency of enzyme and substrate resulting in a higher concentration of product.

In addition, figure 5.9b shows the activity ratio between immobilized and non-immobilized CalB. Taking the error of the activity measurements into account leads to the conclusion that a temperature change during the esterification reaction of the immobilized system has no pronounced influence on the specific activity. One explanation could be that even at high temperatures the mesh sizes of p-NIPAM with a cross-linker content of 0.25 mol-% are large enough for a diffusion of the substrate into the microgel particles. The activity was also investigated for CalB which was immobilized by increasing the temperature to 50°C after mixing with p-NIPAM_{*t*-0.25} to find out if the higher amount of adsorbed enzyme leads to a higher specific activity (see figure 5.7). The activity reaction was done at 32°C and the results are shown in figure 5.10.

Against one's expectations, here the specific activity is lower compared to the system which was immobilized at 25°C which is supported by the decreasing activity ratio between immobilized and non-immobilized CalB (figure 5.10b). As described before, cooling the system in isopropanol down to room temperature after immobilization leads to a complete emersion of CalB. At the reaction temperature of 32°C the p-NIPAM microgel particles are not in a totally collapsed state which can also lead to an emersion of CalB out of the p-NIPAM matrix. For this case, CalB is existent as non-immobilized CalB in n-hexane. As shown in the presented results the specific activity for non-immobilized CalB in n-hexane is lower than for immo-

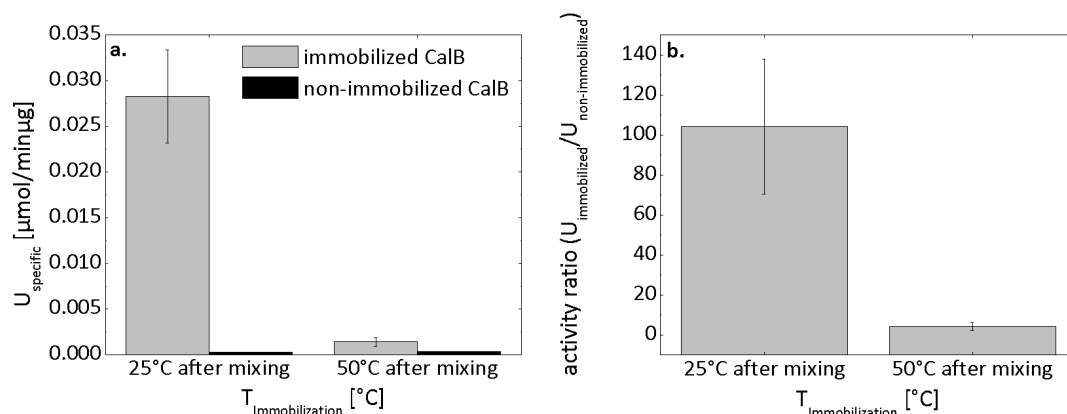


Figure 5.10: Specific activity in *n*-hexane of non-immobilized and immobilized CalB after immobilization at 25°C and 50°C after mixing of CalB and $p\text{-NIPAM}_{l-0.25}$ microgel particles measured at 32°C (a) and the calculated activity ratio (b). For non-immobilized CalB the same temperature treatment was done as for the immobilized system.

bilized CalB which explains the lower specific activity for the system immobilized at 50°C after mixing of the components.

As a next step the stability in *n*-hexane and the reusability of CalB immobilized within $p\text{-NIPAM}_{l-0.25}$ were further investigated. Figure 5.11a shows that the activity decreases by only 10% compared to the starting value within six days.

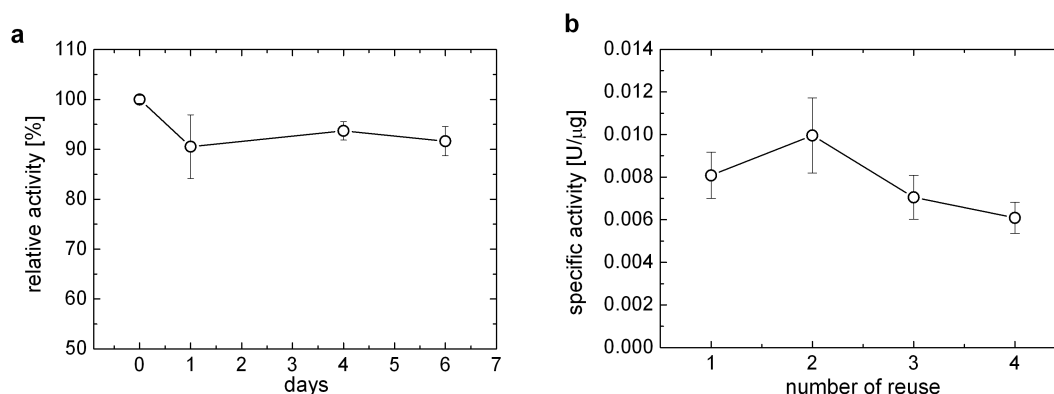


Figure 5.11: Stability of CalB immobilized within $p\text{-NIPAM}_{l-0.25}$ in *n*-hexane (a) and reusability of the system (b).

Interestingly, this decrease is not continuous, but rather occurs at the first measuring point after starting the investigation. This implies that the activity loss is not a consequence of deactivation of the immobilized catalyst, but might be a result of two different populations of CalB after immobiliza-

tion. The first population is fixed within the p-NIPAM particles. The open structure near to the surface of the loosely cross-linked particles leads to a connection of the second population to the polymer particles in this area. The storage in n-hexane leads to a leakage of this second population of CalB.

For catalytic applications the reusability of a system plays also an important role. Figure 5.11b shows a slight increase of the specific activity after the first usage. The catalytic reaction and the washing procedure may affect a folding of the enzyme leading to a better accessibility of the active center. Additionally, it is clearly shown that the immobilized CalB can be used several times with just a slightly decreasing activity.

In order to get information on the influence of the amount of cross-linker on the specific activity, CalB immobilized within p-NIPAM_{l-5} was also investigated after immobilization at 25°C using the esterification reaction (figure 5.8). Therefore, the substrate penetration into the microgel below and above the VPTT was determined by measuring the activity at 25°C and 50°C. Figure 5.12 shows the specific activity at both investigated temperatures of the non-immobilized enzyme and CalB after immobilization within p-NIPAM_{l-5} compared to p-NIPAM_{l-0.25} as well as the activity ratio.

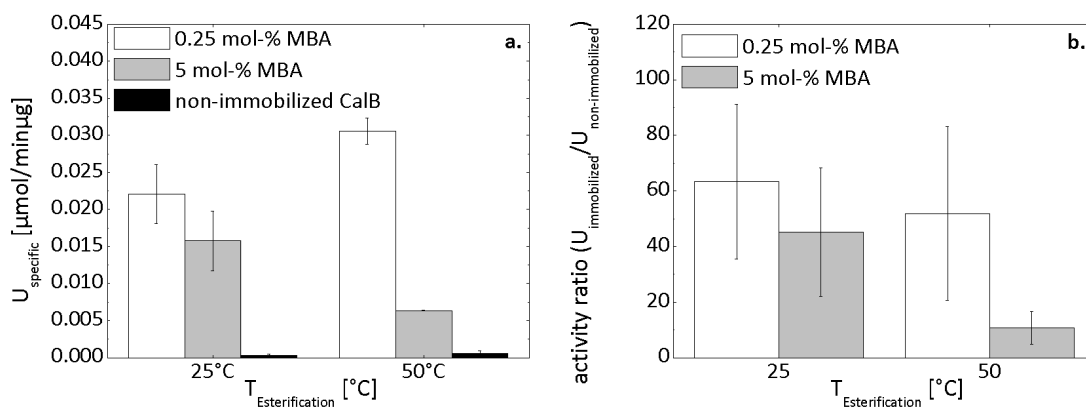


Figure 5.12: Specific activity in n-hexane of non-immobilized and immobilized CalB investigated at 25°C and 50°C after immobilization within p-NIPAM_{l-5} and p-NIPAM_{l-0.25} (a) and the calculated activity ratio (b).

The usage of p-NIPAM_{l-5} leads to a slight decrease in activity at 25°C compared to p-NIPAM_{l-0.25}. Due to the higher density of the polymer network with increasing cross-linker content, the diffusion of the substrate into the polymer particles is decreased. Beside, the substrate is not able to diffuse easily through the denser network which can lead to a decreased collision

frequency. Nevertheless, the system shows still a much higher specific activity than non-immobilized CalB.

Furthermore, the esterification reaction was done below and above the VPTT. As described above, the collapse of p-NIPAM_{l-0.25} has no significant influence on the activity. Using a higher cross-linked p-NIPAM system (5 mol-% MBA) the specific activity decreases clearly by increasing the reaction temperature from 25°C to 50°C (figure 5.12). The shrinkage of the microgel particles by increasing temperature leads to much smaller meshes. Therefore, one reason for the decreased activity could be that the supply of the substrate is partly disabled and the formation of octyloctanoate is decreased. Additionally, the collapsed polymer network leads to a reduced flexibility of the enzyme within the microgel particles which could also lead to a change of the conformation of the active center leading to a disadvantage for substrate binding. p-NIPAM particles offer a suitable matrix to design systems with temperature controlled activity.

5.3.2.3 Localization of CalB within p-NIPAM microgels using CLSM.

In figure 5.11a the specific activity shows a decrease only after the first day. This is an indication for two populations of CalB: 1.) near to the surface and 2.) in the interior of the microgel particles. The activity loss might be related to the desorption of CalB, which is close to the surface, during the storage in the solvent. In contrast, the enzymes which are immobilized within the microgel particles are fixed and show no desorption. In order to look at the location of CalB within the p-NIPAM particles, the enzyme was labeled with FITC before the immobilization procedure. The determined particle sizes for p-NIPAM_{l-0.25} and p-NIPAM_{l-5} allow the application of CLSM for visualization of both microgel particles giving the opportunity to observe the distribution of fluorescently labeled enzyme inside them.

After incubation of the hydrogel particles with FITC-labeled CalB the solution was centrifuged and the p-NIPAM particles were redispersed either in isopropanol or in buffer. Firstly, labeled CalB was immobilized within p-NIPAM_{l-0.25} and the obtained CLSM images of the samples are shown in figure 5.13.

Images a1 and b1 give the fluorescence of the sample and images a2 and b2 reflect the transmission of the sample. Images a3 and b3 display an overlay of the fluorescence and transmission mode and proves whether the fluorescent areas match with the position of the p-NIPAM microgel particles.

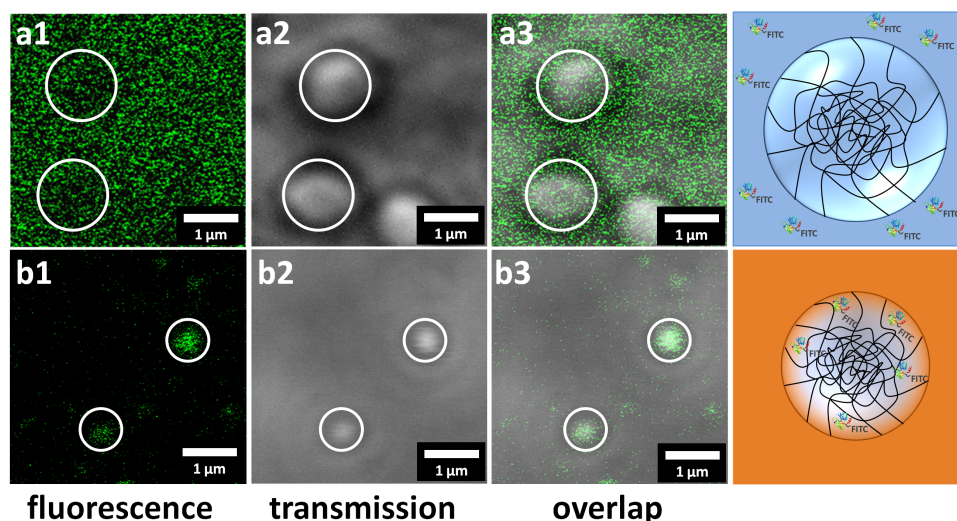


Figure 5.13: CLSM-images of the residue of $p\text{-NIPAM}_{l-0.25}$ after incubation with labeled CalB redispersed in buffer (a) and isopropanol (b) in fluorescence mode, transmission mode and as a super imposed image of both.

The upper series of CLSM-images show the residue after enzyme immobilization and centrifugation redispersed in buffer. Obviously, the fluorescence is distributed over the whole scan area but there also exist some areas with less fluorescence (white circles). These areas fit to the position of the microgel particles shown in the overlay of the first two images. Hence, the labeled enzyme is not located within the $p\text{-NIPAM}_{l-0.25}$ particles but situated outside of the particles.

The lower series of figure 5.13 show the hydrogel particles after redispersion in isopropanol. It can be seen that the measured fluorescence is mainly concentrated at two positions (white circles). The overlay of the fluorescence and the transmission images shows that these fluorescence spots are exactly at the position of the microgel particles which leads to the conclusion that CalB is located within or on the surface of the $p\text{-NIPAM}_{l-0.25}$ particles after solvent exchange.

In order to get information about the distribution of the enzymes, the microgels redispersed in isopropanol were investigated in more detail using the z-stack option of the CLSM. Therefore, the sample was scanned in 18 different x-y-planes with a distance of 50 nm in z-direction between them. Figure 5.14a displays an orthogonal section view of these slices. In the center one of the x-y-planes framed by a blue box is shown. The upper green box frames the x-z-plane of a cut through the sample along the green horizontal line in the central x-y-image. The right hand red framed box represents the

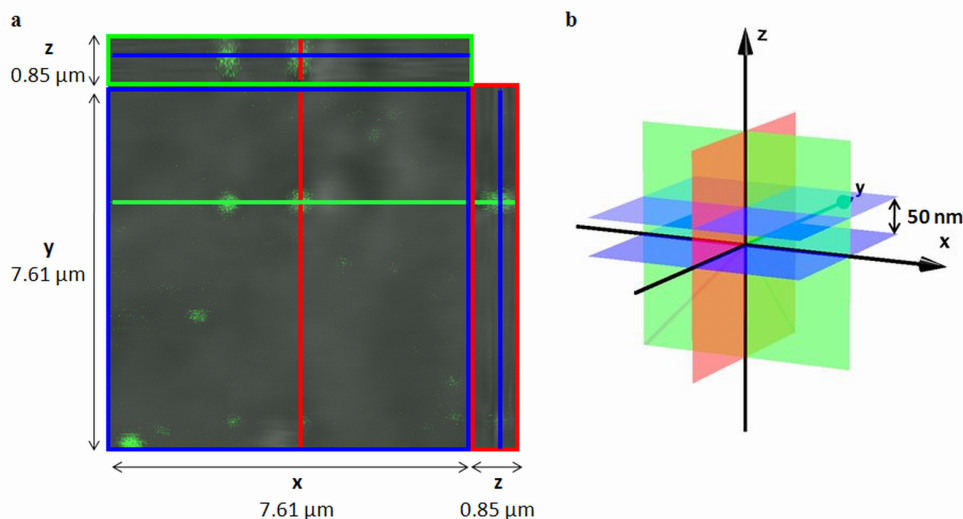


Figure 5.14: Orthogonal section view of one x - y -plane of p -NIPAM _{l -0.25} particles with immobilized CalB after redispersion in isopropanol (a) and schematic explanation of the blue, red and green box (b).

y - z -plane of the cut along the red vertical line. The blue line in the x - z and y - z images represents the z -position of the x - y -plane displayed in the center. Due to the fact that all three planes show a spherically shaped fluorescent object, it can be concluded that CalB is located inside of the particles and not only at the surface.

The distribution of the enzyme between particles and solvent was further observed by CLSM after drying. The sample was dried directly under the microscope and immediately scanned in 23 x - y -planes with 50 nm distance in the z -direction. The orthogonal section view of the z -stack is shown in figure 5.15.

The y - z - and x - z -planes show no more spherical fluorescence images of the particles. Obviously, the labeled enzyme is now located outside of the polymer network, on the top of the dried particles and on the glass surface. To make this more clear separate x - y -scans were analyzed. The fluorescence images and the corresponding intensity profiles for three different z -positions are summarized in figure 5.16. The intensity profiles show that on the bottom of the substrate (scan 6) the fluorescence signal is missing at the particle position. The profile which belongs to a scan through the particle (scan 16) demonstrates that there is no fluorescence signal in the center of the polymer. Going to the surface of the polymer particle (scan 21) leads to a fluorescence signal which fits the particle position. This proves that CLSM is an adequate method to investigate the location of the enzyme

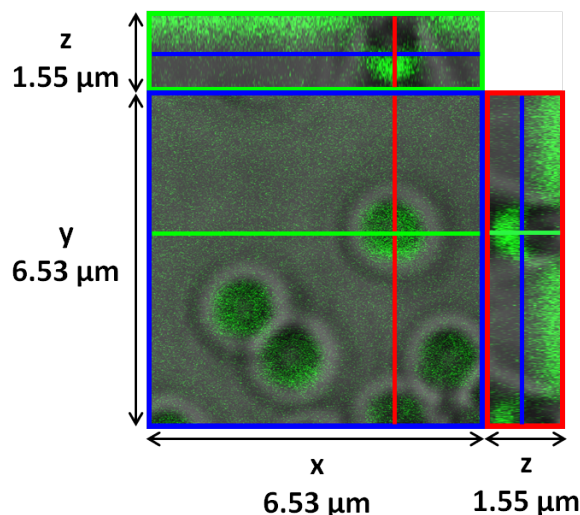


Figure 5.15: Orthogonal section view of $p\text{-NIPAM}_{l-0.25}$ particles with immobilized CalB after drying.

molecules. Probably, the evaporation of the solvent, which is assumed to start at the hydrogel surface, creates a negative pressure (capillary forces) within the hydrogel particles leading to emersion of the enzyme molecules. The release of enzymes by the drying process is an interesting effect which can be used for regeneration of the polymer matrix and reuse by immobilization of unused enzymes.

The immobilization of CalB within $p\text{-NIPAM}_{l-0.25}$ microgel particles by solvent exchange can be explained by the high affinity of CalB to aqueous environment. If the residue is dissolved in buffer, the enzyme can diffuse out of the $p\text{-NIPAM}_{l-0.25}$ microgel particles and mainly stays in the buffer. The exchange of water against isopropanol leads to a decrease of R_h of the $p\text{-NIPAM}_{l-0.25}$ microgel particles from 880 nm to 580 nm at 25°C. Simultaneously, a residual amount of water remains inside the microgel particles and presents a kind of "aqueous cage" for the enzymes. Due to the lower solubility of CalB in isopropanol the enzyme is pressed into the polymer network of $p\text{-NIPAM}$ microgels.

The immobilization of CalB within $p\text{-NIPAM}_{l-5}$ using solvent exchange leads to the CLSM images shown in figure 5.17 in buffer (a) and isopropanol (b). The upper series (in buffer) shows that CalB is distributed over the whole scan range with the exception of some spherically shaped darker areas (white circles). An overlay of the transmission and fluorescence image (figure 5.17a3) proves that these dark areas fit to the position of the microgel particles. This leads to the conclusion that there is no immobilization of

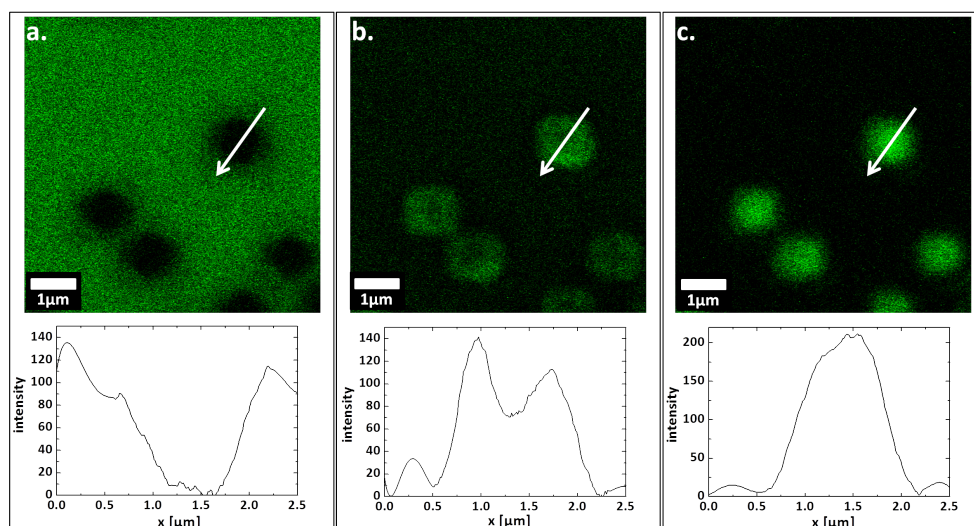


Figure 5.16: Fluorescence images and corresponding profiles of scan 6 (a), scan 16 (b) and scan 21 (c) of 23 scans in x - y -plane monitored for p -NIPAM $_{l-0.25}$ particles with immobilized CalB after drying.

CalB in buffer which is in good agreement with the results of p -NIPAM $_{l-0.25}$. The lower series of figure 5.17 presents the CLSM images after redispersion in isopropanol. Against one's expectation, the microgel particles show no fluorescence. Obviously, some fluorescent aggregates are formed in the solution which are totally independent from the position of microgel particles. The mass of these aggregates seems to be so high that the immobilized system is not purified from them after centrifugation during the washing step with isopropanol. The images show that CalB is not immobilized within p -NIPAM $_{l-5}$ microgel particles after labeling with FITC. Due to the fact that CalB is not soluble in isopropanol, aggregates of enzyme molecules are formed after redispersion in isopropanol. Unlabeled CalB shows an enhanced activity in the immobilized system indicating an embedding of the enzyme within the polymer network. The adsorption only at the surface of the microgel particles can be excluded because the enzyme should also be adsorbed at the surface in the case, where it cannot penetrate the microgel. As it can be seen in figure 5.17 there is no enhanced fluorescence on the particles' surface. Hence, the labeled enzyme that is not able to penetrate into the particles is not adsorbed on their surface which is inconsistent with the case of p -NIPAM $_{l-0.25}$ (figure 5.11a). An increase in the amount of MBA leads to a higher connectivity and denser polymer network also in the outer region of the microgel particles. Therefore, CalB is not adsorbed near to the microgel surface in case of p -NIPAM $_{l-5}$.

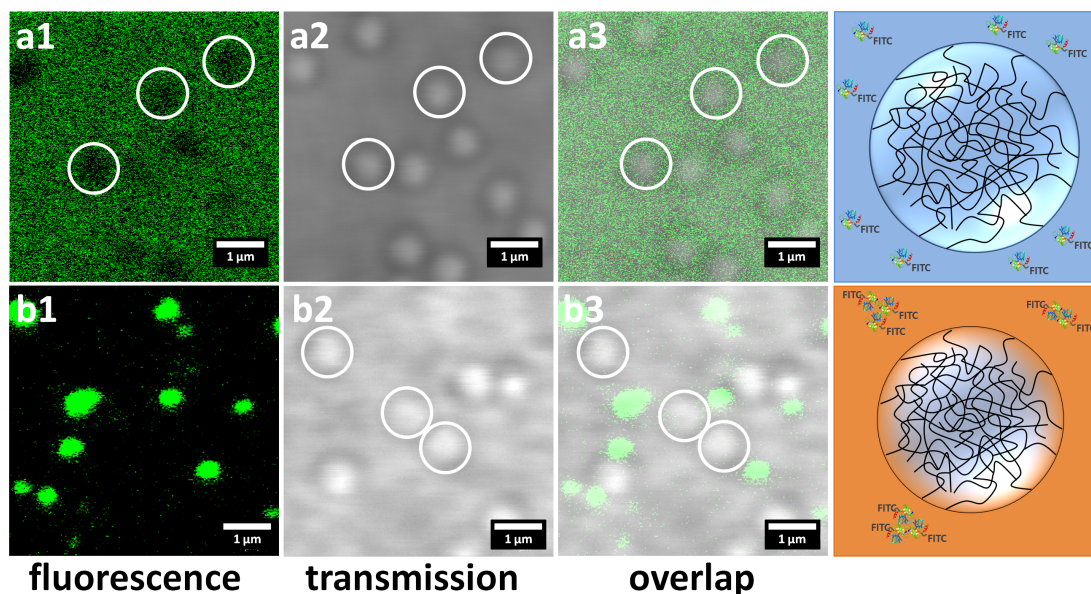


Figure 5.17: CLSM-images of the residue of $p\text{-NIPAM}_{l-5}$ after incubation with labeled CalB redispersed in buffer (a) and isopropanol (b) in fluorescence mode, transmission mode and as a super imposed image of both.

To summarize, without FITC-labeling CalB is small enough to enter into the swollen microgel particles. After labeling the FITC-CalB seems to be too large for penetrating the $p\text{-NIPAM}_{l-5}$ network. Since CalB does not show any strong interaction with $p\text{-NIPAM}$ itself, this result allows an estimation of the mesh size of the polymer network.

The size of CalB is supposed to be 3 nm x 4 nm x 5 nm.¹²⁴ As determined by UV-Vis spectroscopy the average number of bounded FITC molecules per CalB molecule is 1.5. Due to the fact that no labeled enzyme is immobilized within the polymer particles, even CalB with one FITC molecule attached is not able to diffuse inside of the $p\text{-NIPAM}_{l-5}$ network. The largest molecular axis of FITC is 0.7 nm. That means the largest axis of FITC-CalB can be up to $(5 + 1 \times 0.7)$ nm = 5.7 nm. From literature it is known that $p\text{-NIPAM}$ microgels consist of an inhomogeneous network with larger meshes in the outer part¹²¹ which are probed with the described technique. That means that the largest mesh sizes in the outer part of the swollen gel (5 mol-% MBA) are between 3 nm (shortest axis of CalB) and ≈ 6 nm (longest axis of FITC-CalB). According to the temperature sensitive catalytic activity the shrunken gel (5 mol-% MBA) has to have a largest mesh size below 1 nm (longest axis of the substrate) or the mesh sizes are at least close to this value and lead to a reduced mobility of the substrate. In contrast to this

result the largest mesh size of the swollen gel with 0.25 mol-% MBA is well above ≈ 6 nm and the shrunken gel has a largest mesh size below ≈ 5 nm but above 1 nm.

Although the labeled CalB is not immobilized within p-NIPAM_{*l*-5}, the immobilization of unlabeled CalB has been clarified. As described above the assumption is that a residual amount of water remains within the microgel particles after exchange of the solvent. This kind of "aqueous cage" is supposed to be the driving force for the enzyme to stay within the polymer matrix. To support this assumption Karl-Fischer titration was used to determine the water content within p-NIPAM microgel particles after solvent exchange. Due to the fact that p-NIPAM is stored under ambient conditions there is also water left in the dried polymer particles. To exclude this amount from the determined residual water content after solvent exchange, the same experiments were done for "dry" microgel particles. Table 5.4 summarizes the determined water contents of p-NIPAM_{*l*-0.25} and p-NIPAM_{*l*-5} in dried state (ambient conditions) and after solvent exchange. There is a

*Table 5.4: Water contents of p-NIPAM_{*l*-0.25} and p-NIPAM_{*l*-5} after freeze drying (ambient conditions), after solvent exchange and amount of water per p-NIPAM microgel particle.*

MBA [mol-%]	c_{H_2O} [wt%] (dry)	c_{H_2O} [wt%] (after se)	m_{H_2O} [g per p-NIPAM]
0.25	12.0 ± 0.9	46.6 ± 2.4	2.32×10^{-14}
5	12.1 ± 0.7	36.7 ± 2.1	3.60×10^{-14}

huge difference in the water contents before and after solvent exchange. This supports the assumption that a kind of "aqueous cage" remains within the polymer network. Due to the high affinity of enzymes to aqueous environments, these results explain the motivation for CalB to stay within the microgel particles.

Additionally, the water content of p-NIPAM_{*l*-0.25} is higher (46.6 wt%) than the value of p-NIPAM_{*l*-5} (36.7 wt%). In order to compare the results, the mass of water per microgel particle was calculated using the determined M_W values (table 5.1). The values are given in table 5.4. For the higher cross-linked polymer particles a higher content of water is found per particle after exchange of the solvent. At room temperature p-NIPAM microgels absorb a very high amount of water. Due to the fact that p-NIPAM_{*l*-5} has a more narrow structure, the exchange of water against isopropanol is more hindered leading to a higher amount of water compared to p-NIPAM_{*l*-0.25}.

5.3.3 Immobilization of HRP

It has been shown that the immobilization via solvent exchange works well for the enzyme CalB leading to an enhanced specific activity. To prove the general application of this method, the same experiments were done for another enzyme, named *horseradish* peroxidase (HRP). HRP uses hydrogen peroxide to oxidize both organic and inorganic compounds. Therefore, it can catalyze a number of synthetically useful conversions, such as asymmetric epoxidations and sulfoxidations.¹³⁶ Due to the fact that reactions can be not only carried out in water but also in nearly anhydrous solvents, it is important to reach a high specific activity and stability after immobilization, for example within a polymer matrix.

5.3.3.1 Determination of the immobilized amount of HRP. In comparison to the immobilization of CalB, HRP was immobilized within p-NIPAM_{*l*-0.25} at 25°C (figure 5.6). After immobilization the embedded amount of HRP was determined using the Bradford assay (see 5.3.2.1). The determined M_W of the microgel and the M_W of HRP (44000 Da) lead to an immobilized amount of 8.1×10^3 HRP-molecules per p-NIPAM_{*l*-0.25} particle. The determined values are summarized in table 5.5 and compared with the results for CalB.

*Table 5.5: Adsorbed amount of CalB and HRP within p-NIPAM_{*l*-0.25} particles after immobilization at 25°C.*

enzyme	m_{enzyme} [μg per mg p-NIPAM]	N_{enzyme} per p-NIPAM
CalB	$6 \pm 1 \times 10^{-2}$	$5.4 \times 10^3 \pm 1 \times 10^1$
HRP	12 ± 2.6	$8.1 \times 10^3 \pm 2 \times 10^3$

The loading efficiency for HRP is much higher than for CalB. The dimensions of peroxidase are supposed to be 6.2 nm x 4.3 nm x 1.2 nm¹³⁷ and thus slightly smaller than for CalB (3nm x 4nm x 5nm¹²⁴). Due to an easier diffusion within the microgel structure for smaller molecules, this could be one reason for the higher immobilized amount of HRP. Additionally, HRP is a metalloenzyme¹³⁸ and consists of a lower number of hydrophobic amino acids, which makes the enzyme more hydrophilic than CalB. Therefore, it has a higher affinity to the remaining aqueous cage inside of the microgel structure after solvent exchange. The presence of this "aqueous cage" has been proven by Karl-Fischer titration (see 5.3.2.3) and is very impor-

tant, especially for HRP which is usually soluble and active only in aqueous environment. Hence, a higher amount of HRP is immobilized.

5.3.3.2 Activity measurements on the immobilized system. In order to get information on the activity of the immobilized system the oxidation of pyrogallol to purpurogallin in the presence of hydrogen peroxide, isopropanol and HRP was used (figure 5.18). The product can be determined by UV-Vis spectroscopy at a wavelength of 420 nm. The activity reaction was carried out for the immobilized and non-immobilized HRP.

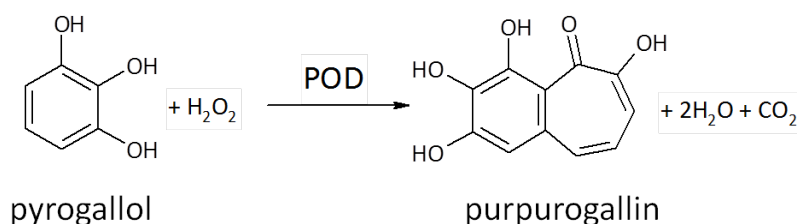


Figure 5.18: Activity reaction for HRP.

Due to the fact that the immobilized amount of HRP in the microgel particles and the amount of HRP in the non-immobilized enzyme is known, the specific activity can be calculated. The results for HRP and CalB are presented in table 5.6.

Table 5.6: Specific activity in [$\mu\text{mol}/\text{min}\mu\text{g}$] of non-immobilized and immobilized HRP and CalB after immobilization at 25°C.

	CalB	HRP
non-immobilized	$3.49 \times 10^{-4} \pm 9 \times 10^{-5}$	$5.55 \times 10^{-6} \pm 1 \times 10^{-6}$
immobilized	$2.21 \times 10^{-2} \pm 4 \times 10^{-3}$	$1.60 \times 10^{-2} \pm 9 \times 10^{-3}$

The results show clearly that a high increase in the specific activity is reached after immobilization of HRP within p-NIPAM_{l-0.25}. This increase is more pronounced than for CalB where the non-immobilized enzyme shows a higher activity than non-immobilized HRP. This can be attributed to the better solubility of non-immobilized CalB in n-hexane than non-immobilized HRP in isopropanol or n-hexane. Additionally, CalB is an enzyme which normally catalyzes reactions with organic substrates and products at the interface between aqueous and organic environment. The investigations emphasize that this immobilization method can be applied to other enzymes leading also to an enhanced specific activity.

5.3.3.3 Localization of HRP within p-NIPAM microgels using CLSM.

The location of HRP within p-NIPAM_{l-0.25} was determined using CLSM in analogy to CalB as described in section 5.3.2.3. The upper series in figure 5.19 shows clearly that there is no FITC-labeled HRP immobilized after re-dispersion in buffer due to the fact that the fluorescence does not match the position of the polymer particles (white circles). The re-dispersion in isopropanol is visualized in series b and proves that the enzyme is located at the same position as the microgel particles.

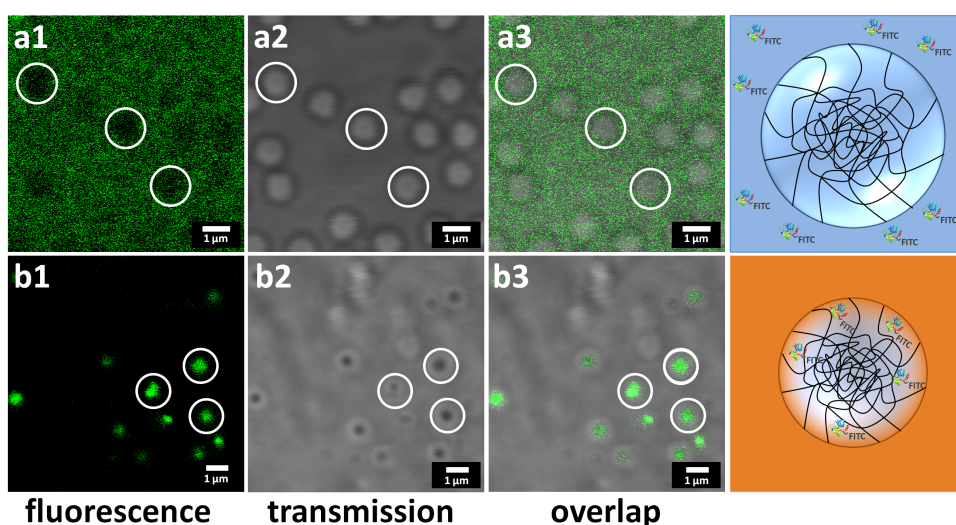


Figure 5.19: CLSM-images of the residue of p-NIPAM_{l-0.25} after incubation with HRP re-dispersed in buffer (a) and isopropanol (b) in fluorescence mode, transmission mode and as a super imposed image of both.

In order to investigate if the enzyme is immobilized within the microgel network and not only adsorbed on the surface, the z-stack option of the CLSM was used. After re-dispersion in isopropanol, the sample was scanned in 32 different x-y-planes with a distance of 50 nm in z-direction between them. An orthogonal section view of these slices is shown in figure 5.20. A precise description of the interpretation of the image is given in section 5.3.2.3. It is shown that there is also a spherical shaped fluorescence signal in all three planes leading to the conclusion that HRP is located within the polymer structure.

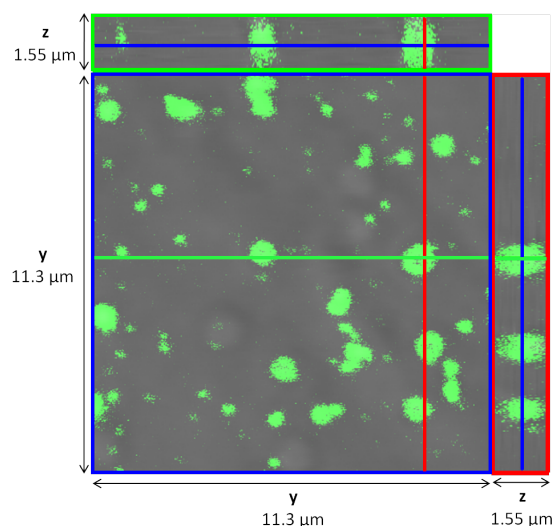


Figure 5.20: Orthogonal section view of one x - y -plane of p -NIPAM_{*l*-0.25} particles with immobilized HRP after redispersion in isopropanol.

5.4 Immobilization of horseradish peroxidase by covalent immobilization using para-benzoquinone

Beside the usage as biocatalysts in organic solvents, it is also important to create systems which show high activity in aqueous environment, e.g. for detergent and food industry.²⁴ The described immobilization by solvent exchange leads to a leakage of the enzymes after transfer to aqueous solution. To overcome this problem the following subsection describes the immobilization within p -NIPAM microgel particles by covalent attachment. Due to its broad application in aqueous environment, e.g. the removal of Chlorophenols from waste water, HRP has been chosen as enzyme.¹³⁹

In literature, the covalent attachment of enzymes is widely used but often leads to a strong reduction of enzyme activity.^{140,141} The usage of coupling agents like aldehydes or esters leads to changes of enzyme conformation or hindrance/delocalization of the active center, thus reducing enzyme activity. Here, the covalent attachment was realized by using p -benzoquinone (BQ) as coupling agent between amine-groups from HRP and from the polymer network.^{86,142}

Due to the fact that the focus of this PhD thesis is on the immobilization of enzymes by solvent exchange, the investigations on the covalent attachment were not finished in the context of the presented work.

5.4.1 Characterization of p-NIPAM-co-AA microgels

In order to get the possibility to covalently bind HRP to p-NIPAM microgels using BQ as coupling agent, it is necessary to produce microgels with amine groups integrated into the polymer network. Therefore, p-NIPAM microgels with 5 mol-% of the cross-linker MBA and 5 mol-% of the comonomer allylamine (AA) were synthesized via surfactant-free precipitation polymerization (p-NIPAM_{AA-5}).

The shape and the monodispersity of the synthesized microgel particles were investigated by AFM measurements against air (figure 5.21). The hexagonal order of the microgels presented in figure 5.21a is a typical order of monodisperse particles. Additionally, a cross-section of one individual polymer particle was done (figure 5.21c, d). The diameter in dried state is around 500 nm but it is also shown that the particle height is only around 35 nm. Therefore, the drying process leads to a flattening and an increase in diameter compared to the particles in solution.

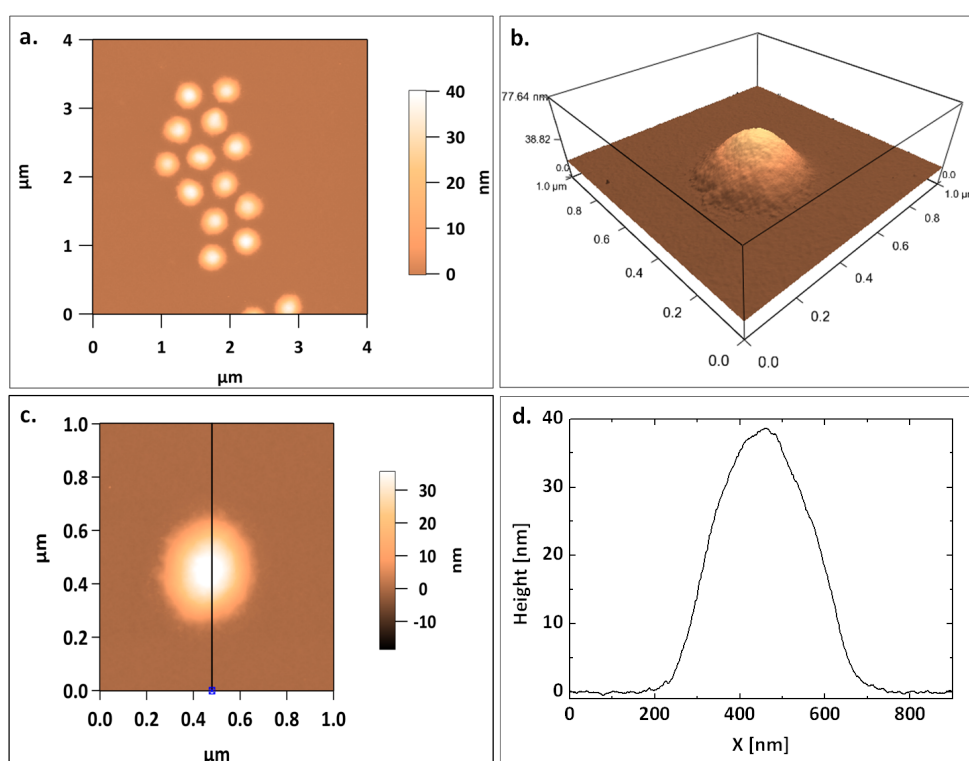


Figure 5.21: AFM images of p-NIPAM_{AA-5} measured against air (a, b, c) and the cross-section of c (d).

The M_W of p-NIPAM_{AA-5} was determined using SLS and Zimm-plot analysis. A residual water content of around 10 wt% which was determined by Karl-

Fischer titration and a refractive index increment $dn/dc = 0.167 \text{ cm}^3/\text{g}^{119}$ were used for calculation. The determined Zimm-plot can be found in the Appendix (figure A5) and the achieved M_W is presented in table 5.7. The lower value compared to $p\text{-NIPAM}_5$ is in good agreement with the smaller size received when AA was used as comonomer.

The size and the swelling behavior of the synthesized microgels was determined using DLS. The measured swelling curve in water ($\text{pH} \approx 6$) and the correlation function including the cumulant fit at 25°C are shown in figure 5.22.

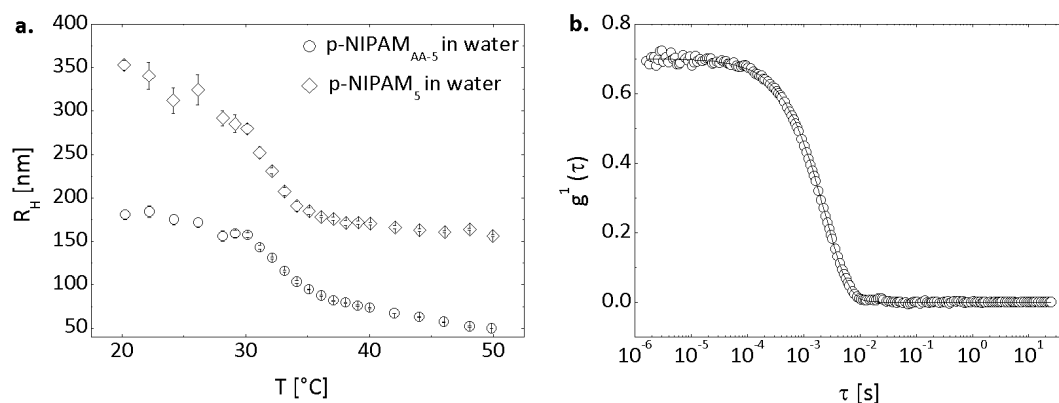


Figure 5.22: Swelling curves of $p\text{-NIPAM}_{AA-5}$ and $p\text{-NIPAM}_5$ from figure 4.1 c (a) and correlation function with cumulant fit at 25°C of $p\text{-NIPAM}_{AA-5}$ (b).

The correlation functions were used to determine R_H . The function shown in figure 5.22b leads to a PDI of 0.112 which proves the low polydispersity of the synthesized microgel particles. The determined R_H values in the swollen and collapsed state, the calculated deswelling ratio α and the VPTT are summarized in table 5.7 and compared with $p\text{-NIPAM}_5$ discussed in section 4.2.1.

Table 5.7: R_H , α , VPTT and M_W of $p\text{-NIPAM}$ microgel particles with 5 mol-% MBA and AA-contents of 0 and 5 mol-%.

mol-% AA	$R_H(25^\circ\text{C})$ [nm]	$R_H(40^\circ\text{C})$ [nm]	α	VPTT [°C]	M_W [g/mol]
0	281 ± 16	173 ± 2	0.23	32	$8.4 \times 10^9 \pm 3 \times 10^8$
5	173 ± 6	73 ± 0.6	0.08	34	$1.5 \times 10^9 \pm 3 \times 10^8$

In order to further characterize the synthesized microgel particles and to prove the presence of the amine groups, zeta potential measurements were done at different pH values and temperatures (figure 5.23a). At a pH value

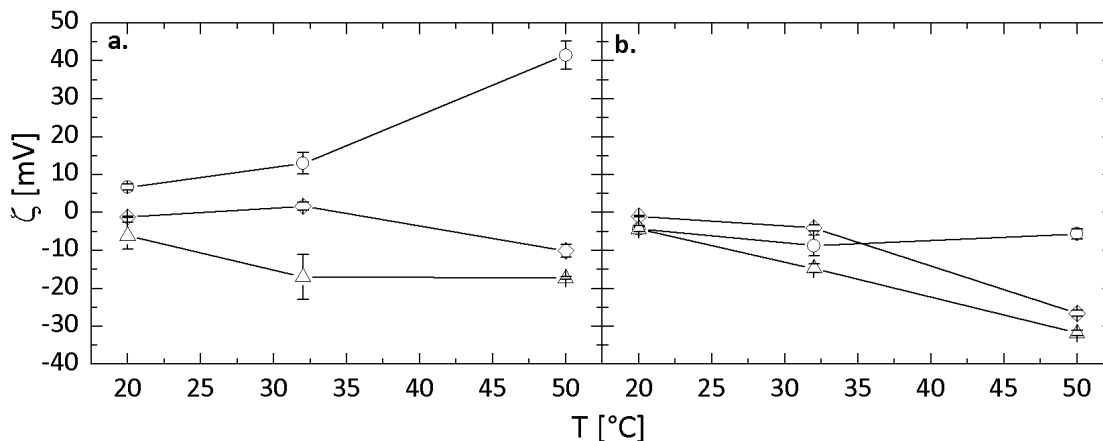


Figure 5.23: Temperature dependance of the zeta potentials of $p\text{-NIPAM}_5$ (a) and $p\text{-NIPAM}_{AA-5}$ (b) at pH 2 (circles), 7 (rhombs) and 12 (triangles).

of 2 the amine groups of the comonomer and the sulfate groups of the initiator KPS are protonated (R-NH_3^+ , $\text{R-SO}_3\text{H}$) resulting in a positive zeta potential. With increasing temperature and the induced VPT the charge becomes more positive. This result proves that the amine groups are situated in the outer region of the polymer network. Changing the pH value to 7 leads to a deprotonation of the sulfate groups (R-NH_3^+ , R-SO_3^-). Therefore, the charges compensate each other and the zeta potential is around 0 mV in the swollen state of the microgel particles. After the temperature induced collapse the negative charges of the sulfate groups predominate and the determined zeta potential becomes negative. A further increase of the pH value to 12 leads to deprotonation of the amine groups (R-NH_2 , R-SO_3^-) and a negative charge even in the swollen state can be obtained. The same zeta potential measurements were performed for pure $p\text{-NIPAM}$ microgels and the results are shown in figure 5.23b. At pH 2 the zeta potential of the polymer particles remains around 0 mV with increasing temperature which proves the protonation of the sulfate groups ($\text{R-SO}_3\text{H}$). Additionally, it has been proven that the positive zeta potential determined for $p\text{-NIPAM}_{AA-5}$ at pH 2 is due to the amine groups integrated within the polymer network. These observations prove that the comonomer AA was successfully integrated within the polymer network during the polymerization.

The assumption that the amine groups are situated in the outer region of the polymer network of $p\text{-NIPAM}_{AA-5}$ can be supported by the swelling curve (figure 5.22a) where two different regions of the shrinking are shown. Above 29°C a strong collapse of the microgel particles is observed. This can be at-

tributed to the shrinking of the inner part of the polymer network where no comonomer is integrated. This temperature is similar to the results of p-NIPAM₅ (figure 5.22a) where no AA was used for the synthesis. The strong collapse is followed by a less steep decrease in size above 36°C. This is related to the shrinking of the outer region of the p-NIPAM microgel particles where the AA groups are situated. The amine groups make this part more hydrophilic and lead to the decrease in size at higher temperatures. Additionally, this is the reason for the increase in the VPTT from 32°C for p-NIPAM₅ to 34°C for p-NIPAM_{AA-5}. Additionally, the determined R_H values (table 5.7) show that the integration of AA as comonomer leads to smaller microgel particles. In contrast, the integration of acrylic acid as comonomer leads to an increase in size due to the increasing electrostatic repulsion between the polymer chains.¹⁴³ The DLS measurements for p-NIPAM_{AA-5} are done at pH 6 where the amine groups are protonated. Hence, the electrostatic repulsion from the negative charged sulfate groups of the initiator is lowered. This leads to a decrease in the hydrodynamic radius. Nevertheless, this effect is not strong enough to lead to a decrease in R_H of 100 nm after synthesis (table 5.7). Acrylic acid forms much more stable radicals than AA. Therefore, AA has a low reaction rate and is integrated at a late point of the polymerization process which supports the assumption of p-NIPAM particles with AA groups situated in the outer region of these microgels. The described structure and swelling behavior is schematically presented in figure 5.24.

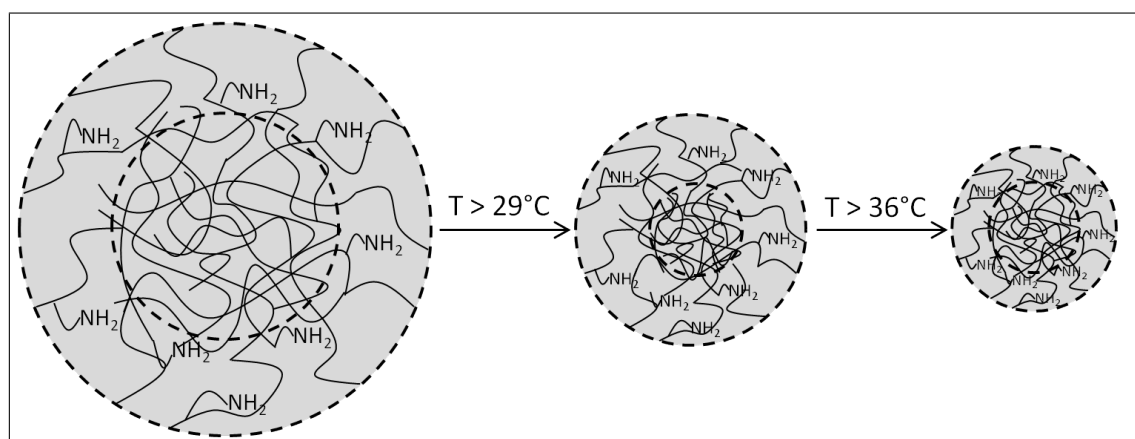


Figure 5.24: Sketch for the structure and swelling behaviour of p-NIPAM_{AA-5}.

5.4.2 Immobilization of HRP using BQ

Due to the fact that HRP shows catalytic activity in aqueous environment it was used for the covalent immobilization within p-NIPAM_{AA-5}. In the first step, the amino groups of the enzyme were used to bind BQ using a Michael-addition. Below, this complex is abbreviated as BQ-HRP. To covalently bind this complex to the microgel particles another Michael-addition was performed leading to p-NIPAM_{AA-5}-BQ-HRP. This coupling is schematically drawn in figure 5.25.

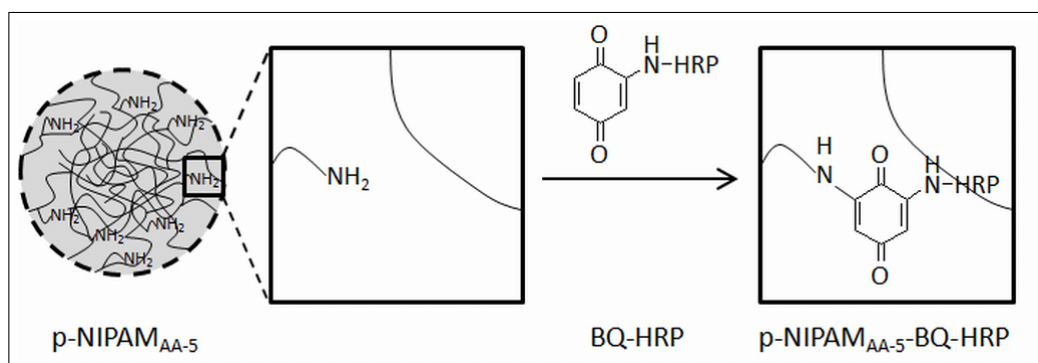


Figure 5.25: Scheme of the covalent immobilization of HRP within p-NIPAM_{AA-5}.

5.4.2.1 Activity measurements on the immobilized system. In order to prove the immobilization of HRP, the catalytic activity of the system was investigated. Therefore, the oxidation of Pyrogallol, which is described in section 5.3.3.2 (figure 5.18), was done in aqueous solution. The colour change of the solution from clear to yellow proves the immobilization of HRP and demonstrates the catalytic activity of the immobilized system (figure 5.26).

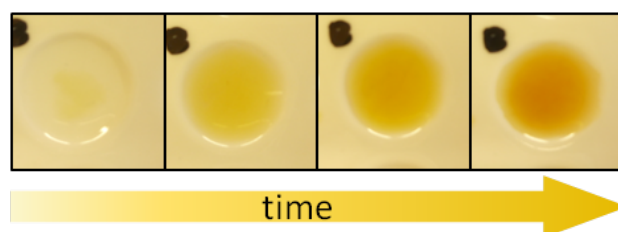


Figure 5.26: Colour change during the activity reaction of p-NIPAM_{AA-5}-BQ-HRP.

The absorption change at 420 nm within 1 minute can be used to calculate

the concentration of the produced purpurogallin. Hence, the catalytic volume activity was determined to be $4.34 \pm 0.3 \mu\text{molmL}^{-1}\text{min}^{-1}$.

The stability of the immobilized system was investigated by storing the samples in buffer solution. The catalytic activity was measured several times during the next 11 days. The same experiment was performed with the non-immobilized HRP. By evaluation of the results as a relative change of the volume activity the stability of immobilized and non-immobilized HRP can be compared. The determined stabilities are presented in figure 5.27.

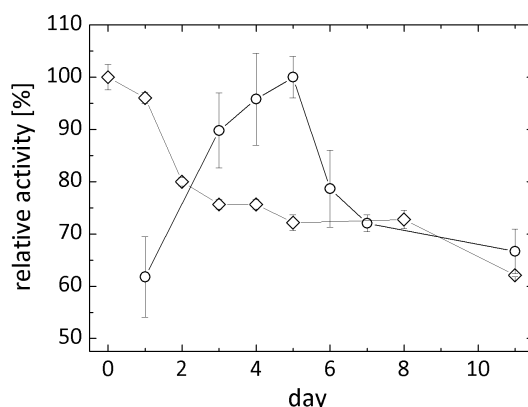


Figure 5.27: Relative stability of $p\text{-NIPAM}_{AA-5}\text{-BQ-HRP}$ (circles) and non-immobilized HRP (rhombs).

Surprisingly, the volume activity of the immobilized system increases within the first days. This could be due to changes in the enzyme conformation by covalent binding to the matrix. By storage in aqueous environment an equilibrium appears and the active center of the enzyme is reachable for the substrates. The maximum activity of the system was measured after 5 days. Afterwards, the activity decreases again reaching a constant value of around 65%. In contrast, the activity of non-immobilized peroxidase decreases strongly during the first days losing roughly 20% of its activity. After day 3 the relative activity slightly decreases further to around 60%. Nevertheless, the immobilized system shows the tendency to be more stable regarding long time stability. To prove this assumption the measurements should be continued after day 11.

5.4.3 Outlook

Although, the stability and the volume activity of the p-NIPAM_{AA-5}-BQ-HRP system has been proven, it is necessary to determine the specific activity for future work. This value can be directly compared to the non-immobilized enzyme which is of huge interest to show further advantages of the immobilized system, especially for industrial application. To calculate the specific activity the immobilized amount of HRP within the microgel particles has to be determined.

In a first attempt, the Bradford assay was used to determine the amount of HRP after covalent immobilization. The idea was to measure a calibration curve of pure p-NIPAM_{AA-5} with Bradford reagent to subtract the absorption value which is produced by the pure microgel from the absorption value after immobilization (see section 5.3.2.1). Due to the fact that p-NIPAM_{AA-5} contains amine groups and the detection of the enzyme concentration via Bradford assay is based on amine groups the measurements led to a huge error. After immobilization the amine groups of pure p-NIPAM_{AA-5} are blocked by the covalently bounded BQ-HRP complexes. This leads to a lower absorption signal of p-NIPAM_{AA-5}-BQ-HRP after subtracting the pure p-NIPAM_{AA-5} than in reality.

To overcome this problem, in a second approach the order of coupling was changed. The idea was to covalently bind BQ to the polymer particles in the first step and to add a known amount of HRP in the second step. Then the amount of immobilized HRP can be calculated by determination of the non-immobilized amount of HRP in the supernatant after immobilization. This experiment failed due to the interparticle reaction of BQ and p-NIPAM_{AA-5}. This led to aggregates of the polymer particles after the first step and no further coupling of HRP could be done.

As conclusion, it is necessary to use a method for determination of the enzyme concentration which is not sensitive to amine groups. Although such methods exist, e.g. determination via fluorescence or absorbance using Amplex Red,^{144,145} they are not included in this PhD thesis and are an interesting approach for the continuation of this project. Due to the fact that the focus of this thesis is on the immobilization by solvent exchange, the investigations on the covalent immobilization were not continued at this point.

Nevertheless, it is shown that covalent attachment of enzymes to microgel

particles by BQ is a promising method to obtain biodegradable catalysts working in aqueous environment.

5.5 Conclusion

Immobilization of enzymes within p-NIPAM microgel particles was investigated to create biocatalysts for the usage in organic and aqueous environment.

The enzymes CalB and HRP were successfully immobilized within large p-NIPAM particles using a solvent exchange from aqueous to organic solvents. Promising catalytic systems working in organic environment were produced which show enhanced activity compared to the free enzyme, high stability and good reusability. The principle of this great method is based on a remaining "aqueous cage" within the p-NIPAM microgels after exchange of the solvent. The high affinity of enzymes to water is the driving force for the immobilization. Another solvent exchange from organic to aqueous solvents can be used to exchange the inactive enzyme against fresh one.

The thermoresponsive behavior as well as the cross-linker density of the microgel matrix are useful to tune the loading efficiency and the activity. A change of the temperature above the VPTT after mixing of the components results in a higher amount of CalB within the p-NIPAM microgels (0.25 mol-% cross-linker) compared to an immobilization at 25°C. In contrast, no entrapment of the enzyme is reached by an increase in temperature above the VPTT before mixing of the components due to the collapsed polymer network.

A tunable supply of the substrate was reached by increasing the amount of cross-linker (5 mol%). By increasing the temperature for the activity reaction above the VPTT a strong decrease in activity was observed. The dependance of the activity on the temperature is a great property to reach systems where a change in temperature leads to either an active or a nonactive biocatalyst.

Compared to other studies in literature^{25,28,130} the localization of the enzymes within the lowly cross-linked polymer structure was determined using confocal laser scanning microscopy (CLSM). Additionally, the immobilization of enzymes is useful to estimate the largest mesh sizes of such polymer particles.

The described immobilization by embedding enzymes in hydrated polymer matrices gives several advantages like a more homogeneous distribution, easier accessibility and easier handling of the enzymes. Furthermore, no chemical adjustment of the polymer matrix is needed for the embedding.

The drawback of the described method is given by the leakage of the enzymes in aqueous solution. As an approach to create a biocatalyst which is active in aqueous environment BQ was used as coupling agent between a p-NIPAM matrix and the enzyme HRP. Although covalent attachment of enzymes often leads to a loss in activity due to structural changes, this procedure leads to an active system in aqueous solvents. The attachment of HRP to a p-NIPAM matrix using BQ is a promising approach to obtain highly active biocatalysts in water which are interesting systems for industrial applications.

The potential to apply these two immobilization methods to other enzymes makes the described procedures promising approaches for creating new biocatalysts, especially for the chemical synthesis in organic solvents (solvent exchange) and detergent industry (covalent attachment).

6 Polyampholyte p-NIPAM-co-AG microgels

6.1 Introduction

The integration of ionic comonomers into the polymer network of microgel particles influences the swelling behavior. These, so called polyelectrolyte (PE) microgels are able to respond to several external stimuli including temperature,¹⁴⁶ pH¹⁴⁷ and ionic strength.¹⁴⁸

When PE microgels contain both cationic and anionic groups they are called Polyampholyte (PA) microgels.²⁹ These systems have the properties of PE microgels but can also show a very different behavior compared to monoionic polymer particles. These properties make them interesting for basic research. The presence of opposite charges lead to multiple interactions which can act simultaneously or compete against each other within the microgel interior. This behavior makes them highly interesting and therefore many studies focused on the synthesis and investigation on the stimuli-responsive properties of PA microgels.^{30,31}

So far, two different comonomers, one cationic and one anionic, were added to receive opposite charges within the polymer network.^{32,33} Due to the different polymerization kinetic of the comonomers the used ratio has to be modified to obtain PA microgels with balanced charges. Their stimuli-responsive properties make PA microgels useful in a broad range of applications, such as sequestration of gold nanoparticles,¹⁴⁹ drug delivery^{150,151} and gene delivery.¹⁵²

In contrast to the other studies in literature, the work presented in this chapter is based on the usage of one amphoteric comonomer. PA microgels were prepared by integrating allylglycine (AG) into the polymer network. The

structure of this comonomer is based on the amino acid glycine which consists of neighbored amine and carboxy groups. The pH dependant charge of the functional groups within the polymer particles is schematically shown in figure 6.1.

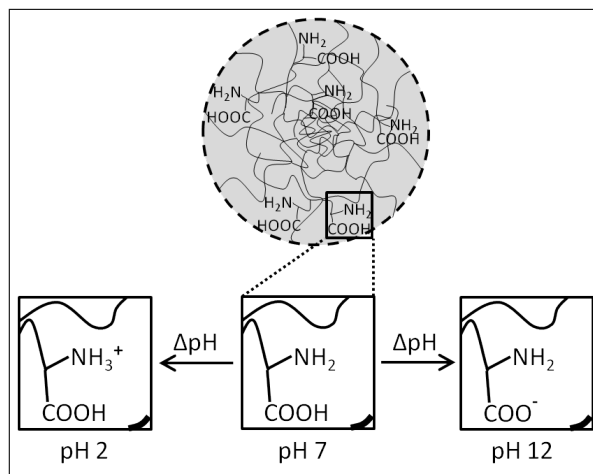


Figure 6.1: PH dependant charges within p-NIPAM microgel particles using AG as comonomer.

AG has the same basic structure as an amino acid which makes this PA microgels a promising system for the immobilization of enzymes. The point where AG has an overall neutral charge (isoelectric point (IEP)) is approximately at a pH of 5.9. Due to the fact that enzymes also consist of amino acids there is a high affinity for building hydrogen bonds to the AG groups within the polymer network. The presented study focuses on the influence of the concentration, pH and amount of AG on the swelling behavior. It is shown that defined aggregates of PA microgels can be formed and separated by changing different external stimuli.

6.2 Results and Discussion

6.2.1 Characterization of p-NIPAM-co-AG microgels

In the present work, balanced PA microgel particles ($N_{COOH} : N_{NH_2} = 1:1$) were received by integrating the comonomer AG within the polymer network. Therefore, two microgels were prepared by surfactant-free precipitation polymerization using a cross-linker content of 0.25 mol-% and a comonomer content of 3 mol-% (p-NIPAM_{AG-3}) on the one hand and 25 mol-% (p-NIPAM_{AG-25}) on the other hand. The size and the swelling behavior of

the synthesized particles dissolved in water were investigated by DLS measurements. The received swelling curves are presented in figure 6.2.

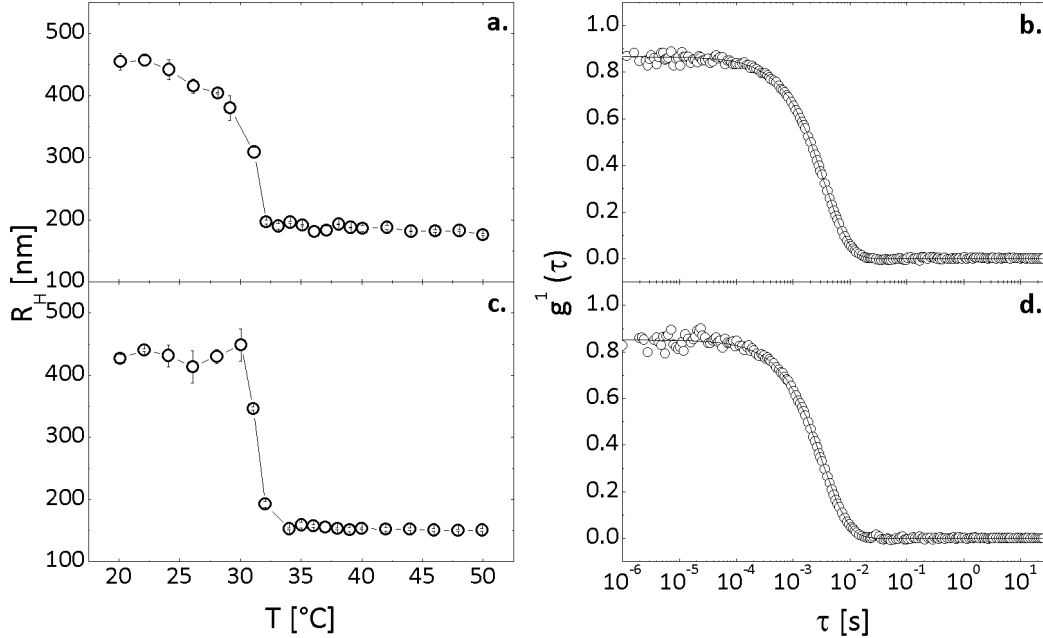


Figure 6.2: Swelling curves of $p\text{-NIPAM}_{AG-3}$ (a) and $p\text{-NIPAM}_{AG-25}$ (c) and correlation functions with cumulant fits at 25°C for $p\text{-NIPAM}_{AG-3}$ (b) and $p\text{-NIPAM}_{AG-25}$ (d) dissolved in water.

The R_H values were determined by fitting the received correlation functions. One correlation function with the cumulant fit for each synthesized sample is given in figure 6.2. This leads to a PDI of 0.024 for $p\text{-NIPAM}_{AG-3}$ (figure 6.2b) and 0.042 for $p\text{-NIPAM}_{AG-25}$ (figure 6.2d) supporting the low polydispersity of the synthesized polymer particles. All characteristic values obtained from DLS measurements are summarized in table 6.1. As comparison to pure $p\text{-NIPAM}$ with the same cross-linker amount, the obtained results from section 4.2.1 were added to the table.

Table 6.1: R_H , α and VPTT of $p\text{-NIPAM}_{0.25}$, $p\text{-NIPAM}_{AG-3}$ and $p\text{-NIPAM}_{AG-25}$.

AG content [mol-%]	$R_H(25^\circ\text{C})$ [nm]	$R_H(40^\circ\text{C})$ [nm]	α	VPTT [°C]
0	238 ± 11	112 ± 2	0.10	31
3	428 ± 11	186 ± 5	0.08	31
25	422 ± 17	153 ± 1	0.05	32

As expected, the synthesized microgel particles show a thermoresponsive behavior with a decrease in the R_H values with increasing temperature. A

nearly discontinuous shrinking can be observed for both types of prepared polymer particles. The same behavior was found for pure p-NIPAM with the same amount of cross-linker integrated into the polymer network (see figure 4.2a). This behavior is related to the low cross-linker content of 0.25 mol-% resulting in an extremely flexible polymer network.

Furthermore, a higher amount of AG as comonomer (p-NIPAM_{AG-25}) results in a stronger decay in the swelling curve after reaching the VPTT. This can be explained by the functional groups of the comonomer. If the microgel is dissolved in water the system has an pH value of around 6.5 which is close to the IEP of the comonomer AG (IEP \approx 5.9). This means that the overall charge of the functional groups is close to zero. As it is known for amino acids like glycine the tendency to build hydrogen bonds at this pH value is very high (see figure 6.5b). In the swollen state of microgel particles the amine and carboxy groups are distributed in the polymer network and too far away from each other to build these hydrogen bonds. If the temperature is increased, the hydrophobic character of p-NIPAM increases and the particles start to collapse. The functional groups approach and are able to build hydrogen bonds. Therefore, the expulsion of water from the microgel interior and the shrinking process are facilitated leading to a sharp VPT.

Table 6.1 shows that the microgel particles with AG as comonomer are larger than the corresponding pure polymer particles. Due to the fact that the polymerization is done above the VPTT one has to compare the R_H values at 40°C. Even in the collapsed state the R_H values of p-NIPAM_{AG-3} and p-NIPAM_{AG-25} are larger than the values of pure microgel particles. As described above hydrogen bonds between the functional groups are formed above the VPTT. The polymer network contracts much more than in case of p-NIPAM_{0.25}. This supports the assumption that the increase in size using AG as comonomer is not an effect of electrostatic repulsion as it was obtained for p-NIPAM-**co**-acrylic acid microgels.¹⁴³ Here, the polymerization process is responsible for the formation of larger polymer particles which are highly compact above the VPTT.

Comparing p-NIPAM_{AG-3} and p-NIPAM_{AG-25} at 40°C shows that an increase in the amount of comonomer leads to a decrease in size. This can be explained by the formation of more hydrogen bonds and a more compact structure of p-NIPAM_{AG-25}. With decreasing temperature the p-NIPAM-**co**-AG particles become more hydrophilic and start to swell. In the swollen state the functional groups in the polymer network are located far away from

each other. Hence, the hydrogen bonds between the functional groups of the comonomer break with decreasing temperature. This leads to an abrupt VPT and a high deswelling ratio. The similar R_H values for p-NIPAM_{AG-3} and p-NIPAM_{AG-25} at 25°C support the assumption that the difference in size at 40°C is related to the formation of hydrogen bonds.

Although the integration of AG makes the polymer network more hydrophilic, the VPTT remains the same for all three investigated microgels. Typically, the increase of hydrophilicity of the microgel network leads to a shift of the VPTT towards higher temperatures. Here, the hydrogen bonds inhibit the swelling at higher temperature. This additionally reinforces the assumption that hydrogen bonds are present in the shrunken state of the microgel particles.

Additionally, the size and the shape of the synthesized microgel particles were measured by AFM against air. Images of individual particles of p-NIPAM_{AG-3} and p-NIPAM_{AG-25} and the corresponding cross-sections are presented in figure 6.3.

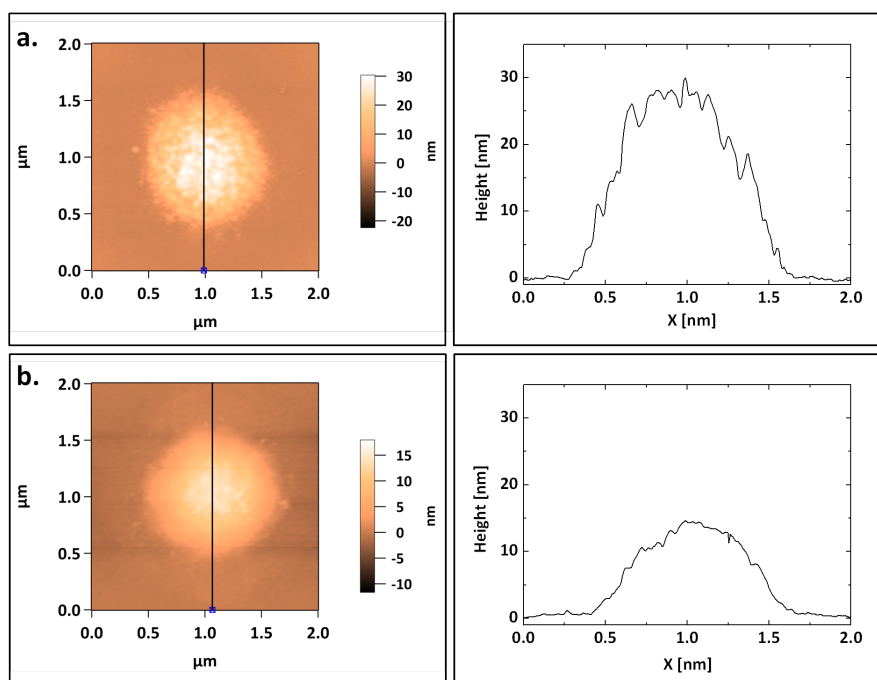


Figure 6.3: AFM images of p-NIPAM_{AG-3} (a) and p-NIPAM_{AG-25} (b) measured against air and the corresponding cross-sections.

The diameter in dried state is around 1.3 μm for both p-NIPAM microgel particles. In comparison to the hydrodynamic diameter measured by DLS

(≈ 840 nm) the size in dried state appears rather large. Investigating the height of the measured particles on the wafer leads to the conclusion that the drying process stimulates a flattening. It is also shown that the height decreases with increasing amount of AG from 25 nm for p-NIPAM_{AG-3} (figure 6.3a) to 12 nm for p-NIPAM_{AG-25} (figure 6.3b) while the diameter stays constant. Assuming that there is no significant change in lateral direction, these results are an additional proof for the presence of hydrogen bonds between the functional groups of the comonomer. The surface of the p-NIPAM microgel particles appears some kind of fluffy which can be addressed to the low amount of cross-linker in the polymer network.

The synthesized microgel particles were further characterized by temperature dependant zeta potential measurements. The measurements were performed at three different pH-values and a concentration of 0.015 wt%. The received curves are presented in figure 6.4.

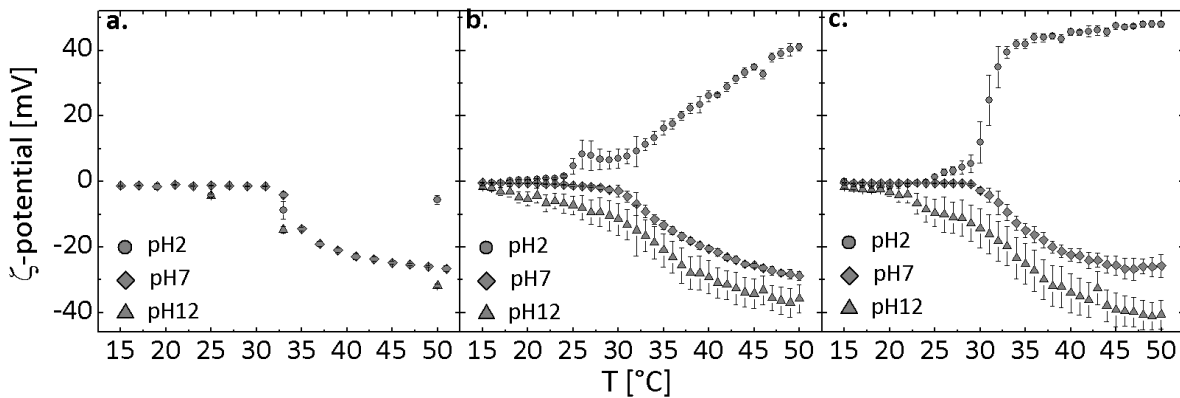


Figure 6.4: Temperature dependant zeta potential measurements for p-NIPAM_{0.25} (a), p-NIPAM_{AG-3} (b) and p-NIPAM_{AG-25} (c) at pH 2, 7 and 12.

The measurements of pure p-NIPAM with 0.25 mol-% MBA shows a constant zeta potential of around 0 mV at low temperatures (figure 6.4a). With increasing the temperature above the VPTT the zeta potential becomes negative. This is related to the functional groups of the initiator KPS at pH 7 and 12 (R-SO_3^-). The change in the zeta potential can be explained by two effects: 1.) The number of charges remains the same after the volume phase transition while the size is decreasing. 2.) The shrinking of the microgel particles presses the charged sulfonate groups to the surface of the polymer particles and a final zeta potential of ≈ -25 mV is reached in the collapsed state. At pH 2 the sulfate groups of KPS are protonated and hence the zeta

potential stays constant with increasing temperature.

The integration of only 3 mol-% AG as comonomer within the polymer network leads to a tunable charge by changing the pH value (figure 6.4b). The charge of the functional groups of AG is schematically shown in figure 6.5.

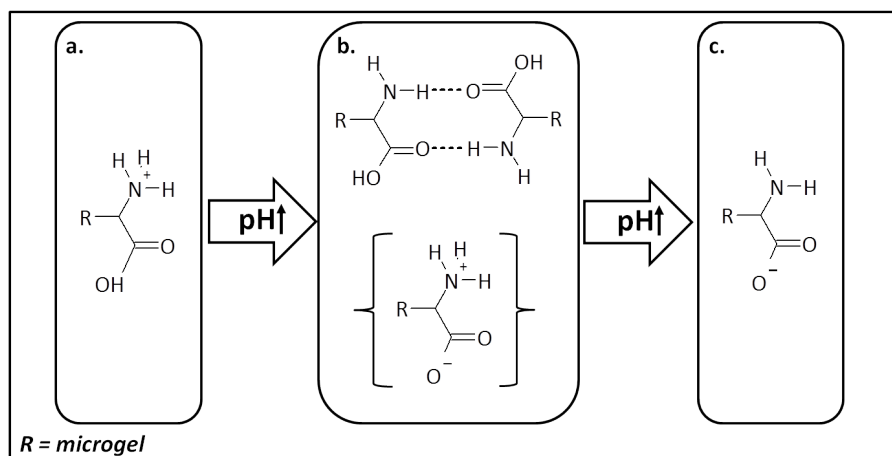


Figure 6.5: Structure of the comonomer AG at pH 2 (a), pH 7 (b) and pH 12 (c).

Due to the fact that the overall charge of the functional groups of AG is nearly neutral at pH 7 p-NIPAM_{AG-3} shows the same temperature dependant zeta potential like p-NIPAM_{0.25}.

Changing the pH value to 2 by adding HCl to the sample results in positive charged amine and neutral carboxy groups (figure 6.5a). Additionally, the sulfonate groups of the initiator are protonated at this point (R-SO₃H). This is reflected by the appropriate zeta potential curve. In the swollen state of the microgel particles the zeta potential is similar to that of the pure p-NIPAM. The charged amine groups are in the interior of the polymer network and the charge density is low for these large particles ($R_H \approx 420$ nm). With increasing temperature the described VPT begins leading to an increase in the charge density on the one hand and an enrichment of the functional groups on the surface on the other hand. Hence, the charge of p-NIPAM_{AG-3} increases clearly to a final zeta potential of ≈ 40 mV in the collapsed state.

By changing the pH value in the opposite direction to 12 the functional groups become deprotonated. This leads to neutral amine groups and negatively charged carboxy (figure 6.5c) and sulfonate groups (R-SO₃⁻). Starting at a similar zeta potential as pure p-NIPAM in the swollen state p-NIPAM_{AG-3}

particles reach a higher negative charge of around -35 mV in the collapsed state.

The increase in the AG amount to 25 mol-% has no significant influence on the charge in the swollen state (figure 6.4c). The zeta potential in the collapsed state increases to ≈ 50 mV at pH 2 and ≈ -40 mV at pH 12 proving a higher amount of AG integrated into the polymer network. Additionally, compared to p-NIPAM_{AG-3} the change in zeta potential is more abrupt at pH 2 when the VPTT is reached. This is due to the faster shrinking process which was observed in the swelling curves. This fact and the higher amount of charged functional groups within the polymer network leads to a stronger increase of the charge density.

In summary, the zeta potential measurements prove the integration of AG into the polymer network and show that the charge of the synthesized microgel particles can be tuned by changing the pH value and the temperature.

6.2.2 Switchable aggregation behavior of p-NIPAM-co-AG microgels

To get more information on the synthesized PA microgels, the swelling behavior was investigated at different pH values. During these studies one effect appears which was also found for pure p-NIPAM microgels by Al-Manasir et al.¹⁵³ While p-NIPAM_{0.25} as well as p-NIPAM_{AG-25} dissolved in water (pH ≈ 6.5) show the expected swelling behavior the addition of a small amount of NaOH to change the pH value to 7 leads to an aggregation above the VPTT. By decreasing the concentration of microgel particles with a factor of 10 this aggregation is not obtained anymore. The measured swelling curves are summarized in figure 6.6. Swelling curves of the microgels in water at concentrations below 0.015% are not shown because aggregation becomes less propable.

Firstly, it is shown that the R_H values of p-NIPAM_{AG-25} in the swollen state increase by changing the pH to 7 (figure 6.6c,d). Due to the fact that the adjusted pH value is slightly above the IEP of AG the amine groups of the comonomer become deprotonated. Therefore, the charges within the microgel particles show electrostatic repulsion and the flexible polymer network is expanded.

The second, more interesting observation is the formation of aggregates at higher concentrations right after the VPT. Due to the fact that these aggregates can be observed for both types of microgels, the interparticle for-

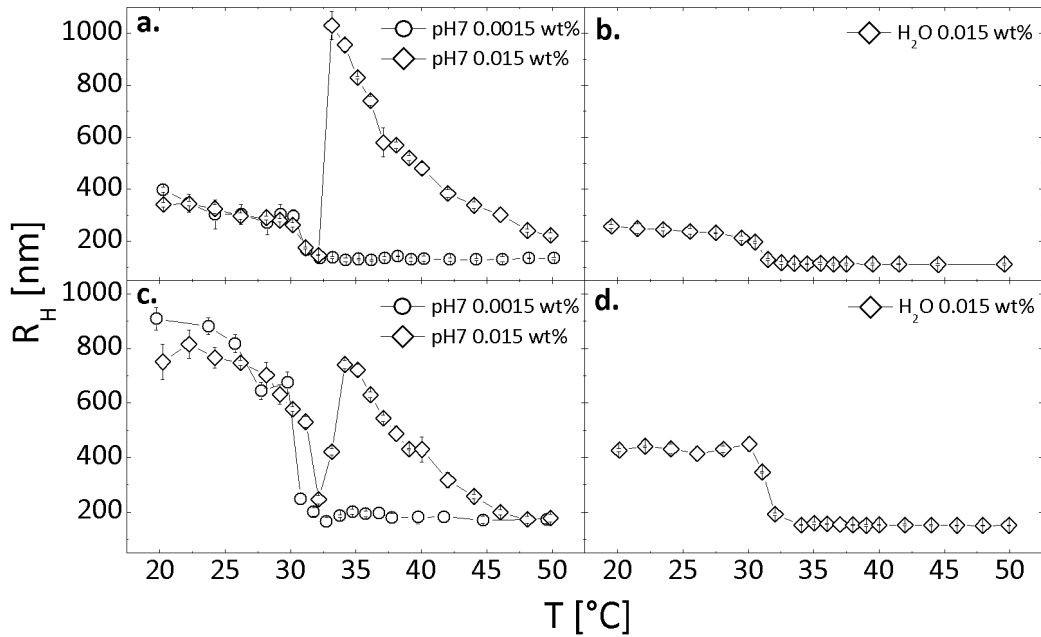


Figure 6.6: Swelling curves of $p\text{-NIPAM}_{0.25}$ at pH7 (a) and in water (b) and of $p\text{-NIPAM}_{AG-25}$ at pH7 (c) and in water (d) using different concentrations.

mation of hydrogen bonds for $p\text{-NIPAM}_{AG-25}$ seems to be not very likely. Although the R_H values of ≈ 1000 nm are at the detection limit of DLS, the small error bars and the narrow size distribution after cumulant analysis show that these aggregates are very homogeneous. This indicates a formation of a complex which consists of a fixed number of polymer particles. The observed aggregation can be explained by increasing hydrophobicity of the polymer network with increasing temperature (see section 2.1). In the swollen state the polymer particles show a hydrophilic character. Hence, they are soluble in water and have no tendency to aggregate. Reaching the VPTT leads to an increasing hydrophobicity and the shrinking of the microgel particles. This hydrophobicity supports the affinity of the polymer particles to each other in a surrounding aqueous environment. Temperature dependant zeta potential measurements at low concentrations proved that the negative charge of the microgel particles increases with increasing temperature at pH 7. This inhibits the aggregation (see section 6.2.1). At higher polymer concentrations the distance between the particles becomes smaller. The presence of ions (NaOH) leads to a screening of the charges and therefore the hydrophobic attraction overcomes the electrostatic repulsion. By a further increase of the temperature the R_H values decrease till the

same values as for the diluted case are reached (figure 6.6c,d). This indicates that the aggregates break up and individual particles are present in the solution in the collapsed state. As shown in section 6.2.1 the size reduction with increasing temperature results in an increase of the negative zeta potential. The amount of added NaOH to reach pH 7 is insufficient for a further screening of the charges. Due to the arising electrostatic interactions the collapsed microgel particles repel each other and the aggregates disappear. The distances are too large for attractive interactions in a highly diluted sample. Hence, these assemblies are not obtained in this case.

To get further information about the formation of aggregates, the scattering intensity of pure p-NIPAM as model system was monitored using temperature dependant DLS. Additionally, the swelling curve was measured in a heating and cooling cycle to investigate the reversibility of the process. The results are summarized in figure 6.7.

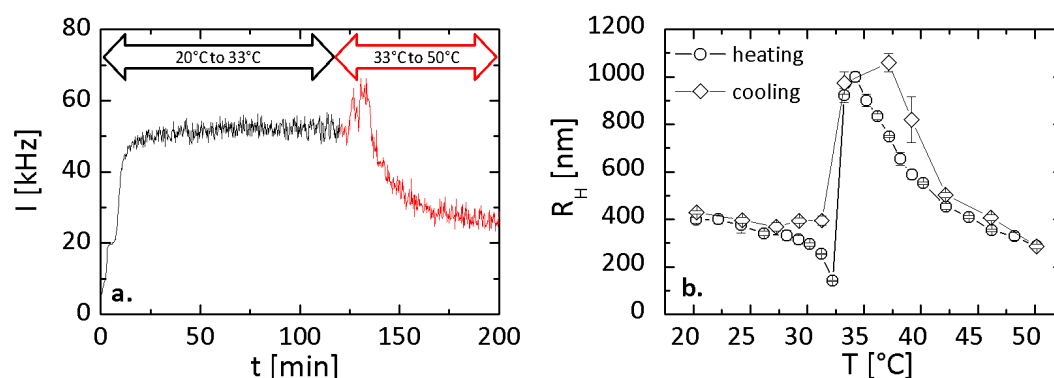


Figure 6.7: Time and temperature dependant scattering intensity (a) and swelling and deswelling curve (b) of p-NIPAM_{0.25}.

The monitored intensity signal for p-NIPAM_{0.25} using a temperature ramp from 20°C to 33°C clearly demonstrates the formation of homogeneous aggregates (figure 6.7). The abrupt increase in the intensity indicates the presence of larger particles. The measured signal remains constant when a temperature of 33°C is reached. That proves a defined number of microgel particles attached to each other. These assemblies are stable at the reached temperature (33°C). If the number of aggregated microgel particles would become higher the intensity signal would increase with time. Additionally, a stronger fluctuation of the measured signal would be observed if there would exist a large size variation of aggregates in the sample.

Going to higher temperatures leads to a temporary increase of the intensity

indicating that 33°C is not equivalent to the temperature where the largest aggregates are formed. However, further heating to 50°C shows that the measured intensity signal decreases again. This proves that the assemblies of microgel particles break up.

Figure 6.7b presents the swelling curve of p-NIPAM_{0.25} in one heating and cooling cycle. The measured temperature dependant radii prove the reversibility of the formation of the formed aggregates. Hence, defined sizes of single microgel particles as well as aggregates can be adjusted by the temperature in high concentration regimes.

To investigate the influence of the comonomer AG and the pH value on the thermoresponsive behavior, the swelling curves of all three synthesized microgel particles were studied at pH 2, 7 and 12 at 0.015 wt%. The received results are presented in figure 6.8.

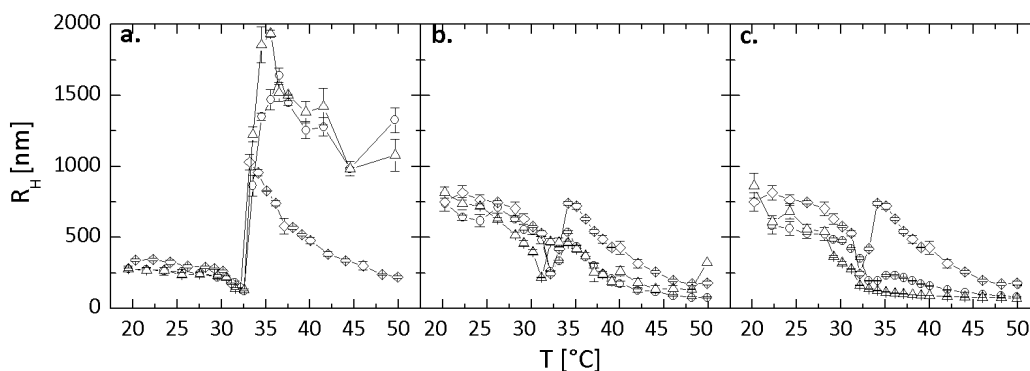


Figure 6.8: Swelling curves of p-NIPAM_{0.25} (a), p-NIPAM_{AG-3} (b) and p-NIPAM_{AG-25} (c) at pH 2 (circles), pH 7 (rhombs) and pH 12 (triangles).

NaOH and HCl were used to adjust the pH values. In case of p-NIPAM_{0.25}, a change of the pH value to 2 or 12 leads to a formation of aggregates with a high polydispersity (figure 6.8a). In contrast to the behavior at pH 7, these particles remain aggregated even in the collapsed state of the microgel particles. At pH 2 the sulfonate groups of the initiator are protonated (R-SO₃H) and the affinity of the considered polymer particles to aggregate increases. At pH 12 the functional groups of KPS are deprotonated (R-SO₃⁻) and the charge of the microgel becomes more negative with increasing temperature (see figure 6.4). Due to the fact that a high amount of base was added to reach a pH value of 12 the charges of the polymer particles are screened even in the total collapsed state. Hence, the hydrophobic attraction is stronger than the electrostatic repulsion and no tendency for a

separation of the formed assemblies at both pH values can be determined. The integration of AG as comonomer within the polymer network has a huge influence on this aggregation behavior. At pH 7 all three synthesized microgel particles show a similar swelling behavior at a concentration of 0.015 wt% regarding the formed assemblies.

Changing the pH to 2 or 12 leads to different swelling behaviors. In case of p-NIPAM_{AG-3} only small aggregates are present at temperatures slightly above the VPTT (figure 6.8b). In contrast to pure p-NIPAM these assemblies separate with increasing temperature as it was observed at pH 7. The integration of a higher amount of AG as comonomer disables the aggregation completely at pH 12 and almost completely at pH 2 (figure 6.8c). The addition of NaOH or HCl, depending on the adjusted pH value, increases the charge within the polymer network due to the integrated amine and carboxy groups. This has been proven by zeta potential measurements (6.2.1). An initial comonomer amount of 25 mol-% is enough to overcome the effect of screening. Hence, the electrostatic repulsion is stronger than the hydrophobic attraction and single p-NIPAM microgel particles are observed.

The described behavior makes the novel PA microgels a promising system for the control of aggregate size. The formation of defined aggregates can be tuned by the amount of comonomer, the concentration, the pH and the temperature of the system.

6.3 Conclusion

In this chapter a PA microgel system is presented which was synthesized by using AG as comonomer. In contrast to other studies from literature,^{30,33} only one comonomer was used to receive the PA polymer particles. Therefore, the preparation leads to a system where both functional groups (R-NH₂, R-COOH) are balanced.

Temperature dependant zeta potential measurements showed that the charge of the PA microgels can be tuned either to positive or negative potentials by variation of the pH value. Especially, in the collapsed state the polymer particles have a high charge density. The swelling behavior was investigated in response to the variation in temperature, pH and concentration. Dissolved in water, which corresponds to the zwitterionic pH range, the PA microgel particles show a sharper VPT than the pure p-NIPAM particles. This can be related to the formation of hydrogen bonds between the

amine and carboxy groups of the integrated AG. Introducing ions to the solution leads to a homogeneous aggregation at pH 7 for the PA microgels as well as for the corresponding pure microgel particles at a concentration of 0.015 wt%. Figure 6.9 illustrates the thermoresponsive behavior and the influence of pH, concentration and amount of comonomer around the VPTT.

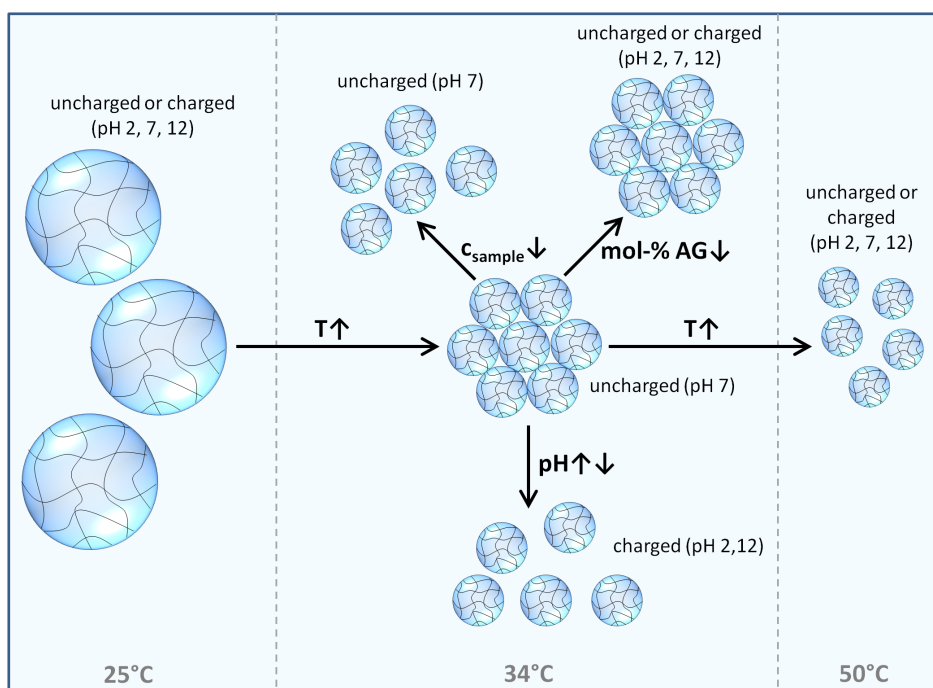


Figure 6.9: Schematic thermoresponsive behavior of $p\text{-NIPAM}_{AG-25}$ and the influence of pH, concentration and amount of comonomer at 34°C.

The sketch makes clear that the integration of AG as comonomer gives the opportunity to switch between defined aggregates and single microgel particles in a temperature range around the VPTT. This novel synthesized system produces either uncharged or charged single particles or charged or uncharged homogeneous aggregates by variation of the sample concentration, the integrated amount of the comonomer or the pH value.

This behavior makes the presented PA microgel particles a promising system in a wide field of applications. Even for processes in which higher microgel concentrations are needed the change of the pH value inhibits the formation of aggregates. The tunable aggregation is also an interesting effect for purification processes.

Additionally, the integration of the amphoteric functional groups leads to

a promising polymer matrix for enzyme immobilization. The structure of the used AG also exists in the structure of enzymes. As known, amine and carboxy groups in combination have a high affinity to build hydrogen bonds or show electrostatic interactions depending on the pH and hence the charge of the groups. At a pH value where enzyme and microgel are neutral, the enzyme can be immobilized using hydrogen bonds as driving force. A change in the pH value afterwards leads to the formation of charges and electrostatic repulsion occurs. Hence, the enzyme will be removed from the polymer matrix. This fact is an advantage regarding two aspects: 1.) Inactive enzyme can be exchanged. 2.) PA microgel particles are useful to fabricate tunable biocatalysts demonstrating switchable behavior.

7 Conclusions and Future Perspectives

7.1 Conclusions

This PhD thesis comprises the study of responsive microgel particles in terms of their structure and different applications. During the last two decades countless studies have been done on these materials. There is still a huge interest in research due to the wide field of applications of this responsive microgels. In this work different stimuli responsive p-NIPAM microgels were synthesized, characterized and used as matrices for inorganic and organic particles. This leads to materials with tunable properties.

Four different types of p-NIPAM microgel particles were investigated:

1. p-NIPAM microgels with different amounts of the cross-linker MBA (0.25 mol-%: p-NIPAM_{0.25}, 5 mol-%: p-NIPAM₅, 10 mol-%: p-NIPAM₁₀)
2. Copolymer microgels made of NIPAM, 5 mol-% MBA and 5 mol-% Allylamine (p-NIPAM_{AA-5})
3. Copolymer microgels made of NIPAM, 0.25 mol-% MBA and different amounts of Allylglycine (3 mol-%: p-NIPAM_{AG-3}, 25 mol-%: p-NIPAM_{AG-25})
4. Large p-NIPAM microgels with different amounts of MBA (0.25 mol-%: p-NIPAM_{l-0.25}, 5 mol-%: p-NIPAM_{l-5})

The size, shape, swelling behaviour and zeta potential of the prepared microgel particles were investigated by DLS and AFM. All p-NIPAM particles show a low polydispersity and the typical thermoresponsive character due to the volume phase transition temperature (VPTT) of the polymer particles.

The results regarding size and swelling behavior are summarized in the appendix (table A.1).

In good agreement with literature the deswelling ratio α increases linearly with increasing amount of MBA for p-NIPAM_{0.25}, p-NIPAM₅ and p-NIPAM₁₀.³⁷ The VPTT of the microgel particles is $\approx 32^\circ\text{C}$ and independent from the cross-linker content. Due to the used initiator potassium peroxydisulfate (KPS), the synthesized microgel particles show a slightly negative zeta potential.

In contrast to acrylic acid,¹⁴³ the integration of allylamine (AA) into the polymer network results in smaller particles than pure p-NIPAM microgels. The presence of amine groups in the polymer network increases the hydrophilicity leading to an increased VPTT. Hence, it has been proven that the usage of comonomers is a nice tool to influence the swelling behavior of the microgel particles.^{15,16} Another advantage of integrating AA into the polymer network, is the possibility to change the charge of the polymer particles by adjusting the pH value. Zeta potential measurements showed that p-NIPAM_{AA-5} is positively charged at pH 2 and negatively charged at pH 7 and 12, especially above the VPTT. Regarding the embedding of particles, this can be used for switching between electrostatic repulsion and attraction. Additionally, the amine groups give the opportunity to covalently bind organic particles.

Furthermore, allylglycine (AG) was used as amphoteric comonomer to prepare Polyampholyte (PA) microgels offering carboxy- and amine groups. In the range of the isoelectric point (IEP ≈ 5.9) the functional groups are able to build hydrogen bonds. This leads to a more pronounced compression of the polymer network in the shrunken state of p-NIPAM_{AG-3} and p-NIPAM_{AG-25}. As expected, this effect is stronger for a higher amount of AG. With decreasing temperature, these hydrogen bonds keep the polymer network compressed till the hydrophilicity of the microgels is strong enough and the volume phase transition occurs. Hence, the VPTT is around 32°C although the hydrophilicity of the microgel particles is increased by the integration of AG. It has been proven that the zeta potential of p-NIPAM_{AG-3} and p-NIPAM_{AG-25} can be changed from negative values at pH 12 to positive values at pH 2. Due to the additional carboxy groups the negative charge at pH 12 is more pronounced than in case of p-NIPAM_{AA-5}. The combination of the amphoteric and thermoresponsive behavior make the polymer particles suitable systems for a wide field of applications. The functional groups are the same

like in peptides or enzymes and offer a suitable point of connection. Another interesting and special property of p-NIPAM_{AG-25} is the switchable aggregation around the VPTT. The addition of NaOH to adjust the pH to 7 leads to a charge screening and the formation of aggregates. These aggregates are stable at different pH values for decreasing amount of AG but can be separated by changing the pH to 2 or 12, changing the temperature below or above the VPTT or decreasing the sample concentration. The fact that the aggregation behavior can be influenced by different external stimuli makes the systems also useful for purification processes.

The size of p-NIPAM microgel particles can be influenced by using a temperature ramp during the polymerization. Comparing the hydrodynamic radii of p-NIPAM_{0.25}, p-NIPAM₅, p-NIPAM_{l-0.25} and p-NIPAM_{l-5} in the swollen state, an increase of around 500 nm can be observed. The VPTT for these polymer particles is dependant from the content of MBA. Hence, the structure of the large p-NIPAM microgel is not directly comparable with that of p-NIPAM_{0.25} and p-NIPAM₅. Nevertheless, the thermoresponsive character is the same which makes them a suitable matrix for the embedding of inorganic and organic particles. The large size is a good property for analyzing the microgels by optical methods, like confocal laser scanning microscopy (CLSM).

Organic and inorganic particles were embedded within the stimuli responsive microgel particles a.) to investigate the structure of the p-NIPAM microgels and b.) to create new materials with tunable functions.

By simply mixing dilute dispersions of p-NIPAM_{0.25}, p-NIPAM₅ and p-NIPAM₁₀ with spherical, citrate-stabilized Au-NPs (average diameter: 18.5 nm) structural information on the microgel particles were obtained. Investigations using TEM and temperature dependant UV-Vis spectroscopy show that the Au-NPs were embedded in the outer region of the polymer network. This proves an inhomogeneous structure of the microgel network.¹²¹ With decreasing cross-linker content a deeper penetration of the Au-NPs was observed indicating a smaller area of large meshes for p-NIPAM₅ and p-NIPAM₁₀ compared to p-NIPAM_{0.25}. Additionally, it has been proven that the largest mesh size for all three microgel particles is above 18.5 nm.

The mesh sizes of p-NIPAM_{l-0.25} and p-NIPAM_{l-5} were estimated by successful immobilization of the enzyme Lipase B (CalB, shortest axis \approx 3 nm). After labeling CalB with the dye FITC (longest axis \approx 3 nm), CLSM was used to prove the immobilization within the polymer particles. In case of p-NIPAM_{l-5},

the labeling with 1 FITC molecule per CalB molecule leads to an increase in size which inhibits CalB to penetrate within the polymer network. Hence, the largest mesh size in the swollen state is between 3 nm and 6 nm for p-NIPAM_{l-5} and above 6 nm for p-NIPAM_{l-0.25}.

The prepared thermosensitive microgels are also suitable matrices for a huge field of applications, e.g. biocatalysis and sensors.

By loading p-NIPAM_{0.25}, p-NIPAM₅ and p-NIPAM₁₀ with spherical, citrate-stabilized Au-NPs, hybrid microgels were obtained. The number density of Au-NPs within the polymer network can be controlled by the initial amount of added NPs. Due to a ligand exchange from citrate to the polymer chains the Au-NPs are strongly fixed to the polymer network. The special characteristic of the prepared hybrid microgels is reflected by the precisely adjustable distance between the Au-NPs within the polymer network with increasing temperature. The received plasmon coupling leads to a stepwise red shift of the absorption maximum to ≈ 675 nm. The shift increases with increasing number of Au-NPs in the polymer network and with decreasing MBA content. This "smart" hybrid microgels show optical properties which can be tuned by changing the temperature. The possibility to modify the properties by variation of the MBA content as well as of the loaded amount of Au-NPs might be interesting for applications like sensor design.

Another part of this PhD thesis deals with a promising method to create biocatalysts which work in organic solvents. By simply exchanging the aqueous against an organic solvent, CalB was successfully immobilized within p-NIPAM_{l-0.25}. The thermoresponsive behavior of the microgel particles offer the possibility to control the amount of immobilized CalB by changing the temperature. By proceeding the uptake at 50°C no CalB is immobilized. Increasing the temperature above the VPTT after mixing CalB and the polymer matrices results in an immobilized amount which is two times higher than at 25°C. The immobilized system shows an enhanced activity compared to non-immobilized CalB as well as a high stability and reusability in n-hexane. Increasing the amount of MBA to 5 mol-% leads to biocatalyst with a tunable supply of the substrate. Above the VPTT the activity decreases due to the denser polymer network and hence a lower collision frequency between substrate and enzyme.

The applicability of this method has been proven by successful immobilization of peroxidase (HRP). Although this enzyme is usually not stable in

organic solvents, the immobilized system also shows an enhanced activity. This supports that the described procedure is a really helpful approach for creating new biocatalysts, especially for the chemical synthesis in organic solvents. Additionally, the embedding in hydrated polymer matrices gives advantages like a more homogeneous distribution, easier accessibility and handling of the enzymes. Furthermore, no chemical adjustment of the polymer matrix for the embedding is needed. Another advantage of this method is the possible exchange of inactive enzymes by another solvent exchange to water. This also leads to the drawback that the produced biocatalysts are not able to work in aqueous environment.

As an approach to create biocatalysts which work in aqueous solvents, HRP was covalently bound to p-NIPAM_{AA-5} using p-benzoquinone (BQ) as coupling agent. It is shown that the covalent binding leads to an active biocatalyst which is quite stable. Hence, this is a promising approach to obtain highly active biocatalysts in water which are interesting systems for industrial applications, e.g. detergent industry.

7.2 Future Perspectives

The present research has provided different strategies for the usage of thermoresponsive p-NIPAM microgels in terms of different applications. However, further work is encouraged to make the current research more appealing for industrial applications.

The production of the hybrid materials presented within this work is based on the strong interaction between the polymer network and the Au-NPs. In order to prove the assumption that the citrate is released from the surface of the Au-NPs a further addition of citrate after the loading is of interest. If the citrate stabilizes the NPs again, a leakage of the Au-NPs should be observed. Additionally, the influence of using different sizes of Au-NPs for the loading procedure is of high interest. If there is a dependence on the mesh size and a density gradient present within the polymer network the penetration depth should be dependant on the size of the loaded Au-NPs.

Regarding the immobilization of enzymes for the usage in organic solvents in industrial applications some general informations are relevant. Within this work the localization of the enzymes was determined to be inside of the polymer network. Due to the fact that the enzymes work at the interface between the "aqueous cage" within the polymer particles and the organic

solvent, it would be interesting to know if the enzymes are located at this interface and where this interface is. Another important aspect is the distribution equilibrium between the substrate outside and inside of the polymer particles as well as the amount of product which is formed by one single enzyme molecule.

The thermoresponsibility of the used p-NIPAM matrices should be optimized to reach a biocatalyst where the activity can be switched on and off by a temperature change. Therefore, microgel particles with a cross-linker content above 5 mol-% have to be used for the immobilization in order to control the supply of the substrate completely by the collapse of the polymer matrix. It is important to produce p-NIPAM microgel particles where the meshes in the swollen state are still large enough for enzyme immobilization on the one hand and where the temperature induced collapse leads to meshes which are small enough to inhibit the supply of the substrate on the other hand. Especially, for the usage in industry it is helpful to create a biocatalyst with a recyclable polymer support. The presented system is suitable due to the fact that the immobilized enzyme can be released again by another solvent exchange back to aqueous environment. This has to be investigated in detail in future studies to determine if new enzyme can be immobilized afterwards.

The immobilization for the usage in aqueous environment by covalent attachment has to be investigated intensively in future studies. The most important aspect is the determination of the immobilized amount of HRP to calculate the specific activity. Therefore, a method has to be figured out which is not based on the interactions with amino groups, e.g. determination via fluorescence or absorbance using Amplex Red.^{144,145}

The novel PA microgel system is a promising matrix for several applications, e.g. enzyme immobilization. Therefore, the system should be used at different pH values, depending on the IEP of the used enzyme, for the immobilization based on hydrogen bonds or electrostatic interactions.

A Further experimental details

A.1 Experimental Section

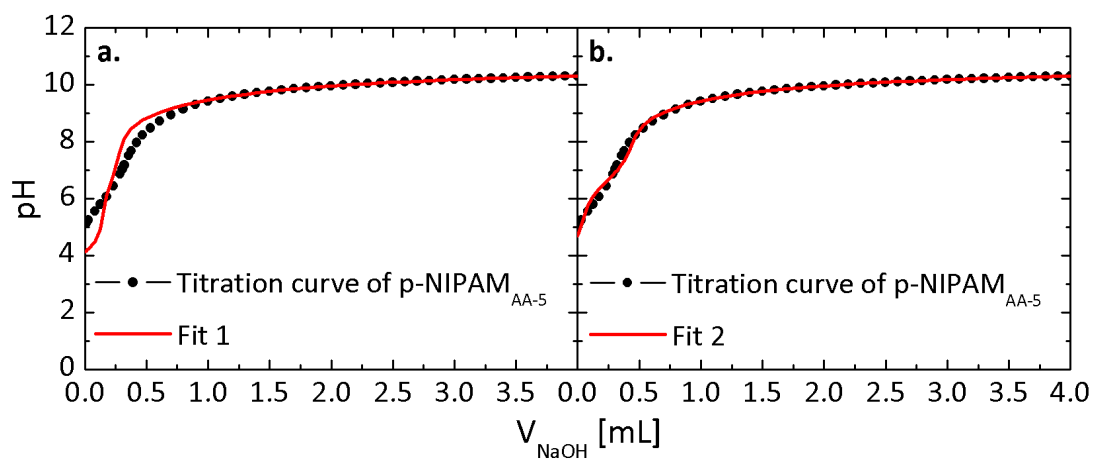


Figure A1: Titration curve of p-NIPAM_{AA-5} and fitting curves taking small amounts of carbonic acid in the titrant (a) or in the titrant and titrand (b) into account.

A.2 P-NIPAM microgels loaded with Au-NPs

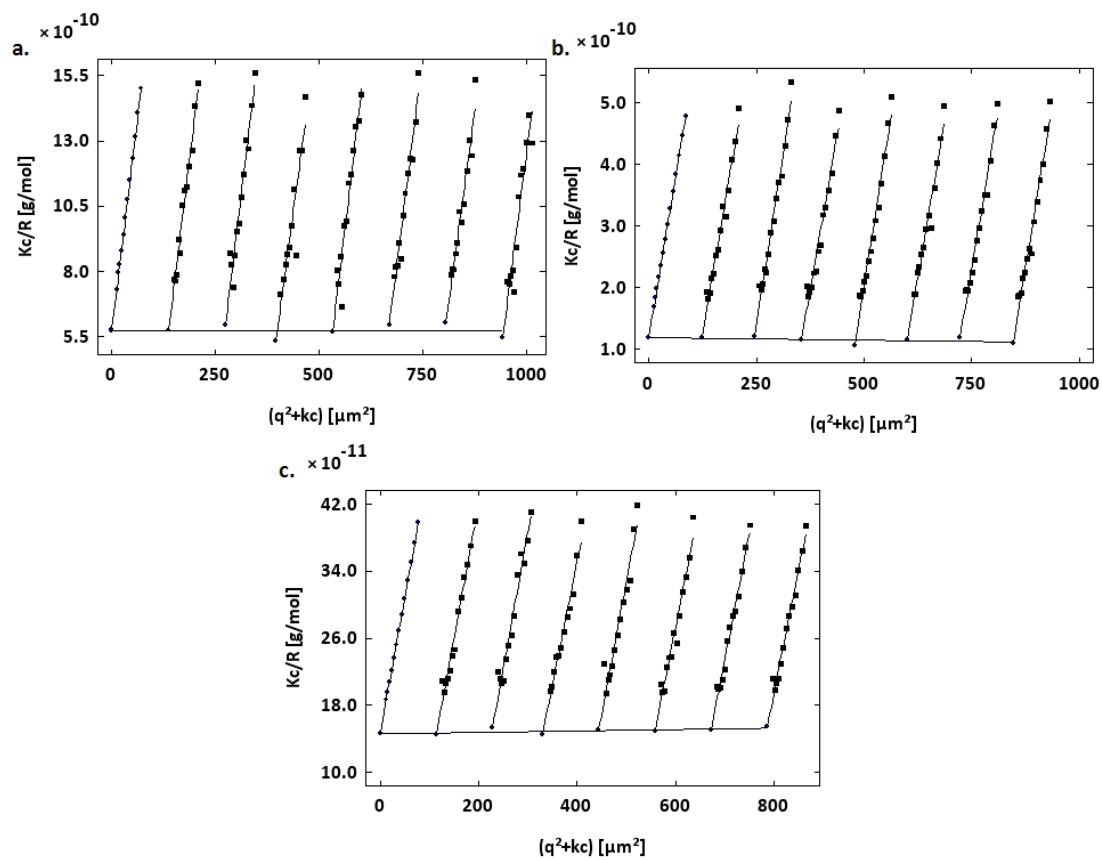


Figure A2: Zimm-Plots of $p\text{-NIPAM}_{0.25}$ (a), $p\text{-NIPAM}_5$ (b) and $p\text{-NIPAM}_{10}$ (c) dissolved in water at 25°C.

A.3 Immobilization of enzymes within p-NIPAM

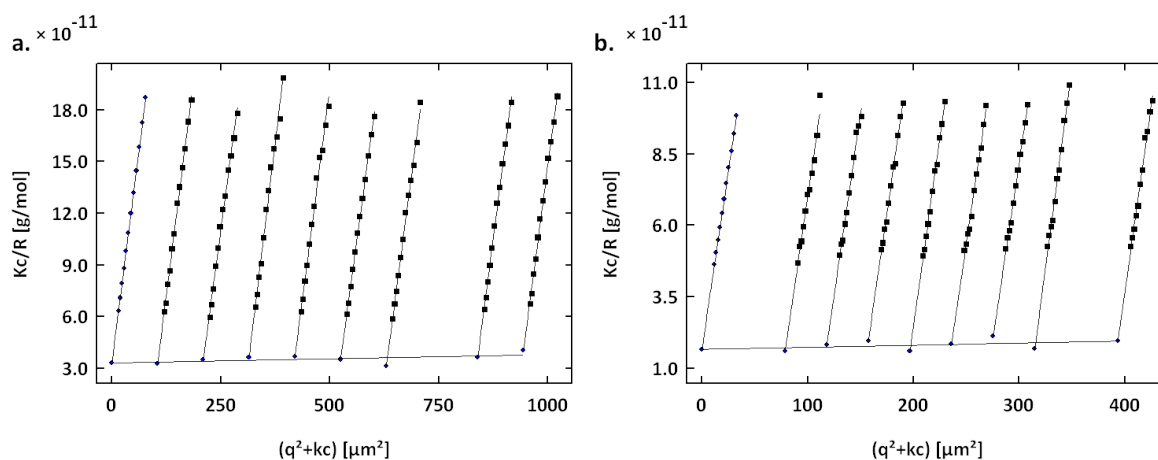


Figure A3: Zimm-Plots of $p\text{-NIPAM}_{l-0.25}$ (a) and $p\text{-NIPAM}_{l-5}$ (b) dissolved in water at 25°C.

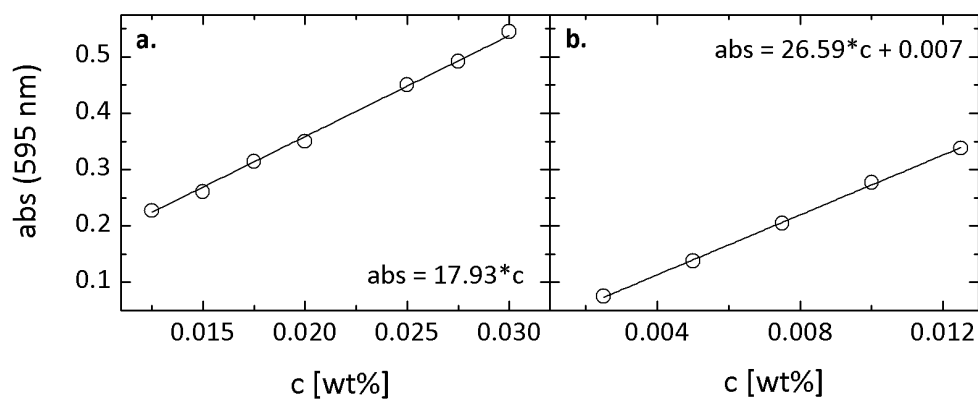


Figure A4: Calibration curves and equations of $p\text{-NIPAM}_{l-5}$ in water (a) and $p\text{-NIPAM}_{l-5}$ in water using Bradford assay (b).

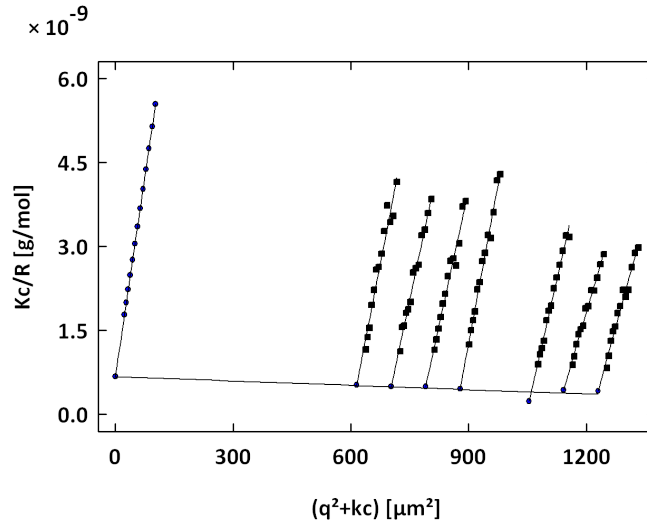


Figure A5: Zimm-Plot of $p\text{-NIPAM}_{AA-5}$ dissolved in water at 25°C .

A.4 Conclusions and Future Perspectives

Table A.1: R_H , α and VPTT of all synthesized $p\text{-NIPAM}$ microgel particles in water.

sample	$R_H(25^\circ\text{C})$ [nm]	$R_H(40^\circ\text{C})$ [nm]	α	VPTT [$^\circ\text{C}$]
$p\text{-NIPAM}_{0.25}$	238 ± 11	112 ± 2	0.10	31
$p\text{-NIPAM}_5$	281 ± 16	173 ± 2	0.23	32
$p\text{-NIPAM}_{10}$	249 ± 10	176 ± 6	0.35	32
$p\text{-NIPAM}_{AA-5}$	173 ± 6	73 ± 0.6	0.08	34
$p\text{-NIPAM}_{AG-3}$	428 ± 11	186 ± 5	0.08	31
$p\text{-NIPAM}_{AG-25}$	422 ± 17	153 ± 1	0.05	32
$p\text{-NIPAM}_{l-0.25}$	881 ± 23	105 ± 2	1.7×10^{-3}	28
$p\text{-NIPAM}_{l-5}$	727 ± 42	175 ± 3	0.01	31

B Abbreviations

α	deswelling ratio
Γ	relaxation rate
ϵ	dielectric constant
ϵ	extinction coefficient
ζ	zeta potential
η	viscosity
θ	scattering angle
κ	Debye-length
λ	wavelength
μ_E	electrophoretic mobility
v	molar volume
Π	osmotic pressure
τ	correlation time
ϕ	volume fraction
χ	polymer-solvent interaction parameter
Ψ	potential
a	particle radius
a_n	scattering coefficient
a_x	amplitudes
AA	allylamine
AG	allylglycine
APS	ammonium persulfate
Au-NPs	gold nanoparticles
AFM	atomic force microscopy
b_n	scattering coefficient
BSA	bovine serum albumine
BQ	para-benzoquinone
C_{ext}	extinction cross-section

CalB	Lipase B from <i>Candida antarctica</i>
CLSM	confocal laser scanning microscopy
d	thickness of the cuvette
d	distance
D	diffusion coefficient
Da	Dalton
DLS	dynamic light scattering
E	electric field
E	extinction
e.g.	example gratia
et al.	et altera
f	number of counterions per chain
F	free energy
F	force
FITC	Fluorescein-5-isothiocyanat
$g^1(\tau)$	field time autocorrelation function
$g^2(\tau)$	intensity time autocorrelation function
H	enthalpy
h	Planck's constant
h	hour(s)
H ₂ CO ₃	Carbonic acid
HCl	hydrogen chloride
HRP	<i>horseradish</i> peroxidase
I	intensity
IEP	isoelectric point
\vec{k}	wave vector
k	spring constant
k_B	Boltzmann constant
KPS	potassium peroxodisulfate
LCST	lower critical solution temperature
m	mass
M	molar
M_W	molecular weight
MBA	N,N'-methylenebis(acrylamide)
min	minute(s)
n	refractive index

N	number
NA	numerical aperture
N_A	Avogadro constant
N_c	number of chains
NaOH	Sodium hydroxide
NIPAM	N-Isopropylacrylamide
PA	polyampholyte
PE	polyelectrolyte
PDI	polydispersity index
p-NIPAM	poly-N-isopropylacrylamide
p-NIPAM _{0.25}	small p-NIPAM with 0.25 mol-% MBA
p-NIPAM ₅	small p-NIPAM with 5 mol% MBA
p-NIPAM ₁₀	small p-NIPAM with 10 mol-% MBA
p-NIPAM _{AA-5}	p-NIPAM with 5 mol-% MBA and 5 mol-% AA
p-NIPAM _{AG-3}	p-NIPAM with 0.25 mol-% MBA and 3 mol-% AG
p-NIPAM _{AG-25}	p-NIPAM with 0.25 mol-% MBA and 25 mol-% AG
p-NIPAM _{l-0.25}	large p-NIPAM with 0.25 mol-% MBA
p-NIPAM _{l-5}	large p-NIPAM with 5 mol-% MBA
\vec{q}	scattering vector
r	resolution
R	radius
R_H	hydrodynamic radius
rpm	rotation per minute
S	entropy
SDS	sodium dodecyl sulfate
SDS-Page	sodium dodecyl sulfate polyacrylamide gel electrophoresis
se	solvent exchange
SLS	static light scattering
T	temperature
TEM	transmission electron microscopy
TEMED	N,N,N,N-tetramethylethylenediamine
TRIS	tris(hydroxymethyl)aminomethane
$U_{specific}$	specific activity
U_V	volume activity
UCST	upper critical solution temperature
v	velocity

V	volume
VPT	volume phase transition
VPTT	volume phase transition temperature
<i>x</i>	cantilever deflection

List of publications

1. Shuo Bai, Changzhu Wu, Kornelia Gawlitza, Regine von Klitzing, Marion B. Ansorge-Schumacher, Dayang Wang. Using hydrogel microparticles to transfer hydrophilic nanoparticles and enzymes to organic media via stepwise solvent exchange. *Langmuir* **2010**, 26 (15), 12980-12987.
2. Kornelia Gawlitza, Changzhu Wu, Radostina Georgieva, Dayang Wang, Marion B. Ansorge-Schumacher, Regine von Klitzing. Immobilization of lipase B within micron-sized poly-*N*-isopropylacrylamide hydrogel particles by solvent exchange. *Phys. Chem. Chem. Phys.* **2012**, 14 (27), 9594-9600.
3. Kornelia Gawlitza, Changzhu Wu, Radostina Georgieva, Marion B. Ansorge-Schumacher, Regine von Klitzing. Temperature Controlled Activity of Lipase B from *Candida Antarctica* after Immobilization within p-NIPAM Microgel Particles. *Z. Phys. Chem.* **2012**, 226, 749-759.
4. Kornelia Gawlitza, Sarah T. Turner, Matthias Karg, Paul Mulvaney, Regine von Klitzing. Interaction of gold nanoparticles with thermoresponsive microgels: Influence of the cross-linker density on optical properties. **2012**, in preparation.

References

- [1] McCrum, N. G., Buckley, C. P., Bucknall, C. B., Eds. *Principles of Polymer Engineering*, 2nd ed.; Oxford University Press Inc., New York, USA, 1997.
- [2] Senff, H.; Richtering, W. *J. Chem. Phys.* **1999**, *111*, 1705–1711.
- [3] Berndt, I.; Richtering, W. *Macromolecules* **2003**, *36*, 8780–8785.
- [4] Stieger, M.; Pedersen, J. S.; Lindner, P.; Richtering, W. *Langmuir* **2004**, *20*, 7283–7292.
- [5] Senff, H.; Richtering, W. *Colloid. Polym. Sci.* **2000**, *278*, 830–840.
- [6] Evans, C. H. (1978):US4199231.Hydrogel contact lens.1980.
- [7] Nayak, S.; Lyon, L. A. *Angew. Chem.* **2005**, *117*, 7862–7886.
- [8] Welsch, N.; Ballauff, M.; Lu, Y. *Adv. Polym. Sci.* **2010**, *234*, 129–163.
- [9] Ballauff, M.; Lu, Y. *Polymer* **2007**, *48*, 1815–1823.
- [10] Pelton, R. H. *Adv. Colloid Interface Sci.* **2000**, *85*, 1–33.
- [11] He, Q.; Kueller, A.; Schilp, S.; Leisten, F.; Kolb, H.-A.; Grunze, M.; Li, J. *Small* **2007**, *11*, 1860–1865.
- [12] Schild, H. G. *Prog. Polym. Sci.* **1992**, *17*, 163–249.
- [13] Hoare, T.; Pelton, R. *Macromolecules* **2004**, *37*, 2544–2550.
- [14] Hoare, T.; Pelton, R. *Langmuir* **2004**, *20*, 2123–2133.
- [15] Karg, M.; Pastoriza-Santos, I.; Rodriguez-Gonzalez, B.; von Klitzing, R.; Wellert, S.; Hellweg, T. *Langmuir* **2008**, *24*, 6300–6306.
- [16] Kratz, K.; Hellweg, T.; Eimer, W. *Colloids Surf., A* **2000**, *170*, 137–149.

- [17] Burmistrova, A.; von Klitzing, R. *J. Mater. Chem.* **2010**, *20*, 3502–3507.
- [18] Contreras-Cáceres, R.; Sanchez-Iglesias, A.; Karg, M.; Pastoriza-Santos, I.; Pérez-Juste, J.; Pacifico, J.; Hellweg, T.; Fernández-Barbero, A.; Liz-Marzán, L. M. *Adv. Mat.* **2009**, *20*, 1666–1670.
- [19] Das, M.; Sanson, N.; Fava, D.; Kumacheva, E. *Langmuir* **2007**, *23*, 196–201.
- [20] Karg, M.; Pastoriza-Santos, I.; Pérez-Juste, J.; Hellweg, T.; Liz-Marzán, L. M. *Small* **2007**, *3*, 1222–1229.
- [21] Lange, H.; Juarez, B. H.; Carl, A.; Richter, M.; Bastus, N. G.; Weller, H.; Thomsen, C.; von Klitzing, R.; Knorr, A. *Langmuir* **2012**, *28*, 8862–8866.
- [22] Jones, C.; Serpe, M.; Schroeder, L.; Lyon, L. A. *J. Am. Chem. Soc.* **2003**, *125*, 5292–5293.
- [23] Jones, C.; Lyon, L. A. *J. Am. Chem. Soc.* **2003**, *125*, 460–465.
- [24] Kirk, O.; Borchert, T. V.; Fuglsang, C. C. *Curr. Opin. Biotechnol.* **2002**, *13*, 345–351.
- [25] Arica, M. Y.; Öktem, H. A.; Öktem, Z.; Tuncel, S. A. *Polym. Int.* **1999**, *48*, 879–884.
- [26] Johansson, C.; Hansson, P.; Malmsten, M. *J. Phys. Chem. B* **2009**, *113*, 6183–6193.
- [27] Johansson, C.; Gernandt, J.; Bradley, M.; Vincent, B.; Hansson, P. *J. Colloid Interface Sci.* **2010**, *347*, 241–251.
- [28] Welsch, N.; Wittemann, A.; Ballauff, M. *J. Phys. Chem. B* **2009**, *113*, 16039–16045.
- [29] Neyret, S.; Vincent, B. *Polymer* **1997**, *38*, 6129–6134.
- [30] Das, M.; Kumacheva, E. *Colloid. Polym. Sci.* **2006**, *284*, 1073–1084.
- [31] Li, X.; Zuo, J.; Guo, Y.; Cai, L.; Tang, S.; Yang, W. *Polym. Int.* **2007**, *56*, 968–975.

- [32] Tan, B. H.; Tam, K. C. *Adv. Colloid Interface Sci.* **2008**, *136*, 25–44.
- [33] Ogawa, K.; Nakayama, A.; Kokufuta, E. *Langmuir* **2003**, *19*, 3178–3184.
- [34] Sepeur, S., Ed. *Nanotechnologie*; Vincentz Network, Hannover, Germany, 2008.
- [35] Shibayama, M.; Tanaka, T. *Adv. Polym. Sci.* **1993**, *109*, 1–62.
- [36] Kratz, K. Intelligente Poly-N-Isopropylacrylamid Mikrogele unterschiedlicher Zusammensetzung. Einfluss von Konnektivität, Ladungsdichte und Ionenstärke auf das Quellverhalten von PNIPA-Kolloiden. Ph.D. thesis, University of Bielefeld, 1999.
- [37] Kratz, K.; Hellweg, T.; Eimer, W. *Polymer* **2001**, *42*, 6631–6639.
- [38] Kratz, K.; Eimer, W. *Ber. Bunsenges. Phys. Chem.* **1998**, *102*, 848–853.
- [39] Shibayama, M.; Tanaka, T. *J. Chem. Phys.* **1992**, *97*, 6829–6841.
- [40] Shibayama, M.; Tanaka, T. *J. Chem. Phys.* **1992**, *97*, 6842–6854.
- [41] Shibayama, M. *J. Chem. Phys.* **1995**, *15*, 9392–9400.
- [42] Hirokawa, Y.; Tanaka, T. *J. Chem. Phys.* **1984**, *81*, 6379–6380.
- [43] Hirotsu, S.; Hirokawa, Y.; Tanaka, T. *J. Chem. Phys.* **1987**, *87*, 1392–1395.
- [44] Shibayama, M.; Mizutani, S.; Nomura, S. *Macromolecules* **1996**, *29*, 2019–2024.
- [45] Kawasaki, H.; Sasaki, S.; Maeda, H. *J. Phys. Chem. B* **1997**, *101*, 5089–5093.
- [46] Gan, L. H.; Gan, Y. Y.; Deen, G. R. *Macromolecules* **2000**, *33*, 7893–7897.
- [47] Shibayama, M.; Ikkai, F.; Inamoto, S.; Nomura, S.; Han, C. C. *J. Chem. Phys.* **1996**, *105*, 4358–4366.
- [48] Suzuki, A.; Tanaka, T. *Nature* **1990**, *346*, 345–347.

- [49] Mamada, A.; Tanaka, T.; Kungwatchakun, D.; Irief, M. *Macromolecules* **1990**, *23*, 1517–1519.
- [50] Osada, Y. *Adv. Polym. Sci.* **1987**, *82*, 1–46.
- [51] Osada, Y.; Umezawa, K.; Yamauchi, A. *Makromol. Chem.* **1988**, *189*, 597–605.
- [52] Tanaka, T. *Sci. Am.* **1981**, *244*, 124 – 138.
- [53] Tanaka, T. *Phys. Rev. Lett.* **1978**, *40*, 820–823.
- [54] Baker, W. O. *Ind. Eng. Chem.* **1949**, *41*, 511–520.
- [55] Fernandez-Nieves, A., Wyss, H. M., Mattsson, J., Weitz, D. A., Eds. *Microgel Suspensions*; Wiley-VCH, Weinheim, Germany, 2011.
- [56] Brugger, B.; Rosen, B. A.; Richtering, W. *Langmuir* **2008**, *24*, 12202–12208.
- [57] Kim, J.; Nayak, S.; Lyon, L. A. *J. Am. Chem. Soc.* **2005**, *127*, 9588–9592.
- [58] Serpe, M. J.; Yarmey, K. A.; Nolan, C. M.; Lyon, L. A. *Biomacromolecules* **2005**, *6*, 408–413.
- [59] Hoare, T.; Pelton, R. H. *J. Phys. Chem. B.* **2007**, *111*, 11895–11906.
- [60] Duracher, D.; Elaissari, A.; Mallet, F.; Pichot, C. *Langmuir* **2000**, *16*, 9002–9008.
- [61] Lev Bromberg, M. T.; Hatton, T. A. *Langmuir* **2003**, *19*, 8675–8684.
- [62] Nerapusri, V.; Keddie, J. L.; Vincent, B.; Bushnak, I. A. *Langmuir* **2006**, *22*, 5036–5041.
- [63] Serpe, M. J.; Jones, C. D.; Lyon, L. A. *Langmuir* **2003**, *19*, 8759–8764.
- [64] Höfl, S.; Zitzler, L.; Hellweg, T.; Herminghaus, S.; Mugele, F. *Polymer* **2007**, *48*, 245–254.
- [65] Wiedemair, J.; Serpe, M. J.; Kim, J.; Masson, J.-F.; Lyon, L. A.; Mizaikoff, B.; Kranz, C. *Langmuir* **2007**, *23*, 130–137.

- [66] Pelton, R. H.; Chibante, P. *Colloids Surf.* **1986**, *20*, 247–256.
- [67] Flory, P. J.; Rehner, J. *J. Chem. Phys.* **1943**, *11*, 512–520.
- [68] Hunt, L. B. *Gold Bull.* **1976**, *9*, 134–139.
- [69] Mulvaney, P. *Langmuir* **1996**, *12*, 788–800.
- [70] Liz-Marzán, L. M.; Giersig, M.; Mulvaney, P. *Langmuir* **1996**, *12*, 4329–4335.
- [71] Pérez-Juste, J.; Pastoriza-Santos, I.; Liz-Marzán, L. M.; Mulvaney, P. *Coord. Chem. rev.* **2005**, *249*, 1870–1901.
- [72] Enüstün, B. V.; Turkevich, J. *J. Am. Chem. Soc.* **1963**, *85*, 3317–3328.
- [73] Malikova, N.; Pastoriza-Santos, I.; Schierhorn, M.; Kotov, N. A.; Liz-Marzán, L. M. *Langmuir* **2002**, *18*, 3694–3697.
- [74] Nehl, C. L.; Liao, H.; Hafner, J. H. *Nano Lett.* **2006**, *6*, 683–688.
- [75] Mie, G. *Ann. Phys.* **1908**, *25*, 377–445.
- [76] Underwood, S.; Mulvaney, P. *Langmuir* **1994**, *10*, 3427–3430.
- [77] Illanes, A., Ed. *Enzyme Biocatalysis: Principles and Applications*; Springer Science and Business Media B.V., Dordrecht, Netherlands, 2008.
- [78] Sheldon, R. A. *Adv. Synth. Catal.* **2007**, *349*, 1289–1307.
- [79] Katchalski-Katzir, E. *Trends Biotechnol.* **1993**, *11*, 471–478.
- [80] Guisan, J. M., Ed. *Methods in Biotechnology: Immobilization of Enzymes and Cells*; Humana Press Inc., Totowa, New Jersey, 2006.
- [81] Taylor, R. F., Ed. *Protein Immobilization. Fundamentals and Applications*; Bioprocess Technology Series/14; J. Pharm. Pharmacol., 1992; Vol. 44.
- [82] Hartmeier, W. *Trends Biotechnol.* **1985**, *3*, 149–153.

- [83] Ansorge-Schumacher, M. B. In *Handbook of Heterogeneous Catalysis*; Ertl, G., Knözinger, H., Schüth, F., Weitkamp, J., Eds.; Wiley VCH, Weinheim, Germany, 2008; Chapter Immobilization of Biological Catalysts, p 644.
- [84] Klibanov, A. M. *Science* **1983**, *219*, 722–727.
- [85] Walker, J. M., Rapley, R., Eds. *Molecular Biology and Biotechnology*; Springer Science and Business Media B.V., Dordrecht, Netherlands, 2009.
- [86] Brandt, J.; Andersson, L.-O.; Porath, J. *Biochim. Biophys. Acta* **1975**, *386*, 169–202.
- [87] Berne, B. J.; Pecora, R. *Dynamic Light Scattering with Applications to Chemistry, Biology, and Physics*; Dover Publications Inc., Mineola, New York, 2000.
- [88] Koppel, D. E. *J. Chem. Phys.* **1972**, *57*, 4814–4820.
- [89] Frisken, B. J. *Appl. Opt.* **2001**, *40*, 4087–4091.
- [90] Michov, B., Ed. *Elektrophorese: Theorie und Praxis*; Walter de Gruyter, New York, USA, 1995.
- [91] Bauer, D., Ed. *Adsorption von kationischen Polyelektrolyten verschiedener Molmassen und Ladungsdichten und deren Einfluss auf das Stabilitäts- und Flockungsverhalten von Silika-Suspensionen*; Herbert Utz Verlag Wissenschaft, München, Germany, 1997.
- [92] Dörfler, H.-D., Ed. *Grenzflächen und kolloid-disperse Systeme*; Springer, Berlin-Heidelberg, 2002.
- [93] Nitzsche, R. *Malvern Short Course - Zetapotential*; 1998.
- [94] Pawley, J. B., Ed. *Handbook of Biological Confocal Microscopy*; Springer, New York, USA, 2006.
- [95] Minsky, M. (1957):US3013467.Microscopy Apparatus.1961.
- [96] Davidovits, P.; Egger, M. D. *Nature* **1969**, *223*, 831.
- [97] Davidovits, P.; Egger, M. D. *Appl. Opt.* **1971**, *10*, 1615–1619.

- [98] Claxton, N. S.; Fellers, T. J.; Davidson, M. W. *Laser Scanning Confocal Microscopy*; 2008.
- [99] Heydenreich, J., Picht, J., Eds. *Einführung in die Elektronenmikroskopie*; VEB Verlag Technik, Berlin, 1966.
- [100] Binnig, G.; Quate, C. F.; Gerber, C. *Phys. Rev. Lett.* **1986**, *56*, 930–934.
- [101] Blanchard, C. R. *Chem. Educ.* **1996**, *1*, 1–8.
- [102] Meng, Z.; Smith, M. H.; Lyon, L. A. *Colloid. Polym. Sci.* **2009**, *287*, 277–285.
- [103] Gutz, I. G. R. Curtipot program, Version 3.5.4, pH and Acid-Base titration curves: Analysis and Simulation. 2010; http://www2.iq.usp.br/docente/gutz/Curtipot_.html.
- [104] Laemmli, U. K. *Nature* **1970**, *227*, 680–685.
- [105] Nargessi, R. D.; Smith, D. S. *Methods in Enzymology* **1986**, *122*, 67–72.
- [106] Provencher, S. W. *Comput. Phys. Commun.* **1982**, *27*, 213–227.
- [107] Provencher, S. W. *Comput. Phys. Commun.* **1982**, *27*, 229–242.
- [108] Horcas, I.; Fernandez, R.; Gomez-Rodriguez, J. M.; Colchero, J.; Gomez-Herrero, J.; Baro, A. M. *Rev. Sci. Instrum.* **2007**, *78*, 1–8.
- [109] Schmidt, S.; Motschmann, H.; Hellweg, T.; von Klitzing, R. *Polymer* **2008**, *49*, 749–756.
- [110] Karg, M.; Hellweg, T. *J. Mater. Chem.* **2009**, *19*, 8714–8727.
- [111] Agrawal, M.; Gupta, S.; Stamm, M. *J. Mater. Chem.* **2011**, *21*, 615–627.
- [112] Das, M.; Zhang, H.; Kumacheva, E. *Annu. Rev. Mater. Res.* **2006**, *36*, 117–142.
- [113] Pich, A. Z.; Adler, H.-J. P. *Polym. Int.* **2007**, *56*, 291–307.

- [114] Karg, M.; Pastoriza-Santos, I.; Liz-Marzán, L. M.; Hellweg, T. *Chem. Phys. Chem.* **2006**, *7*, 2298–2301.
- [115] Karg, M.; Jaber, S.; Hellweg, T.; Mulvaney, P. *Langmuir* **2011**, *27*, 820–827.
- [116] Pich, A.; Karak, A.; Lu, Y.; Ghosh, A. K.; Adler, H.-J. P. *Macromol. Rapid Commun.* **2006**, *27*, 344–350.
- [117] Lu, Y.; Proch, S.; Schrunner, M.; Drechsler, M.; Kempe, R.; Ballauff, M. *J. Mater. Chem.* **2009**, *19*, 3955–3961.
- [118] Karg, M.; Lu, Y.; Carbó-Argibay, E.; Pastoriza-Santos, I.; Pérez-Juste, J.; Liz-Marzán, L. M.; Hellweg, T. *Langmuir* **2009**, *25*, 3163–3167.
- [119] Gao, J.; Hu, Z. *Langmuir* **2002**, *18*, 1360–1367.
- [120] Burmistrova, A.; Richter, M.; Üzüüm, C.; von Klitzing, R. *Colloid. Polym. Sci.* **2011**, *289*, 613–624.
- [121] Stieger, M.; Richtering, W.; Pedersen, J. S.; Lindner, P. *J. Chem. Phys.* **2004**, *120*, 6197–6206.
- [122] Patel, R. N. *Biomol. Eng* **2001**, *17*, 167–182.
- [123] Patel, R. N. *Adv. Synth. Catal.* **2001**, *343*, 527–546.
- [124] Uppenberg, J.; Hansen, M. T.; Patkar, S.; Jones, T. A. *Structure* **1994**, *2*, 293–308.
- [125] Carrera, G.; Riva, S. *Angew. Chem.* **2000**, *112*, 2312–2341.
- [126] Koeller, K. M.; Wong, C.-H. *Nature* **2001**, *409*, 232–240.
- [127] Klibanov, A. M. *Nature* **2001**, *409*, 241–246.
- [128] Kawaguchi, H.; Fujimoto, K.; Mizuhara, Y. *Colloid. Polym. Sci.* **1992**, *270*, 53–57.
- [129] Fujimoto, K.; Mizuhara, Y.; Tamura, N.; Kawaguchi, H. *J. Intell. Mater. Syst. Struct.* **1993**, *4*, 184–189.

- [130] Ortega, N.; Busto, M. D.; Perez-Mateos, M. *Bioresour. Technol.* **1998**, *64*, 105–111.
- [131] Wack, H.; Nellesen, A.; Schwarze-Benning, K.; Deerberg, G. *J. Chem. Technol. Biotechnol.* **2011**, *86*, 519524.
- [132] Chauhan, G. S.; Mahajan, S.; Sddiqui, K. M.; Gupta, R. *J. Appl. Polym. Sci.* **2004**, *92*, 3135–3143.
- [133] Milasinovic, N.; Krusica, M. K.; Knezevic-Jugovic, Z.; Filipovic, J. *Int. J. Pharm.* **2010**, *383*, 53–61.
- [134] Chen, H.; Liu, L.-H.; Wang, L.-S.; Ching, C.-B.; Yu, H.-W.; Yang, Y.-Y. *Adv. Funct. Mater.* **2008**, *18*, 95–102.
- [135] Kratz, K.; Lapp, A.; Eimer, W.; Hellweg, T. *Colloids Surf., A* **2002**, *197*, 55–67.
- [136] van Deurzen, M. P.; van Rantwijk, F.; Sheldon, R. A. *Tetrahedron* **1997**, *53*, 13183–13220.
- [137] Zhang, J.; Chi, Q.; Dong, S.; Wang, E. *Bioelectrochem. Bioenerg.* **1996**, *39*, 267–274.
- [138] Veitch, N. C. *Phytochem.* **2004**, *65*, 249259.
- [139] Tatsumi, K.; Wada, S.; Ichikawa, H. *Biotechnol. Bioeng.* **1996**, *51*, 126–130.
- [140] Schachschal, S.; Adler, H.-J.; Pich, A.; Wetzels, S.; Matura, A.; van Pee, K.-H. *Colloid. Polym. Sci.* **2011**, *289*, 693–698.
- [141] Hartmeier, W. *Immobilisierte Biokatalysatoren*; Springer, Berlin, 1986.
- [142] Morrison, M.; Steele, W.; Danner, D. J. *Arch. Biochem. Biophys.* **1969**, *134*, 515–523.
- [143] Burmistrova, A.; Richter, M.; Eisele, M.; Üzümlü, C.; von Klitzing, R. *Polymers* **2011**, *3*, 1575–1590.
- [144] Held, P. *Determination of Horseradish Peroxidase (HRP) Using Amplex Red and the SynergyHT Microplate Reader*; 2003.

- [145] Haughland, R., Ed. *Handbook of Fluorescent Compounds and Research Products*; Molecular Probes, Inc., 2002.
- [146] Jones, C. D.; Lyon, L. A. *Macromolecules* **2000**, *33*, 8301–8306.
- [147] Pinkrah, V. T.; Snowden, M. J.; Mitchell, J. C.; Seidel, J.; Chowdhry, B. Z.; Fern, G. R. *Langmuir* **2003**, *19*, 585–590.
- [148] English, A. E.; Mafe, S.; Manzanares, J. A.; Yu, X.; Grosberg, A. Y.; Tanaka, T. *J. Chem. Phys.* **1996**, *104*, 8713–8720.
- [149] Das, M.; Mordoukhovski, L.; Kumacheva, E. *Adv. Mater.* **2008**, *20*, 2371–2375.
- [150] Bradley, M.; Vincent, B.; Burnett, G. *Colloid. Polym. Sci.* **2009**, *287*, 345–350.
- [151] Liu, Z.; Jiao, Y.; Wang, Y.; Zhou, C.; Zhang, Z. *Adv. Drug Delivery Rev.* **2008**, *60*, 1650–1662.
- [152] Taira, S.; Du, Y.-Z.; Kodaka, M. *Biotechnol. Bioeng.* **2006**, *93*, 396–400.
- [153] Al-Manasir, N.; Zhu, K.; Kjniksen, A.-L.; Knudsen, K. D.; Karlsson, G.; Nyström, B. *J. Phys. Chem. B* **2009**, *113*, 11115–11123.